International Conference on Mathematical Applications 2019

July 8-11, 2019
Azores-Portugal

Editors:
Fernando Morgado-Dias
Filipe Quintal

ISSN 2184-3945

2nd International Conference on Mathematical Applications

PROCEEDINGS

July 8-11, 2019
Azores-Portugal

Organized by

Institute of Interactive Technologies

Madeira Interactive Technologies Institute

Universidade da Madeira

Universidade dos Açores

Institute of Knowledge and Development

General Information

Official Language

The official language of the conference is English. All presentations, including discussions and submissions, must be made in the official language. No translation will be provided.

Proceedings

Each accepted paper reaching the secretariat in time will be published in the proceedings.

Opening Hours of the Registration Desk

July 8, Monday: 08:00 – 10:00
July 9, Tuesday: 8:00 – 17:30
July 10, Wednesday: 8:00 – 14:00
July 11, Thursday: 8:00 – 14:00

Presentation

Presentations can be done using a data projector. All authors are kindly asked to take their presentations in a flashdrive. All conference rooms are supplied with data projector, PC and internet.

Smoking

Please, be so kind to your lungs and your colleagues by not smoking during the sessions and social events.

WELCOME MESSAGE FROM THE GENERAL CHAIR

On behalf of the Institute of Knowledge and Development, it is our pleasure to welcome you to the International Conference on Mathematical Applications 2019 (ICMA19) in Ponta Delgada (Portugal).

Mathematics is at the core of Sciences and Engineering and is still the key to modeling and characterizing systems and processes, whether natural or artificial.
At ICMA we are looking for cross fertilization between areas that need Mathematics tools and that can provide the applications for different theoretical approaches.
With this conference the organization expects to contribute to this development and foster the integration of Mathematics with application areas.
The Organization would like to acknowledge the efforts of all the people and agents which have collaborated in the event.

The Chairman:
João Cabral, University of the Azores

The General Chairman:
Morgado-Dias, University of Madeira, Madeira Interactive Technology Institute and Interactive Technology Institute

Committees

GENERAL CHAIRS

Fernando Morgado-Dias, UMA – M-ITI, Portugal

TECHNICAL PROGRAM COMMITTEE

Almeida Antonio Mario, University of Minho
Andreica Anca, Babes-Bolyai University
Barreira Raquel, Polytechnic Institute of Setúbal
Camarinha Margarida, University of Coimbra
Catarino Paula, Departamento de Matemática-Universidade de Trás-os-Montes e Alto Douro
Clímaco João, Faculty of Economics University of Coimbra
Czibula Gabriela, Department of Computer Science, Babes-Bolyai University
Davidrajuh Reggie, University of Stavanger
Faria Susana, University of Minho
Ferreira Marta, University of Minho
Fontes Fernando A C C, University of Porto
Forjaz Maria Antónia, University of Minho
Garapa Marco, Universidade da Madeira
Gomes Teresa, University of Coimbra
Gonçalves A. Manuela, University of Minho
Luís Rafael, University of Madeira and CAMGSD (Centro de Análise Matemática, Geometria e Sistemas Dinâmicos)
Morais Eva, UTAD
Nagy A. M., Benha University
Pop Horia, Babes-Bolyai University, Cluj
Quaresma Pedro, Department of Mathematics, School of Science and Technology, University of Coimbra
Reis Maurício, Universidade da Madeira
Silva Jaime, University of Coimbra
Soares Filomena, Polytechnic of Porto – Porto Accounting and Business School
Sousa Ines, University of Minho
Temido Maria Da Graça, University of Coimbra
Vasconcelos Vítor V., Princeton University
Villar José Ramón, University of Oviedo
Zelina Ioana, Technical University of Cluj Napoca, North Center in Baia Mare, Romania

ORGANIZING COMMITTEE

Morgado Dias, University of Madeira and Madeira Interactive Technology Institute
Filipe Quintal, University of Madeira and Madeira Interactive Technology Institute
Francisco Martins, University of the Azores
Hélia Guerra,University of the Azores
Herlander Mata-Lima, Universidade Federal da Integração Latino-Americana
João Cabral,University of the Azores
José Machado,University of Minho
Lucas Pereira, University of Madeira and Madeira Interactive Technology Institute
Rafael Luís,University of Madeira
Mary Barreto, University of Madeira and Madeira Interactive Technology Institute
Tiago Meireles, University of Madeira and Madeira Interactive Technology Institute
Dario Baptista, Madeira Interactive Technology Institute
Fábio Mendonça, Madeira Interactive Technology Institute
Luis Rodolfo Sousa, University of Madeira and Madeira Interactive Technology Institute
Roham Torabi, Madeira Interactive Technology Institute
Sandy Rodrigues, Madeira Interactive Technology Institute
Sheikh Mostafa, Madeira Interactive Technology Institute

Keynote Abstracts

Professor Dr. Jair Minoro Abe

Jair Minoro Abe received B.A. and MSc in Pure Mathematics – University of Sao Paulo, Brazil. Also received the Doctor degree and Livre-Docente title fromthe same University. He is currently coordinator of Logic Area of Institute of Advanced Studies – University of Sao Paulo Brazil and Full Professor at Paulista University – Brazil. His research interest topics include Paraconsistent Annotated Logics and AI, ANN in Biomedicine and Automation, among others. He is Senior Member of IEEE.

Professor Abe is a studious of a family of Paraconsistent Annotated Logic which is used to solve many complex problems in engineering. He has authored/edited books on Paraconsistent and related logic published by Springer Germany and other reputed publishers.

He is the recipient of many awards including medals for his academic performance and also received many best papers awards. Professor Abe was the Editor-in-Chief of Publicações da Sociedade Paranaense de Matemática de 1990 – 1994. Presently, Professor Abe serves as Associate Editor and member of the Editorial Board of some journals related to the intelligent systems and applications.

Professor Abe has supervised a number of PhD candidates successfully and presented a number of keynote addresses.

He has authored/co-authored around 300+ publications including books, research papers, research reports, etc.

Professor Abe's research interests include System design using conventional and Artificial Intelligence techniques, Paraconsistent Annotated Logic, Human factorsin Aviation, Intelligent Decision Making, Teaching &Learning practices, and Cognitive Studies.

Title: Towards Paraconsistent Engineering

Abstract

Non-classical logics have played an important role in AI and Technology. In this talk we present an overview of Paraconsistent Annotated Logic and some its important applications. Roughly such systems allow to deal with imprecise, inconsistent and incomplete systems of information. We show its usefulness in Biomedicine, Automation, Decision-making themes, among others.

Ph. D. Reinhard Haas, PhD

Energy Economics Group, Institute of Energy Systems and Electric Drives, Vienna University of Technology

Title: Heading towards sustainable and democratic electricity systems

Abstract

In the history of the electricity systems in several countries different boundary conditions existed and exist with respect to price formation in the market. After the periods of state regulation and the first phase of liberalisation of the wholesale markets currently the electricity system faces the third huge challenge: the change towards a bidirectional system, which should be more democratic and sustainable allowing also prosum(ag)ers – consumers with own generation units and storage – to play a specific role. This process is currently under way in many countries world-wide and in these countries also a change in the principle how prices come about is already under way. A major reason for this development is that in recent years the electricity generation from variable renewable energy sources especially from wind and photovoltaic power plants increased considerably. The major objective of this contribution is to analyze and provide insights on how to bring about a sustainable and competitive electricity system with even higher shares of renewable energy sources (RES) and an energy economically balanced system but without escalating political interventions. It is triggered by the current discussion on how to integrate large shares of variable RES but the fundamental intention goes beyond that. The major conclusion is that the electricity system of the future will be built on a very broad portfolio of technologies and demand-side options, allowing a higher number of players to participate in the system and, hence, heading towards a much more democratic approach.

Prof. D. Maria Teresa Restivo

Maria Teresa Restivo has a Physics degree in Solid State Physics and a Ph.D. in Engineering Sciences, both at the University of Porto, Portugal. Her teaching activities are within the Automation, Instrumentation and Control Group of the Mechanical Engineering Department, Faculty of Engineering, University of Porto. Her research activities are within the System Integration and Process Automation Research Unit (UISPA) in the Associated Laboratory for Energy, Transports and Aeronautics (LAETA) funded by the Portuguese Science and Technology Foundation and hosted in the Research Pillar of the Institute of Science and Innovation in Mechanical and Industrial Engineering (INEGI). She was Member of the Faculty of Engineering Scientific Board since 2001-19. She is Director of the UISPA within INEGI Currently, topics of interest of applied research are among the development of Medical Instrumented Devices, Smart Devices and Online Experimentation and the Use of Emerging Technologies in Training and in Education. She has participated in the creation of several non-formal learning activities for the Society organized at University of Porto and by its Faculty of Engineering and collaborated with some of those editions. She is author (co-author) of articles and 6 books at National and International publishers (one awarded at national and international levels, among different other prizes in R&D). She has been project co-ordinator and team member at national level and as FEUP's partner in European projects. She has been involved in supervising MSc and PhD theses. She has five national patents and one international. Two international claims are still pending. She is institutional member of the Global Online Laboratory Consortium (GOLC), Co-Chair of the Scientific Advisory Board of International Association of Online Engineering (IAOE). She is Past-President of International Society for Engineering Pedagogy (IGIP) and member of its Executive Committee. She was the first President of the Portuguese Society of Engineering Education (2010-12). She has the “ING PAED IGIP” diploma of International Engineering Educator.

Title: Experimental activity, engineering students’ skills, innovation, industry and society

Abstract

The role of universities, and especially of their engineering schools, to plan and optimize their output of future professionals, represents a terribly demanding challenge due to our globalization era, with an unprecedented speed of change in the global environment.

The traditional slow adjustment of past curricular reforms in engineering schools has been accelerated to provide student profiles suitable to the global industry and to society demands. Topics such as project management, technology evaluation, engineering innovation and product testing are a few examples of current student skills to be add to scientific and technical knowledge.

As a simple example, I will look at the approach of the Laboratory of Instrumentation for Measurement (LIM) at the Faculty of Engineering of University of Porto and I will try to analyse its initiatives either in involving students in applied research activities and their outputs or in other activities within the society, with intensive gain in complementary skills.

LIM has provided resources, inspiration topics and freedom to their collaborators to work on innovating solutions, in contact with different areas of academic knowledge and listening society needs, gaining skills required by any successful engineering professional.

In each one practical activity, where creativity, and problem-solving where required, these students have engaged in higher-order thinking processes that benefits them, their peers, their instructors, and society.

Different examples could be presented where LIM has been sharing with its students or young granted graduated members, international and national Awards, patents, publications, communications at international and national events, etc.

Additionally, to this discussion, some demonstrations of smart equipment developed under these approaches will be performed.

Table of papers

Software For Six Sigma Projects with the Use of the Paraconsistent Logic

Giovanna Albertini
Graduate Program in Production Engineering
Paulista University
São Paulo- SP
anne.albertini@live.com

Jair Minoro Abe
Graduate Program in Production Engineering
Paulista University
São Paulo - SP
jairabe@uol.com.br

Luiz Antônio de Lima
Graduate Program in Production Engineering
Paulista University
São Paulo - SP
aula.prof@gmail.com

Kazumi Nakamatsu
Human Science and Environment/H.S.E
University of Hyogo
Hyogo - Japan
nakamatu@shse.u-hyogo.ac.jp

***Abstract*—Companies of products and services, implement the six sigma methodology in several scenarios, however, without taking into account factors (organizational climate, organizational culture) that are fundamental to the success of the implementation in the pre-project phase and even in the selection of its six sigma projects. The purpose of this study is the development of a system that uses the Paraconsistent Decision Method to study the feasibility of its implementation in Six Sigma in a given scenario, making the decision making more precise. The Paraconsistent Decision Method allows the support of paraconsistent logic in the (pre-project) phase of choice in consideration of six sigma projects; we have the quest to enable improvement in success accuracy in scenarios where there are factors (organizational climate, organizational culture) critical of success. This article aims to contribute to the constant search for quality (reduction of defects) and mitigation of costs by companies in low-quality scenarios (defects in products and services).**

Keywords— Six Sigma; Quality; Paraconsistent Annotated Evidential Logic Eτ; Paraconsistent Decision-Making Method.

I. INTRODUCTION

According to Mikel Harry, he recognizes as a six-sigma methodology process improvement that achieves defect levels of 3.4 ppm (parts per million) for critical quality characteristics of customers. Deming in 1990, in his vision of states, reinforces that in every process there is some variation in greater or lesser quantity; the key to improving processes is to attack and reduce the cause of variation systematically. From the tools applied logically and structured in a scenario that has the essential for the operation and proper performance of the system, in this scenario, a scene with an excellent organizational climate and an ethical corporate culture, preventing human factors can affect system performance. [2]

The question is related to the fact that the organizational culture and organizational climate can be considered as unstable and ephemeral since both are mostly human and suffer constant changes which can affect the behavior of the system.

Noticeably, or not, the most significant difficulty in the deployment of Six Sigma is in exercising our knowledge and their tools, where the system depends on both the team collaboration and the environment, as well.

There are fundamentally human interactions, where these interactions may not suffer from the human inconsistencies or attitudes as vitiate the data obtained through the Six Sigma projects. [6].

Problems and inconsistencies occur naturally in the scenario with humans, not impeding the ability of reasoning or human thought, the system can perform its knowledge of the situation, together with the humans correctly when finding themselves in a scenario that meets their needs entirely. [6]

Given this assumption, we have sought to establish the feasibility of implementing the Six Sigma system, considering the critical success factors, the organizational climate, the organizational culture and the scenario. [6]

Considering that the decision-making has always been a painful process for both the machine and the human, the vast amount of data, possibility and possible results made this task a problem that needed something new to resolve; it needed a system capable of accurately calculate and show the possible scenarios, a method to support decision-making. [6].

However, in addition to a support system for the decision, a precise system, capable of calculating all the inconsistencies of the scenario, working with a calculation which includes all the variables and brings.

As a result, the feasibility of the System of choice for pre-Six Sigma projects with the use of Paraconsistent Logic becomes patent, since such logic has the ability to process uncertain, inconsistent and even incomplete data in a non-trivial way.

Hence we have chosen the said logical system as the logic underlying our studies.

II. EASE OF USE

A. Six Sigma

In the mid 80's, Six Sigma was born in the company Motorola. Directly and indirectly, the company, at that time, was spending around 10% and 20% of revenues in low quality. After studying the scenario, the bond between the experience of apparent failure on clients and, also, the knowledge of internal defects in their factories, Motorola started to be aware of the fact that the low quality obtained a significant impact on its profitability of primary line. [2]

ISSN 2184-3945

Soon after its deployment at Motorola, Six Sigma has different settings that in short, were linked to efficiency in processes and operations, the improvement of business processes, achieving excellence in our processes. [3]

However, the primary objective of Six Sigma continues to lead the continuous improvement of the process of troubleshooting methodology, being documented and verifiable repetition. [3]

Another definition that can be attributed to this system, which is the definition of a management philosophy, which seeks to achieve challenging objectives considered, reduction of defects in products, using processes and services, through a careful analysis of the results obtained and data collection. [1]

The level of the Six Sigma identification is taken into account as main inputs: total opportunities (number of units tested * possible quantities of opportunities) along with the number of defects found. In a given hypothesis (errors found in production) as shown in table 1, we considered the total of opportunities = 1; then we had the perception of how impotent means the search for the 6sigma level, which represents the almost total extinction of defects, and consequently to the almost 100% success.

TABLE1. PROJECT SIX SIGMA WITH TOTAL OPPORTUNITIES = 1 AND FORMULA.

Sigma Level	DPMO-Defects per Million Opportunities(DPO x 1.000.000)	% Error - Six Sigma	% No Error - Six Sigma
6	3,4	0,00034%	99,99966%
5	233	0,02330%	99,97670%
4	6210	0,62100%	99,37900%
3	66807	6,68070%	93,31930%
2	308538	30,85380%	69,14620%
1	691492	69,14620%	30,85380%

(Source: Author)

In the Six Sigma system is used the tool DMAIC (Define, Measure, Analyse, Improve and Control)

Defines: an accurate definition of the scope of the project;

Measure: Find the focus of one or more problems in the scenario;

Analyze Definition of the causes of each problem;

Improve: Evaluate, present and calculate possible solutions to questions;

Control: Ensure that the answer will keep for a long-term goal. [6].

The logical way to use the DMAIC tool, follow the steps as shown in figure:

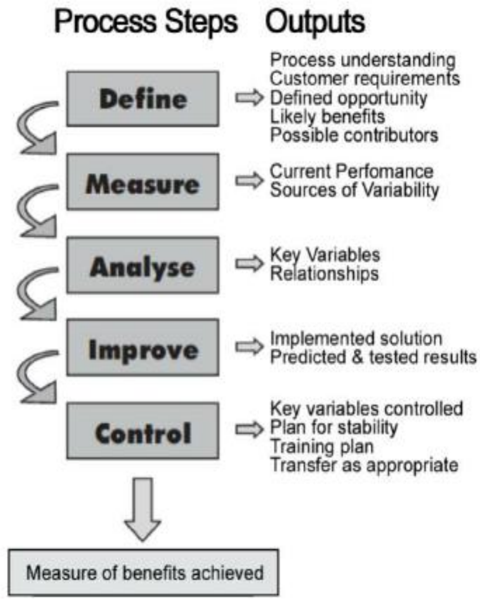

Fig. 1 – *DMAIC – Source:* [10]

B. Success Factors of Six Sigma

It can be identified as factors affecting the system: assigned projects and the environment in which it is being implemented, team preparation and top management, lack of structure and necessary knowledge to work with the system, lack of leadership and team monitoring. Add to that the internal processes of the company. All this leads to the prevention of the achievement of objectives and improvement in the operations and products of the company. [2]

The leadership can be singled out as essential and indispensable for achieving the success of Six Sigma. Monitoring progress and ensuring team commitment is monitored through meetings. Such commitment constitutes one of the fundamental tasks that an active leadership and senior management need to realize. [2]

In addition to the performance of the high administration, customer focus, the use of a structured method and the proper infrastructure are considered the factors of success of Six Sigma. [2]

C. Organizational Climate

The organizational climate can be roughly defined as the work environment, the corporate environment, and psychological atmosphere. Within this environment, it is easier to detect the effects of climate change on people, affecting mainly the performance and teamwork, both significantly essential pillars for the performance of the system Six Sigma, which detect for what reasons the environment is this way.[4]

Even when, understood that the organizational climate is fundamental of inconsistencies and unforeseen changes, makes it essential for the study and the importance of balance in the environment that the system works mainly with human interactions and develops its methodology in the team. [4]

It makes the current mood is the motivation of the members which, as a result, make the environment more productive and satisfying, generating positive effects and animation, collaboration and interest.

Changes happen all the time, preventing the balance still and stable. However, control the variation and seek that doesn't happen an extreme contrast, making the climate with foci of disinterest, depression, dissatisfaction, in more severe cases, which may lead to strikes, nonconformism, unrest among the members of the scenario that consequently also become dissatisfied with the company. [8]

The organizational climate must be studied and thoroughly analyzed by the administrator, then, toil to encourage their decisions, and then find it necessary, interfering in the environment to generating positive changes and gradual climate and organizational culture. [9]

D. Organizational culture

Speak of regulatory climate makes consequent need to speak of corporate culture since one refers to the other. [5]

Organizational culture is what influences and defines the regulatory environment. Would the reasons by which, the atmosphere is the climate in which is, he is a particular climate or not, the study of the culture, is the study of attitudes, habits, gestures, speech, among many others, that establish the environment and team collaboration among themselves. [5]

After setting a set of norms, values, and beliefs that guide and normalize the behavior of particular team, becomes noticeable that culture is broader than the organizational climate. The importance of organizational culture is the significant influence that it has on the environment and people. [9]

If the environment is detrimental to the team and the processes, changes must also come from the culture, essential points for a motivational change are communication, competence, commitment, continuity, and understanding. [9].

E.. Paraconsistent Method of Decision

The Paraconsistent Method of Decision (MPD) was developed by Carvalho (2006) through their studies. To recognize the factors that influence in the enterprise, causing the success or failure, in other words, what can influence the decision of continuity of particular project or not. [7]

It was possible to recognize that specific factors may present different results, as favorable conditions, in other cases, unfavorable terms, or else, can still submit circumstances indifferent to the project. [7]

TABLE II
EXTREME AND NON-EXTREME STATES

Extreme States	Symbol
True	V
False	F
Inconsistent	T
Paracomplete	⊥
Non-extreme states	**Symbol**
Quasi-true tending to Inconsistent	QV→T
Quasi-true tending to Paracomplete	QV→⊥
Quasi-false tending to Inconsistent	QF→T
Quasi-false tending to Paracomplete	QF→⊥
Quasi-inconsistent tending to True	QT→V
Quasi-inconsistent tending to False	QT→F
Quasi-paracomplete tending to True	Q⊥→V
Quasi-paracomplete tending to False	Q⊥→F

The MPD receives data from the members of the decision-making process, as the experience, uses the so-called "experts" for evaluation, making them essential tools in the assessment of a specific issue. Moreover, through the information obtained, performs the calculation considering all the possibilities, not only of the members, as well as the scenario and the company. [7]

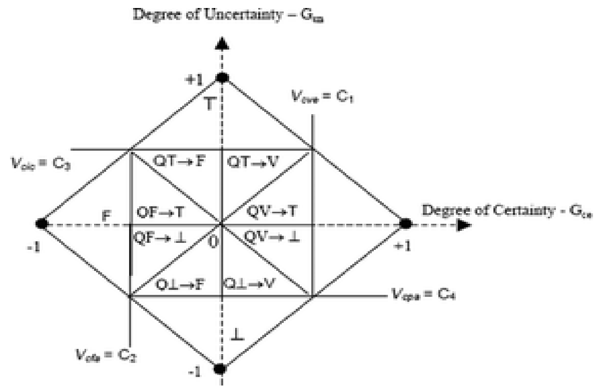

Fig.3.Extreme and non-extreme States. Source[13]

III. THE PROJECT

This study proposes the development of software that can calculate the feasibility of pre-projects of Six Sigma system through the use of the Paraconsistent Method of Decision, aiding in the decision-making process. By using the Paraconsistent Method of Decision, a questionnaire is considered to collect the necessary data on the project.

The user will define the experts who will provide the information on the project and the importance (weights) of each expert, making the report of a particular expert more relevant, in comparison with the other information from other experts. Once completed the questionnaire, it will be done the calculations with the evidence degrees, and it will be delivered the result of viability to the user.

Whereas it is necessary to calculate many variables, the software will be responsible for providing more accurate information essential for the decision-making process. Obviously precision and accuracy of the results are paramount in this process, and of utmost importance for the scenario.

To reflect the joint influence of all factors with weight in each decision, one must take into account the Global Analysis and are collected by the favorable and contrary evidence degree.

The calculation of the Global Analysis can be extracted by the weighted average of the evidence of conviction and uncertainties resulting from all the factors. When the weights in each decision are equal, the Global Analysis should be calculated by the arithmetic mean of the evidence of belief and uncertainty, becoming the geometric center.

At this point, the study advances and reinforces the importance of data collection by forms filled by experts to the implementation of algorithms represented in flowcharts in a way to implement in any computational technology and that support the decision support by the proposed system. The decision-making process consists of choosing one of several alternatives. The unified process of annotated paraconsistent logic is proposed as an aid in the decision-making of recounting, as follows:

TABLE III. UNIFIED MACRO PROCESS PARACONSISTENT ANNOTATED LOGIC

Item	Process	SubProcess
A	Definition	Define Proposition; Define Factors; Define Section; Define Database;
B	Transformation	Generate Normalization; Use Evidence (favorable and unfavorable);
C	Calculation	Calculate Maximization; Calculate Minimization; Calculate Evidence (Resultant Min, Resultant Max); Calculate Degree (Gce: Certainty, Gco: Contradiction); Calculate Globals Analysis (Gce: Certainty, Gco: Contradiction);
D	Parameterization	Parametrize Limitvalues;
E	Processing	Process Para-Analyzeralgorithm;
F	Decision-making Support	Assists decision-making;

The use of Paraconsistent Logic Annotated as support in decision-making in implementing six sigma projects should fill a significant gap in the demands for products and services that are based on the six sigma methodology. In this new proposed form, factors of climate and/or culture should be taken into account in the implementation of the six sigma by managers who decide success.

IV. DISCUSSION OF RESULTS

The study for the development of software capable of bringing the Paraconsistent Method of Decision to calculate the inconsistencies of the scenario and the people who are part, brought more reliability and accuracy to the decision-making process, giving due importance to the calculations and the results obtained.

The study necessary for the development was about the whole process from the pre-project the decision of deployment of the system Six Sigma. The approach by the proposed system must be based on the form that meets propositions able to foment data in the possibility to allow the use of paraconsistent logic and to obtain results that will aid in the whole of decision making by six sigma projects.

Other ways of representing the paraconsistent logic with possible implementation in a particular programming language are to launch the use of the flowchart, where we have:

In this stage of the flowchart, there is an excellent possibility of being quasi-true tending to the inconsistent, or inconsistent tending to the True,

because the Gce and Gco conditions result in some response and when there is no possibility to answer, it follows in the "Y" flow to explore the possible answers offered by the paraconsistent logic

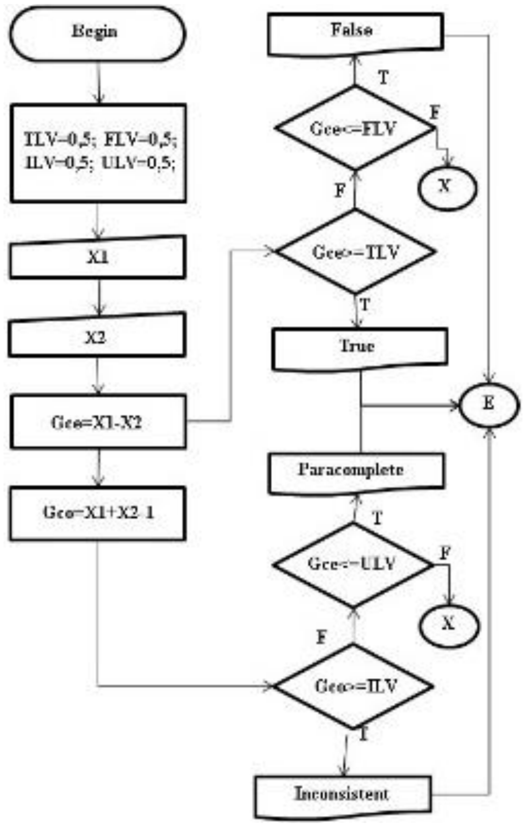

Fig. 4. Paraconsistent logical flowchart: True, False, Inconsistent, Paracomplete. (Source: Luiz A. de Lima).

The flowchart (Fig. 4) shows that there is a possibility of being quasi-true tending to the inconsistent, or quasi-inconsistent tending to the True because the Gce and Gco degrees conditions result in some response. When there is no possibility to answer, it follows in the "Y" flow to explore the possible answers offered by the structure of paraconsistent logic.

The flowchart (Fig. 5) shows that there is a possibility of being quasi-true tending to the inconsistent, or inconsistent tending to the True because the Gce and Gco conditions result in some response. When there is no possibility to answer, it follows in the "Y" flow to explore the possible answers offered by the paraconsistent logic.

The next flowchart (Fig. 6), there is a possibility of being quasi-true tending to the Paracompleteness or Paracompleteness tending to the True, since the Gce and Gco conditions result in some response. Moreover, when there is no possibility to answer, it follows in the stream "Z" to explore the possible answers offered by the paraconsistent logic.

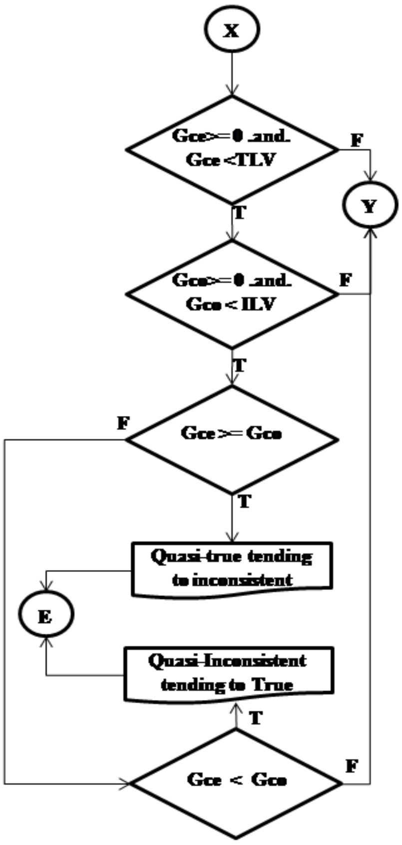

Fig. 5. Paraconsistent logical flowchart: Quasi True tending to the Inconsistent, Inconsistent tending to True. (Source: Luiz A. de Lima).

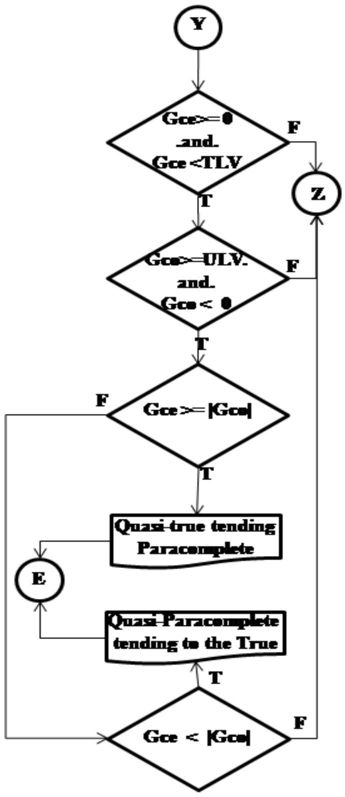

Fig. 6. Paraconsistent logical flowchart: Quasi True tending to Paracompletenessn, Paracompletenessn tending to the True . (Source: Luiz A. de Lima).

V. FINAL CONSIDERATIONS

Inconsistencies and human errors continue making the decision-making processes involved, as well as affect the production within an organization. Calculate is not enough, it is necessary to make these calculations automated, easy access to the user. Make the decision-making process more accurate, reliable and fast. The production and operations grew to become the most common errors within the activities, the search for the improvement of operations and the quality of the same, brought the study and development of Six Sigma, which proved to be a useful tool and produced results that demonstrate the improvement in processes and production. In addition to this study, in order to support managers for the implementation of the six sigma methodology, we seek artificial intelligence techniques and, in particular, parachutist logic, aid in decision making with more accuracy and even allowing the refuse in the implementation of six sigma projects, when considering factors such as climate and / or organizational culture.

Acknowledgment

Thanks to the Software Engineering Research Group and the University Paulista.

References

[1] D. Nevalainen, L. Berte, C. Kraft, E. Leigh, L. Picaso, & T. Morgan, “Evaluating Laboratory Performance on Quality Indicators With the Six Sigma Scale”, Archives of Pathology & Laboratory Medicine: April 2000, Vol. 124, No. 4, pp.516-519, 2000.

[2] J. Antony, R. Banuelas, "Key ingredients for the effective implementation of Six Sigma program", Measuring Business Excellence, Vol. 6 Issue: 4, pp.20-27, 2002.

[3] M. Van Houtte, “Tracking effects on school achievement: A quantitative explanation regarding the academic culture of school staff”, American Journal of Education, 110(4), pp.354–388, 2004.

[4] D. Venanzi, B.P. Laporta, “Learn six sigma”, South American Development Society Journal, [s.l.], v. 1, n. 2, ISSN 2446-5763, pp. 66 - 84, 2017.

[5] J. Prosser, “The evolution of school culture research” In J. Prosser (Ed.), School culture, London: Paul Chapman, pp.1–14, 1999.

[6] C.Z. Kirilo, “Método Paraconsistente de Decisão aplicado ao Seis Sigma”, São Paulo, 2017, to appear.

[7] J.M. Abe, “Paraconsistent logics and applications”, In: 4th International Workshop on Soft Computing Applications.. - [s.l.] : IEEE, pp. 11–18, 2010.

[8] R. Payne & D. Pugh, Organizational Structure and Climate. In M. Dunnette (Ed.), “Handbook of Industrial and organizational psychology” Chicago: RandMcNally, pp.1125–1173, 1976..

[9] F.T.T. Phua, The role of organizational climate in socially embedding construction firms’ sustainability goals, Construction Management and Economics, (1), 2018.

[10] https://www.researchgate.net/figure/The-Six-Sigma-DMAIC-Process-and-Key-Outputs-17_fig4_273524820

[11] J.M. Abe, S. Akama, and K. Nakamatsu Introduction to Annotated Logic – Foundations for Paracomplete and Paraconsistent Reasoning, Series Intelligent Systems Reference Library, Vol. 88, Springer International Publishing, ISSN 1868-4394, Ed. 1, 190 pages, 2015.

[12] http://www.demneuropsy.com.br/detalhe_artigo.asp?id=95

[13] http://www.revistaespacios.com/a18v39n09/18390915.html

On continuous deformations of monohedral spherical tilings by spherical pentagons

Ana Maria Reis d'Azevedo Breda
Departamento de Matemática
Universidade de Aveiro
Aveiro, Portugal
ambreda@ua.pt

José Manuel Dos Santos Dos Santos
Instituto GeoGebra Portugal
Escola Superior de Educação - Politécnico do Porto
Porto, Portugal
santosdossantos@ese.ipp.pt

***Abstract*—In a previous work it was described a procedure to obtain certain classes of spherical tilings with GeoGebra, starting from a specific subset of spherical segments. This innovative way of generating spherical tilings has made emerged a class of monohedral spherical tiling by four spherical pentagons and classes of dihedral spherical tiling by twelve spherical pentagons. Here, we shall show how we can generate a class of a 2-parameter monohedral spherical tilings by convex pentagons, $\mathfrak{P}^*_{(\mathscr{C},\theta 1,\theta 2)}$, made of sixty congruent tiles, changing the gluing rules of the edge-tiles, being the new ones ruled by a local action of a particular subgroup of spherical isometries with support on the regular spherical dodecahedral tiling. In relation to these new classes of pentagonal tilings, combinatorial and geometric properties will be given. All monohedral spherical tilings by pentagons whose pentagonal prototile is of the form *a.a.b.b.c* are shown. This family of spherical tilings has emerged as a result of an interactive construction process using newly produced GeoGebra tools and the dynamic interaction capabilities of this software.**

***Index Terms*—Spherical Geometry, Spherical Tilings, GeoGebra.**

I. Introduction

By a spherical tiling we mean a tiling of the 2-dimensional sphere [13]. A spherical tiling is monohedral if all tiles are congruent. Additionally, a spherical tiling is edge-to-edge if no vertex of a tile lies in the interior of an edge of another tile. In this paper we are interested in the study of new classes of monohedral and edge-to-edge spherical tilings by spherical pentagons.

The spherical tilings by congruent rigth triangles were obtained by Yukako Ueno and Yoshio Agaoka in 1996, [22]. Later, in 2002, the complete classification of monohedral edge-to-edge triangular spherical tilings was achieved by the same authors [23]. They have extended the classification of triangular f-spherical foldings, studied and characterised by Ana Breda, in 1992, [1].

The classification of spherical tilings by triangles is not yet completed. In fact, little is known when the condition of being monohedral or edge-to-edge is dropped out.

The combinatorial study of spherical tilings by twelve pentagons, with vertex valency greater or equal to three has been also achieved, see [12] for details. Recently, a family of spherical monohedral tiling by four congruent and non-convex spherical pentagons has been characterised [7].

Besides the theoretical mathematical aspects involved in the study of spherical tilings, they are also object of interest in other areas of knowledge and in technological applications. Walter Kohn pointed the year 1984 as the year where a big surprise in the field of crystallography has occurred. In [15, p. s70] he mentions: "D. Schechtman and co-workers that reported a beautiful x-ray pattern with unequivocal icosahedral symmetry for rapidly quenched AlMn compounds. The appropriate theory was independently developed by D. Levine and P. Steinhardt, who coined the words quasicrystal and quasiperiodic. Even more curious was the fact that R. Penrose (1984) had anticipated these concepts in purely geometric [terms], the so-called Penrose tilings" [15, p. s70].

Spherical tilings and their properties have been used in chemistry, for instance, in the study of periodic nanostructures [11], making emerge new forms of molecular association notably fullerenes [10], leading to a deeper study of spherical tilings by triangles, quadrilaterals and pentagons [19]. In the same line of reasoning other tilings including heptagons [21], and, heptagons and octagons [20] had emerged. Applications to new possibilities for new molecular patterns are exposed in [8], [14], [17], [18], [24]. Nowadays, in engineering there is a need to merge the computer aided design and computer aided engineering into a single approach, contributing to an increasing interest in studying relationships between spherical tilings and spherical Bezier curves [9]. The knowledge of spherical tilings can also be useful for the developed of some issues in computational algebra [16]. The facility location problems, spherical designs and minimal energy point configurations on spheres [2], [3] are other fields where the study of spherical tilings is quite useful.

In this paper we intend to extend the knowledge of spherical tilings describing a set of spherical tilings, here denoted by $\mathfrak{T}$, presenting and characterising, in detail, some subsets of $\mathfrak{T}$ composed by pentagonal monohedral spherical tilings with sixty tiles, providing a continuous deformation path among elements of this class. We also present a way to obtain all monohedral spherical tilings by convex spherical pentagons whose their tile configurations are of the type *a.a.b.b.c*.

II. Related Work

In previous work, making use of the dynamic capabilities of GeoGebra, that have been proved to be interesting for our research, findings about monohedral and dihedral spherical tilings by spherical convex and non convex pentagons were obtained.

The creation of GeoGebra tools for spherical geometry, used initially to obtain some well known spherical tilings, provide geometric concretization of some new spherical tilings [6].

In fact, GeoGebra gives the possibility of interacting, simultaneously, with graphic, algebraic and calculus views. It also gives the chance to create new tools and commands. All tools was created from the combination of existing tools or commands. The new tool and the corresponding commands can be used in new constructions or may be integrated in the construction of new tools. Spherical GeoGebra tools were constructed among the purpose to explore, among others spherical tilings. Whiting these spherical tools we mention the following ones: *Spherical Segment, Minor*, *Spherical Segment, Great*, *SphericalAngleMeasure*, *Spherical Equidistant Points*, *Spherical Compass*, *Spherical Equilateral Triangle*, *SphericalTriangleVertice3Angles*, *SphericalTriangle*$\beta AB\alpha$.

Here, by way of example, we describe how the Spherical Segment tool was constructed.

Given two non antipodal spherical points A and B, the minor spherical segment joining them is a great circular arc of extremes A and B. These spherical segment can be obtained in GeoGebra using the command $SphereSegmentMinor[A,B]$ described below (see figure 1).

Tool Name	Spherical Segment, minor
Command Name	SphericalSegmentMinor
Syntax	SphericalSegmentMinor[A,B]
Help	Given A,B and a spherical, s, draw the spherical segment joining A to B.
Icon	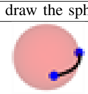
Script	s=Sphere[(0,0,0), 1] A=PointIn[s] B=PointIn[s] If[Distance[A,B]≠2,CircularArc[(0,0,0), A,B,Plane[(0,0,0),A,B]]]

Figure 1: Construction of the spherical segment minor tool

Observed that if we use, in the the last line of the script of figure 1, the command $Plane[(0,0,0),B,A]$ we get the greater spherical segment between two points and, by these way, we can record a different tool.

These new tools allowed us to get new families of spherical tilings, namely, the 2-parameter family, $\widehat{\mathfrak{B}_{\frac{p}{q}}}, p,q\in\mathbb{N}$, obtained by a global action of a subgroup of spherical isometries, which contains the well known antiprismatic tilings see [5]. Later, using similar procedures, the one-parameter family of tilings, $\mathfrak{P}_{(\mathscr{C},\tau)}$ with $\tau\in]0,\pi[\setminus\{\frac{1}{2}\arccos(-\frac{1}{3})\}$, was revealed, see [7]. Recently, the one-parameter family of monohedral spherical non-convex hexagonal tiling with six faces, $\mathfrak{H}_{(\mathscr{C},\tau)}, \tau\in\left]0,\arcsin\left(\frac{\sqrt6}{3}\right)+\frac{\pi}{2}\right[\setminus\{\arctan\left(\frac{\sqrt2}{2}\right)\}$ was described [4].

As we shall see, in the next sections, an adequate adaptation of the previous procedures permit us to characterise a 2-parameter class of monohedral spherical tiling composed of sixty congruent pentagonal tiles, $\mathfrak{P}^*_{(\mathscr{C},\theta1,\theta2)}$, with parameters $\theta1\in[0,\arccos(l_1)]$ and $\theta2\in[0,\arccos(l_2)]$ where

$$l_1=\frac{1}{10}\sqrt{10\left(\sqrt5+5\right)}$$

and

$$l_2=\frac{\alpha\left((4-2\sqrt5)\beta-\sqrt2\sqrt{(4\beta^2-3)(\sqrt5-3)}\right)}{3(\sqrt5-3)}+\beta^2$$

with $\alpha=\cos(\theta1)$ and $\beta=\sin(\theta1)$.

III. Construction of $\mathscr{C}$, the tiling generation cell.

Consider one of the pentagonal tiles, $[ABCDE]$, of the regular dodecahedral spherical tiling. Without loss of generality we may assume that the equilateral spherical pentagon $[ABCDE]$ of angles $\frac{2\pi}{3}$, has as vertices the points A,B,C,D,E whose coordinates are:

$A=\left(\frac{\sqrt{15}+\sqrt3}{6},\frac{-\sqrt{15}+\sqrt3}{6},0\right)$; $B=\left(\frac{\sqrt{15}+\sqrt3}{6},\frac{\sqrt{15}-\sqrt3}{6},0\right)$; $C=\left(\frac{\sqrt3}{3},\frac{\sqrt3}{3},\frac{\sqrt3}{3}\right)$; $D=\left(\frac{\sqrt{15}-\sqrt3}{6},0,\frac{\sqrt{15}+\sqrt3}{6}\right)$; $E=\left(\frac{\sqrt3}{3},-\frac{\sqrt3}{3},\frac{\sqrt3}{3}\right)$.

The centroid of the prototile is the point $C_t=\left(\frac{\sqrt{10\sqrt5+50}}{10},0,\frac{\sqrt{-10\sqrt5+50}}{10}\right)$ and the coordinates of the midpoint of the geodesic joining the spherical points A and B is $M_{AB}=(1,0,0)$. It should be noted that C_t is determined by the intersection of the geodesic segments $M_{AB}D$ and AM_{CD} where $M_{CD}=\left(\frac12,\frac{\sqrt5-1}{4},\frac{\sqrt5+1}{4}\right)$.

The side lengths of the spherical triangle $[AM_{AB}C_t]$ are:

$\widehat{AM_{AB}}=\arccos\left(\frac{\sqrt3+\sqrt{15}}{6}\right)$;

$\widehat{M_{AB}C_t}=\arccos\left(\frac{1}{10}\sqrt{10\left(\sqrt5+5\right)}\right)$;

$\widehat{C_tA}=\arccos\left(\frac{\sqrt{15\left(2\sqrt5+5\right)}}{15}\right)$.

Having in mind the use of an adaption to the procedure performed in previous work and using the dynamic displacement of a point P in the region defined by the spherical triangle $[AM_{AB}C_t]$, we end up, as we shall see, with a class of pentagonal tilings. In fact, some elements of this class are monohedral tilings by triangles and quadrilaterals. They are limit cases of the pentagonal ones, see Fig.2.

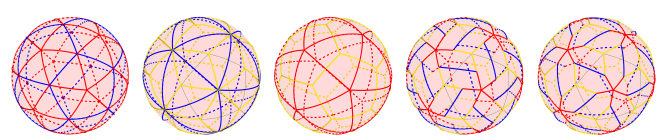

Figure 2: Some elements of $\mathfrak{P}^*_{(\mathscr{C},\theta1,\theta2)}$, monohedral spherical tilings by triangles, kites, quadrilaterals and pentagons.

Consider the set

$\mathscr{C}=\{X\in S^2: X\in\widehat{PA}\vee X\in\widehat{PM_{AB}}\vee X\in\widehat{PC_t}\}$, $P\in[AM_{AB}C_t]$, which represents the starting cell of the generating tilings. In Figure 3, we illustrate a tiling obtained through the generating procedure described bellow, with $\theta1,\theta2$ the midpoints of the corresponding admissible intervals.

Let $\theta1$ be an angle in $[0,l_1]$. To obtain a dynamic variation of P in all points of the fundamental region, $[AM_{AB}Ct]$, let us

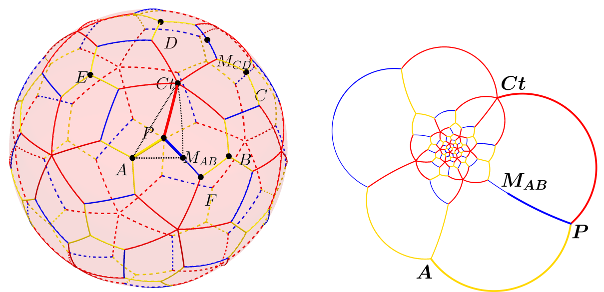

(a) $\mathfrak{P}^*_{(\mathscr{C},\theta 1,\theta 2)}$ (b) Cell $\mathscr{C}$ in the and planar graph.

Figure 3: Element of the monohedral spherical tiling family $\mathfrak{P}^*_{(\mathscr{C},\theta 1,\theta 2)}$ and one of its planar graph.

take an arbitrary point $X_{\theta 1} \in \widehat{OM_{Ab}Ct}$ and consider the point $\hat{X}_{\theta 2}$ obtained by the intersection of the plane $z = \sin\theta 1$ with the spherical segment $\widehat{ACt}$. Let P be an arbitrary point in the spherical segment $\widehat{X_{\theta 1}\hat{X}_{\theta 2}}$. Denoted by $\theta 2$ the $\widehat{X_{\theta 1}P}$, see figure 4.

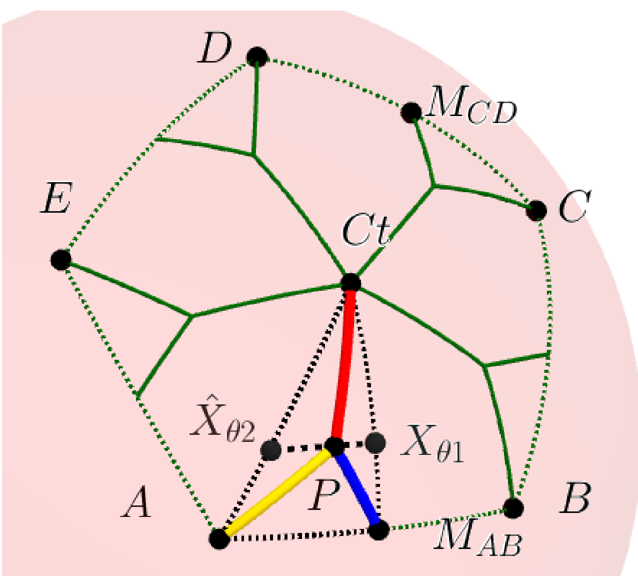

Figure 4: Detail of construction of P in $\mathscr{C}$ of $\mathfrak{P}^*_{(\mathscr{C},\theta 1,\theta 2)}$.

Thus, P is in the intersection of the planes $OM_{AB}C_t$ and $z = \sin\theta_1$ with the sphere. Consequently, the coordinates of P fulfil the equations: $x^2 + y^2 + z^2 = 1$; $z = \sin\theta_1$; $-\frac{1}{15}x\sqrt{15\left(-2\sqrt{5}+5\right)} - \frac{1}{30}y\sqrt{30\left(\sqrt{5}+5\right)} + \frac{1}{30}z\sqrt{30\left(-\sqrt{5}+5\right)} = 0$; leading to $\frac{1}{2}\sin{\theta_1}^2\left(-\sqrt{5}+5\right) + \frac{1}{2}x^2\left(-3\sqrt{5}+9\right) + \sin\theta_1 x\left(-2\sqrt{5}+4\right) - 1 = 0$, which mean that $\theta 1 \in \left[-\frac{1}{2}\arccos\left(\frac{\sqrt{5}-10}{15}\right), \frac{1}{2}\arccos\left(\frac{\sqrt{5}-10}{15}\right)\right]$.

Having in account the definition of $\hat{X}_{\theta 2}$, we may conclude that its coordinates are:

$$\frac{-\sqrt{2}\sqrt{\left(\sqrt{5}-3\right)\left(4\sin^2(\theta 2)-3\right)}-2\sqrt{5}\sin(\theta 2)+4\sin(\theta 2)}{3\left(\sqrt{5}-3\right)};$$

$$\frac{-\sqrt{2}\sqrt{\left(\sqrt{5}-3\right)\left(4\sin^2(\theta 2)-3\right)}+\sqrt{5}\sin(\theta 2)+\sin(\theta 2)}{6};$$

and $\sin(\theta 2)$, respectively.

Accordingly, $(\cos(\theta 1)\cos(-\theta 2), \cos(\theta 1)\sin(-\theta 2), \sin(\theta 1))$ was the coordinates of point P, that is one of the vertices of the generated tiling.

IV. From $\mathscr{C}$ to the $\mathfrak{P}^*_{(\mathscr{C},\theta 1,\theta 2)}$

Let us consider the set of the following eighth spherical rotations:

$$\mathscr{I} = \left\{ \left(\mathscr{R}_{(Ct,k\frac{2\pi}{5})}\right)_{k\in\{1,\ldots,4\}}, \mathscr{R}_{(M_{AB},\pi)}, \mathscr{R}_{(A,\frac{4\pi}{3})}, \mathscr{R}_{(A_2,\frac{2\pi}{3})}, \mathscr{R}_{(C,\frac{2\pi}{3})} \right\},$$

where:

$$A_2 = \mathscr{R}_{(A,\frac{2\pi}{5})}\left(\mathscr{R}_{(M_{AB},\pi)}(Ct)\right) = \left(\frac{\sqrt{3}}{3}, -\frac{\sqrt{3}}{3}, -\frac{\sqrt{3}}{3}\right).$$

vspace0.2cmnoindent The matricial representation of the elements of $\mathscr{I}$ are:

$$\mathscr{R}_{(Ct,\frac{2\pi}{5})} = \begin{pmatrix} \frac{\sqrt{5}+1}{4} & -\frac{1}{2} & \frac{\sqrt{5}-1}{4} \\ \frac{1}{2} & \frac{\sqrt{5}-1}{4} & \frac{-\sqrt{5}-1}{4} \\ \frac{\sqrt{5}-1}{4} & \frac{\sqrt{5}+1}{4} & \frac{1}{2} \end{pmatrix};$$

$$\mathscr{R}_{(Ct,\frac{4\pi}{5})} = \begin{pmatrix} \frac{1}{2} & \frac{-\sqrt{5}+1}{4} & \frac{\sqrt{5}+1}{4} \\ \frac{\sqrt{5}-1}{4} & \frac{-\sqrt{5}-1}{4} & -\frac{1}{2} \\ \frac{\sqrt{5}+1}{4} & \frac{1}{2} & \frac{-\sqrt{5}+1}{4} \end{pmatrix};$$

$$\mathscr{R}_{(Ct,\frac{6\pi}{5})} = \begin{pmatrix} \frac{1}{2} & \frac{\sqrt{5}-1}{4} & \frac{\sqrt{5}+1}{4} \\ \frac{-\sqrt{5}+1}{4} & \frac{-\sqrt{5}-1}{4} & \frac{1}{2} \\ \frac{\sqrt{5}+1}{4} & -\frac{1}{2} & \frac{-\sqrt{5}+1}{4} \end{pmatrix};$$

$$\mathscr{R}_{(Ct,\frac{8\pi}{5})} = \begin{pmatrix} \frac{\sqrt{5}+1}{4} & \frac{1}{2} & \frac{\sqrt{5}-1}{4} \\ -\frac{1}{2} & \frac{\sqrt{5}-1}{4} & \frac{\sqrt{5}+1}{4} \\ \frac{\sqrt{5}-1}{4} & \frac{-\sqrt{5}-1}{4} & \frac{1}{2} \end{pmatrix};$$

$$\mathscr{R}_{(A,\frac{4\pi}{3})} = \begin{pmatrix} \frac{\sqrt{5}+1}{4} & \frac{-\sqrt{5}-3}{4} & \frac{\sqrt{5}+1}{4} \\ \frac{-\sqrt{5}-3}{4} & \frac{\sqrt{5}+1}{4} & \frac{\sqrt{5}+1}{4} \\ \frac{-\sqrt{5}-1}{4} & \frac{-\sqrt{5}-1}{4} & -\frac{1}{2} \end{pmatrix};$$

$$\mathscr{R}_{(M_{AB},\pi)} = \begin{pmatrix} 1 & 0 & 0 \\ 0 & -1 & 0 \\ 0 & 0 & -1 \end{pmatrix};$$

$$\mathscr{R}_{(A_2,\frac{2\pi}{3})} = \begin{pmatrix} 0 & 1 & 0 \\ 0 & 0 & -1 \\ -1 & 0 & 0 \end{pmatrix};$$

$$\mathscr{R}_{(C,\frac{2\pi}{3})} = \begin{pmatrix} 0 & 0 & 1 \\ 1 & 0 & 0 \\ 0 & 1 & 0 \end{pmatrix}.$$

Consider:

$\mathscr{C}^0 = \mathscr{C}$ (graphically represented in figure 3(b)),

$\mathscr{C}^1 = \bigcup_{i=1}^{4} \mathscr{R}_{(Ct,i\frac{2\pi}{5})}(\mathscr{C}^0)$,

$\mathscr{C}^2 = \mathscr{R}_{(M_{AB},\pi)}(\mathscr{C}^1)$,

$\mathscr{C}^3 = \mathscr{R}_{(A,\frac{4\pi}{3})}(\mathscr{C}^2)$,

$\mathscr{C}^4 = \mathscr{R}_{(A_2,\frac{2\pi}{3})}(\mathscr{C}^3)$,

$\mathscr{C}^5 = \mathscr{R}_{(C,\frac{2\pi}{3})}(\bigcup_{i=1}^{4}\mathscr{C}^i)$ and
$\mathscr{C}^6 = \mathscr{R}_{(C,\frac{2\pi}{3})}(\mathscr{C}^5)$.

Under these conditions the set $\bigcup_{i=0}^{6}\mathscr{C}^i$ define the spherical class of tilings $\mathfrak{P}^*_{(\mathscr{C},\theta 1,\theta 2)}$.

Besides each tile has internal angles of the form $(\frac{2\pi}{3}, *i, \frac{2\pi}{5}, *i, *i)$, where the $*i$, $i \in \{1,2,3\}$, are uniquely determined for each value of $\theta 1, \theta 2$.

The pentagonal tilings in $\mathfrak{P}^*_{(\mathscr{C},\theta 1,\theta 2)}$ are composed by sixty pentagonal congruent tiles, and so the sum of the internal angles of each tile is $\frac{13\pi}{5}$.

Thus, given the coordinates of the points A, P, M_{AB} and Ct, we may compute the angle measure defined by them:

$$\begin{aligned}\cos\left(\widehat{APM_{AB}}\right) = {} & \frac{1}{12}\left(\sin(\theta 1+\theta 2)-\sin(\theta 1-\theta 2)\right)\\ & \left(\left(\cos(\theta 1)\cos(\theta 2)\left(-\sqrt{3}+\sqrt{15}\right)\right.\right.\\ & \left.+\cos(\theta 1)\sin(\theta 2)\left(-\sqrt{3}-\sqrt{15}\right)\right)\\ & +\frac{1}{6}\sin^2(\theta 1)\left(-\sqrt{3}-\sqrt{15}\right);\end{aligned}$$

$$\begin{aligned}\cos\left(\widehat{M_{AB}PC_t}\right) = {} & -\frac{1}{10}\cos(\theta 1)^2\sin(\theta 2)^2\sqrt{10\left(\sqrt{5}+5\right)}\\ & -\frac{1}{10}\sin(\theta 1)^2\sqrt{10\left(\sqrt{5}+5\right)}\\ & +\cos(\theta 1)\cos(\theta 2)\sin(\theta 1)\frac{1}{10}\sqrt{10\left(-\sqrt{5}+5\right)};\end{aligned}$$

$$\begin{aligned}\cos\left(\widehat{C_tPA}\right) = {} & -\frac{1}{15}\cos(\theta 1)^2\sin(\theta 2)^2\sqrt{15\left(2\sqrt{5}+5\right)}\\ & -\frac{1}{15}\sin(\theta 1)^2\sqrt{15\left(2\sqrt{5}+5\right)}+\cos(\theta 1)\cos(\theta 2)\sin(\theta 1)\times\\ & \frac{1}{30}\sqrt{30\left(\sqrt{5}+5\right)}+\cos(\theta 1)\sin(\theta 1)\sin(\theta 2)\times\\ & \frac{1}{15}\sqrt{15\left(-2\sqrt{5}+5\right)}+\cos(\theta 1)^2\cos(\theta 2)\sin(\theta 2)\times\\ & \frac{1}{30}\sqrt{30\left(-\sqrt{5}+5\right)},\end{aligned}$$

and so all the internal angle measure of the tile are known.

The dynamic process described above allow us to characterise all the elements of the family $\mathfrak{P}^*_{(\mathscr{C},\theta 1,\theta 2)}$. First, we note that there are elements in this family which do not correspond to pentagonal spherical tilings. In fact, only angles, $\theta 1$ and $\theta 2$, taken in the interior of their admissibility intervals correspond to pentagonal monohedral tilings, being these composed by sixty spherical tiles (as we can see one example in Fig. 3(a)). The remaining cases correspond to monohedral spherical tilings by triangles and quadrilaterals.

The elements of $\mathfrak{P}^*_{(\mathscr{C},\theta 1,\theta 2)}$ with $\theta 1 \in]0,l_1[$ and $\theta 2 \in]0,l_2[$ belong to a family of a two parameter not yet described in the literature.

Any element of this family is composed by sixty 60 spherical pentagons, with 150 edges and 92 vertices, 12 of them of valence 5 and the others 80 vertices of valence 3, and have the tile configuration $y.y.r.r.(2b)$.

The process here described can be applied generate spherical tilings supported in the others regular spherical tilings, i.e, tetrahedral, $\mathscr{T}$; hexahedral, $\mathscr{H}$; octahedral, $\mathscr{O}$; and icosahedral, $\mathscr{I}$.

We get three monohedral spherical tilings by pentagon, $\mathfrak{P}^*_{(\mathscr{C}_\mathscr{K},\theta_1^\mathscr{K},\theta_2^\mathscr{K})}$ where $\mathscr{K} \in \{\mathscr{T},\mathscr{H},\mathscr{O},\mathscr{I}\}$. For each $\mathscr{C}_\mathscr{K}$, we proceed changing the gluing rules of the edge-tiles according a local action of particular subgroups of spherical isometries related with the corresponding regular $\mathscr{K}$ spherical tiling. It should be note that: $\mathfrak{P}^*_{(\mathscr{C}_\mathscr{D},\theta_1^\mathscr{D},\theta_2^\mathscr{D})}$ and $\mathfrak{P}^*_{(\mathscr{I}_\mathscr{I},\theta_1^\mathscr{I},\theta_2^\mathscr{I})}$ defines the same families of tilings; $\mathfrak{P}^*_{(\mathscr{C}_\mathscr{H},\theta_1^\mathscr{H},\theta_2^\mathscr{H})}$ and $\mathfrak{P}^*_{(\mathscr{C}_\mathscr{O},\theta_1^\mathscr{O},\theta_2^\mathscr{O})}$ defines the same families of tilings .

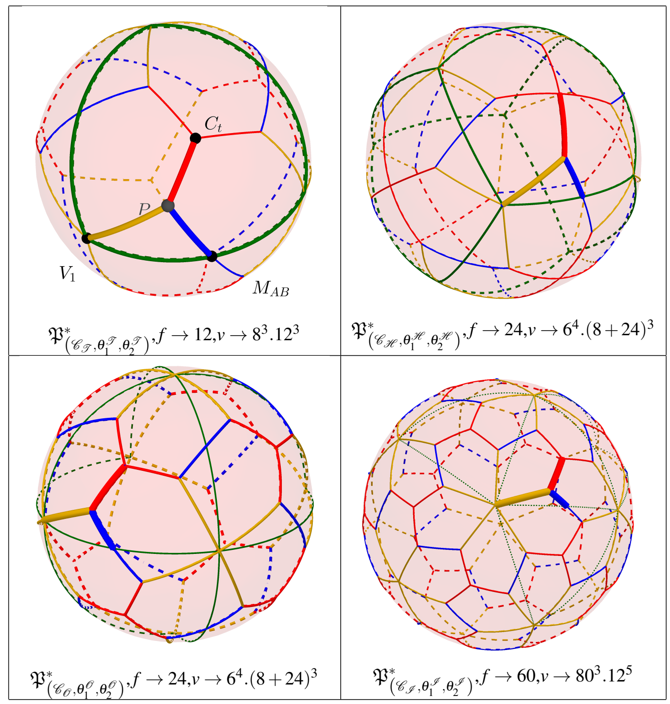

Figure 5: Elements of $\mathfrak{P}^*_{(\mathscr{C}_\mathscr{K},\theta_1^\mathscr{K},\theta_2^\mathscr{K})}, \mathscr{K} \in \{\mathscr{T},\mathscr{H},\mathscr{O},\mathscr{I}\}$.

These procedures led to the characterisation of three class of monohedral pentagonal spherical tilings, where all the tilings have the tile configuration $y.y.r.r.(2b)$, whose some geometrical and combinatorial characterisation are specified in figure 5.

V. Conclusion

Here, we have shown how a suitable adaptation of a procedure for generating spherical tilings starting from a cell, composed by three spherical arcs, and described in previous work, with support in the regular dodecahedral spherical tiling, led to a two parameter family of pentagonal monohedral tiling of the sphere with sixty faces. This approach was possible by mean of computational tools. We also show some of the results of the adaptation of the procedure here described in order to present all the monohedral pentagonal tiling with the tile configuration $y.y.r.r.(2b)$. Next step will be the detailed description of these new pentagonal tilings.

This work highlights the potential of the geometric approach supported by a dynamic geometry software for the search and analysis of spherical tilings, revealing connections that a combinatorial approach would not have.

ACKNOWLEDGMENT

This research was supported by the Portuguese national funding agency for science, research and technology (FCT), within the Center for Research and Development in Mathematics and Applications (CIDMA), project UID/MAT/04106/2019.

REFERENCES

[1] Ana M. R. Azevedo Breda. A class of tilings of s^2. *Geometriae Dedicata*, 44(3):241–253, Dec 1992.

[2] Carlos Beltrán. A facility location formulation for stable polynomials and elliptic fekete points. *Foundations of Computational Mathematics*, 15(1):125–157, 2015.

[3] Johann S Brauchart and Peter J Grabner. Distributing many points on spheres: minimal energy and designs. *Journal of Complexity*, 31(3):293–326, 2015.

[4] Ana Maria D'Azevedo Breda and José Manuel Dos Santos Dos Santos. New classes of monohedral spherical tilings by non-convex spherical hexagons and non-convex spherical pentagons with geogebra. In Gordon Lee and Ying Jin, editors, *Proceedings of 34th International Conference on Computers and Their Applications*, volume 58 of *EPiC Series in Computing*, pages 75–82. EasyChair, 2019.

[5] Ana M d'Azevedo Breda and José M Dos Santos Dos Santos. Spherical geometry and spherical tilings with geogebra. *Journal for Geometry and Graphics*, 22(2):283–299, 2018.

[6] Ana M d'Azevedo Breda and José M Dos Santos Dos Santos. Spherical tiling with geogebra - new results, challenges and open problems. 2019in press.

[7] Ana M d'Azevedo Breda and José M Dos Santos Dos Santos. A new class of monohedral pentagonal spherical tilings with geogebra. *Portugaliae Mathematica*, 74(3):257–266, 2018.

[8] Bart De Nijs, Simone Dussi, Frank Smallenburg, Johannes D Meeldijk, Dirk J Groenendijk, Laura Filion, Arnout Imhof, Alfons Van Blaaderen, and Marjolein Dijkstra. Entropy-driven formation of large icosahedral colloidal clusters by spherical confinement. *Nature materials*, 14(1):56, 2015.

[9] Sander Dedoncker, Laurens Coox, Florian Maurin, Francesco Greco, and Wim Desmet. Bézier tilings of the sphere and their applications in benchmarking multipatch isogeometric methods. *Computer Methods in Applied Mechanics and Engineering*, 332:255 – 279, 2018.

[10] Michel Deza, Patrick W Fowler, A Rassat, and Kevin M Rogers. Fullerenes as tilings of surfaces. *Journal of chemical information and computer sciences*, 40(3):550–558, 2000.

[11] Mircea V Diudea and Csaba L Nagy. *Periodic nanostructures*, volume 7. Springer Science & Business Media, 2007.

[12] Honghao Gao, Nan Shi, and Min Yan. Spherical tiling by 12 congruent pentagons. *Journal of Combinatorial Theory, Series A*, 120(4):744 – 776, 2013.

[13] Branko Grünbaum and Geoffrey Colin Shephard. *Tilings and patterns*. Freeman, New York, 1987.

[14] Giuliana Indelicato, Newton Wahome, Philippe Ringler, Shirley A. Müller, Mu-Ping Nieh, Peter Burkhard, and Reidun Twarock. Principles governing the self-assembly of coiled-coil protein nanoparticles. *Biophysical Journal*, 110(3):646 – 660, 2016.

[15] Walter Kohn. An essay on condensed matter physics in the twentieth century. *Reviews of Modern Physics*, 71(2):S59, 1999.

[16] Joachim König, Arielle Leitner, and Danny Neftin. Almost-regular dessins d'enfant on a torus and sphere. *Topology and its Applications*, 243:78 – 99, 2018.

[17] Majid Mosayebi, Deborah K. Shoemark, Jordan M. Fletcher, Richard B. Sessions, Noah Linden, Derek N. Woolfson, and Tanniemola B. Liverpool. Beyond icosahedral symmetry in packings of proteins in spherical shells. *Proceedings of the National Academy of Sciences*, 114(34):9014–9019, 2017.

[18] Manica Negahdaripour, Nasim Golkar, Nasim Hajighahramani, Sedigheh Kianpour, Navid Nezafat, and Younes Ghasemi. Harnessing self-assembled peptide nanoparticles in epitope vaccine design. *Biotechnology Advances*, 35(5):575 – 596, 2017.

[19] Ali Asghar Rezaei. Polygonal tiling of some surfaces containing fullerene molecules. *Iranian Journal of Mathematical Chemistry*, 5(2):99–105, 2014.

[20] Ali Asghar Rezaei. Tiling fullerene surface with heptagon and octagon. *Fullerenes, Nanotubes and Carbon Nanostructures*, 23(12):1033–1036, 2015.

[21] Yuan-Zhi Tan, Rui-Ting Chen, Zhao-Jiang Liao, Jia Li, Feng Zhu, Xin Lu, Su-Yuan Xie, Jun Li, Rong-Bin Huang, and Lan-Sun Zheng. Carbon arc production of heptagon-containing fullerene [68]. *Nature communications*, 2:ncomms1431, 2011.

[22] Yukako Ueno and Yoshio Agaoka. Tilings of the 2-dimensional sphere by congruent right triangles. *Memoirs of the Faculty of Integrated Arts and Sciences, Hiroshima University. IV, Science reports: studies of fundamental and environmental sciences*, 22:1–23, 1996.

[23] Yukako Ueno, Yoshio Agaoka, et al. Classification of tilings of the 2-dimensional sphere by congruent triangles. *Hiroshima Mathematical Journal*, 32(3):463–540, 2002.

[24] Zhi Wang, Hai-Feng Su, Yuan-Zhi Tan, Stan Schein, Shui-Chao Lin, Wei Liu, Shu-Ao Wang, Wen-Guang Wang, Chen-Ho Tung, Di Sun, et al. Assembly of silver trigons into a buckyball-like ag180 nanocage. *Proceedings of the National Academy of Sciences*, 114(46):12132–12137, 2017.

Road map for Bifurcations of Real Rational maps

João Cabral
CIMA - Research Centre for Mathematics and Applications
Faculty of Science and Technology - University of Azores
Ponta Delgada, Portugal
joao.mg.cabral@uac.pt

***Abstract*—With the help of a proper parameter space $P_{a,b}$, defined for the class of real rational maps (1), in this work, we define lines in the form $b = \varphi(a)$, that will be used as roads in a traffic map, which will contribute to a better understanding of their behaviour, under iteration. This family of maps have a very interesting dynamic, where we can confirm the existence of several bifurcation types. Using tools, from Combinatorial Dynamics, Entropy and Bifurcation Analysis, with common use in Low Dimension Dynamical Systems studies, it is shown that these roads clearly depend on the relationship between variables a and b, highlighting some important aspects of this relationship, which help to describe the dynamics of map (1).**

$$f_{a,b}(x) = 1 + \frac{b-a}{x^2-b}, \quad b < a, \quad b < 1 \tag{1}$$

***Index Terms*—Real Rational Maps, Iteration, Bifurcation**

I. Introduction

Discrete time dynamical systems generated by iterated maps appear in many scientific areas, such as economics, engineering, and ecology. To understand better the behaviour of these systems is used, frequently, some results derived from bifurcation analysis, establishing some order in chaotic events, classifying possible behaviours, whose may explain computational simulation results, with different values of control parameters.

The notion of iterated function system was introduced by M. F. Barnsley and S. Demko, in 1985, but the concept is usually attributed to Joan P. Hutchinson. According Edward R. Vrscay the idea is traced further back to the works of Leggett and Williams, who studied fixed points of contractive maps finite composition. Iterated function systems are interacting with many fields of mathematics. For example, they are useful for creating fractals, learning models, interesting probability distributions and analysing stochastic processes with Markovian properties.

In this paper it will be presented some numerical and geometrical results, supported by high and extensive analytical calculus, but not fully shown in this paper, due to size and complexity usually found in real rational maps, under iteration.

Let $f^n_{a,b}(x)$ be the $n-iterate$ of $f_{a,b}$, *i. e.*, the map composition, by itself, $n-times$. The sequence

$$\{x_i\}_{i=0,1,...,n} = \{x_0, x_1, ..., x_n\}$$

is the orbit of x_0, under iteration by $f_{a,b}$. It means that $x_{i+1} = f_{a,b}(x_i)$, $i = 0, 1, \ldots, n$. Each solution $x = \xi$ of $f^n_{a,b}(x) = x$, using fixed parameters $a = a_0$ and $b = b_0$, is designated fixed point of order n for f_{a_0,b_0}. These values, under iteration by f_{a_0,b_0}, are invariant. They can be classified as attractors if $|f'_{a,b}(\xi)| < 1$, repulsors if $|f'_{a,b}(\xi)| > 1$ and neutral if $|f'_{a,b}(\xi)| = 1$. The solution set of $f'_{a,b}(x) = 0$ is the critical set of $f_{a,b}$, where we will include the values $x = \pm\infty$. In this family of maps (1), by a simple graphic observation, we can see that $\lim\limits_{x\to\pm\infty} f_{a,b}(x) = 1$. So, under iteration of $f_{a,b}$, the values present in some neighbourhood of infinite, have the same behaviour of the value $x = 1$, under iteration. It is now obvious that the singularities of $f_{a,b}$, $x = \pm\sqrt{b}$, under iteration, will have also the same behaviour of the value $x = 1$, since $f_{a,b}(\pm\sqrt{b}) = \infty \Leftrightarrow f_{a,b}(f_{a,b}(\pm\sqrt{b})) = f_{a,b}(\infty) = 1$, so we will use the orbit $x = 1$ to represent the orbit of $x = \pm\infty$ and $x = \pm\sqrt{b}$. If, by any chance, the orbit of $x = 1$ would be periodic then we say that the orbits of $\pm\infty$ and $\pm\sqrt{b}$ are eventually periodic.

In classical low-dimension dynamics, as the study of *m*-modal maps under iteration, classified as interval maps [1] and [4], the analysis of critical orbit set is enough to have a full description of the map dynamics [4]. And the most important orbits, in continuous maps, are the ones with period 3, due to its connection to Sharkovsky's theorem, as shown very deeply in chapter 2 of [1].

Since our map (1) is discontinuous, and real, in the last decades small attempts where made to develop some consistent theory similar to the one developed to continuous interval maps in [4], but so far with no any relevant progress. We have excellent contributions from James Yorke [5] and Laura Gardini [6], among others referenced by these authors, attempts to minimize the damage caused by the presence of singular values, but the full description of the real rational maps dynamics is a stronghold very hard to conquer, even with the use of emerging computational tools of 21st century allied to the newest analytic tools. But one idea is clear, if we cannot deal very well with the singularities, at least we can use the continuous part of the function and make some restrictions to the dynamical domain and compare the findings, building a Scottish quilt of knowledge that can be close to that should be the full dynamical description of the real rational map.

Since $f'_{a,b}(x) = 0 \Leftrightarrow x = 0$ and $\lim\limits_{x\to\pm\infty} f'_{a,b}(x) = 0$ then the critical set of $f_{a,b}$ will be $\Lambda = \{0, \infty\}$. Assuming that

This paper was produced with support from the Portuguese Foundation for Science and Technology, project UID/MAT/04674/2019.

the critical orbits are the ones produced by the critical values, and following the road of discovery like Milnor and Thurston did in [4], for continuous maps, then we will try to reveal the dynamical secrets of this class of maps $f_{a,b}$. To do that we used some computational work, and construct the proper analytical tools to prove some results. Numerically, we create a process to identify regions in $P_{a,b}$, defined as the parameter space for $f_{a,b}$, where, for some fixed $a = a_0$ and $b = b_0$ we can find periodic orbits for $x = 0$ and $x = 1$. To do an organized search we will study the map's behaviour following the lines $b = \varphi(a)$, the paths or roads, with $a \in I$ (see section III). We define the set $\Sigma = \{(a, b) \in I : f^n_{a,b}(0) = 0 \vee f^n_{a,b}(1) = 1, n \in \mathbb{N}\}$, where to any fixed pair $(a, b) = (a_0, b_0)$, we can find roads in the parameter set $P_{a,b}$, such the map f_{a_0,b_0} will have periodic super-stable orbits, under iteration. Since we will work, mostly, with the geometric view of the orbits, it is usual to call them trajectories.
Studying the geometry of $P_{a,b}$ and Σ, it is our goal to show that $f_{a,b}$, as a piecewise differentiable map, presents some behaviour similar to the one exhibited by bi-modal and one-modal class of maps studied by Milnor and Thurston [4], among so many other authors, that followed their work. To fulfil the goal, we use techniques derived from combinatorial dynamics, such as Bifurcation Analysis, Entropy Study and Interpretation of Lyapunov Exponents value [3], to study the relation between periodic orbits and the behaviour of map (1) under iteration.

II. Lyapunov and Bifurcation Theory

Chaotic behaviours are characterized by a high sensitivity to initial conditions: Starting from arbitrarily close to each other, the trajectories rapidly diverge.
The map (1) is discontinuous, then the results, already known for continuous maps, cannot be applied to this map's family, but we can use some of them as a start point to understand its dynamics. One of these tools are the Lyapunov Exponents, integrated in a very large field of research known as Lyapunov Theory. The connection between this Theory and the study of the dynamics of real maps is, undoubtedly, very important, since help to understand the connection between analytic results and computational. The power of Lyapunov Theory comes from the fact that it is used to make conclusions about the dynamics of a system, without finding exactly the values of the trajectories, saving computational time and endless analytic efforts. Young [7] and Katok [3] have a splendid description of use and properties of Lyapunov exponents.
For a function $f(x)$, each trajectory $\{x_i\}$ have the Lyapunov Exponent defined as

$$\lambda = \lim_{n\to\infty} \frac{1}{n} \sum_{i=0}^{n-1} ln \left| f^{'}(x_i) \right| \tag{2}$$

Since λ is the same for all x_i on the basin of attraction of ξ, if ξ is an attractor, the sign of λ defines the attractor type. If $\lambda < 0$ we are in the presence of limit cycle or stable fixed points; If $\lambda > 0$ we have chaotic attractors. For bifurcation values of the function, we will have $\lambda = 0$, and $\lambda \to \infty$ for values where $f(x)$ have super stable orbits. Lyapunov Exponent are also used to calculate an estimative to the Topological Entropy, from which we can obtained detailed information about the orbit behaviour. See [7] for a more complete description.
The bifurcation of a function is characterized as being a splitting of a specific orbit, occurring with the modification of a parameter that controls the function. For example, for $f_\lambda(x) = \lambda x(1 - x)$, with the change of parameter λ, we will assist to a double period bifurcation, with periodic orbit $n = 2$ splitting to $n = 4$, then goes $n = 8$, and so on. But it can occur also the splitting from $n = 1$ to $n = 3$, then $n = 7$, and so on, like the maps studied by Laura Gardini in [6].
The map (1) have parameters a and b, and for certain values of the pair (a, b), the structure of fixed points and periodic orbits changes. In the same way as the maps with only parameter, we define this change as a bifurcation. The graphic, where we can analyse, geometrically, the period variations regarding the parameter change is called Bifurcation Diagram. To build the bifurcation diagram of (1) we need to make $b = \varphi(a)$, in order to transform $f_{a,b}$ in a function of one parameter only. There are many types of bifurcations present in a simple bifurcation diagram for $f_{a,\varphi(a)}$, and we will explore it in section (IV), as we can see, for example, in figure 4. We can find *saddle-node bifurcations*, occurring when a pair of fixed points appears in a region where there were none, with one stable fixed point and one unstable fixed point; *period-doubling bifurcation*, characterized by the loss of stability of the original fixed point, the period doubles, and the nature of attractor changes; *border-collision bifurcations*, as described in detail by Helena E. Nusse and James Yorke in [5] and complemented by Roya Makrooni, Farhad Khellat and Laura Gardini in [6] is mainly characterized by a suddenly change of one fixed point attractor in a *m-piece* chaotic attractor. Also, we can find the reverse bifurcation phenomena.

III. Parameter space $P_{a,b}$ for $f_{a,b}(0)$.

To study the behaviour, under iteration, of the map (1) we need some simple results about the variables domain, in order to build a parameter space where we will get useful information. In [2], we can found complementary data about the map (1).
We establish the domain for the parameters a and b as the set

$$I = \left\{ (a, b) \in \mathbb{R}^2 : 1 - \frac{2\sqrt{3}}{9} < a < 1 + \frac{2\sqrt{3}}{9}, b < a, b < 1 \right\}.$$

As we can check in [4], due to the Sharkovskii theorem, the orbits of period $n = 3$, of the critical points, assumes in the dynamics of a continuous map a very important role, since their existence in continuous maps assures the existence of all others orbits. So, will use, as reference, the period 3 orbit of the critical values $x = 0$ and $x = 1$.
As explained before, whenever a value, under iteration, falls in a neighbourhood of some $f_{a,b}$ discontinuity, the forward image will be ∞, and the next iteration will be trapped in the

orbit of $x = 1$. For our map (1), the lines $b = \varphi(a)$, where this phenomena occurs, will play an important role in the function dynamics, since the computational calculus will tend to be unstable near these lines. Solving the equation $f^3_{a,b}(1) = 1$, we will have two possible lines: $b = a$, that reduces the map to a trivial one, and

$$b = \frac{1}{3}\left(2 - \left(\frac{2}{\omega}\right)^{1/3} - \left(\frac{\omega}{2}\right)^{1/3}\right),$$

with $\omega = -25+54a-27a^2+\sqrt{-4+(-25+54a-27a^2)^2}$. For $4+(25-54a+27a^2)^2 = 0$, will have $a = \frac{1}{9}\left(9 \pm 2\sqrt{3}\right)$. These values are the ones used to set the range for a in I.
We define the parameter space

$$P_{a,b} = \{(a,b) \in I : f^n_{a,b}(x) = x, n = 3, 4, \ldots\},$$

represented in figure 1.

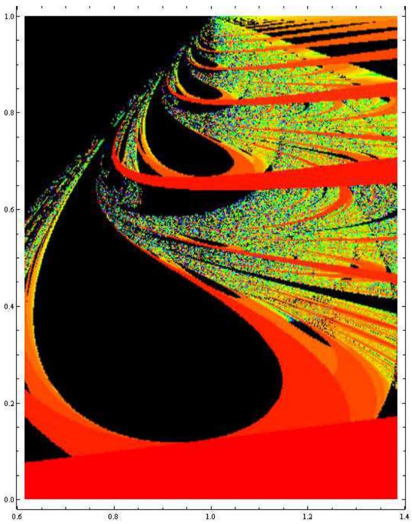

Fig. 1. Parameter space $P_{a,b}$ with $n < 120$ for $f^n_{a,b}(x)$.

It appears to have fractal properties, since we can see a process of self-similarity. Each one of the big black regions, after excluding the upper-left black region where $b > a$, are sets, designated by *n*-Bulbs in [2], geometric neighbourhoods of all solutions lines $b = \varphi(a)$ of the equation $f^n_{a,b}(0) = 0$, which each pair (a, b) produces maps with critical super-stable orbits with period n.
We can, in $P_{a,b}$, identify important lines, see figure 2, where the solution line $b = \varphi(a)$ of $f^3_{a,b}(0) = 0$ is coloured in white; the solution of $f^3_{a,b}(0) = -\sqrt{b}$ in yellow; the solution of $f^3_{a,b}(0) = \sqrt{b}$ in green and the solution of $f^3_{a,b}(1) = 1$ in blue.

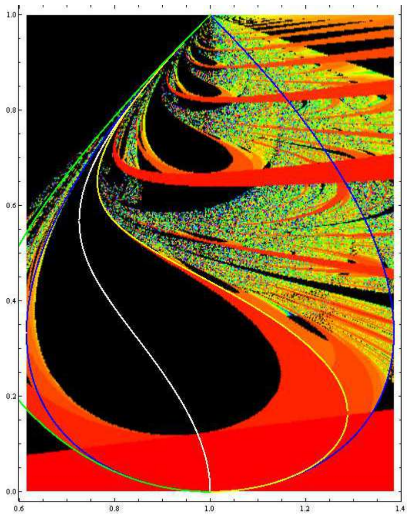

Fig. 2. Relation between $P_{a,b}$ and the lines $b = \varphi(a)$ in $f^3_{a,b}(p_1) = p_2$, with $p_1, p_2 \in \{0,\ 1,\ \pm\sqrt{b}\}$

Definition 1. *Let the solution line $b = \varphi(a)$ of the equation $f^3_{a,b}(1) = 1$, such that all the points are included in I. This line is the border of a region that we will define as the locus L_f.*

L_f will help us to understand the diagrams in the next section.

IV. Bifurcations Exploration

Now, we will transform our map (1) in one parameter map.

Let $b = \varphi(a)$, with $(a, b) = (a, \varphi(a)) \in P_{a,b}$ with $\varphi \in C^1$, then we will have

$$f_{a,\varphi(a)}(x) = f_a(x) = 1 + \frac{\varphi(a) - a}{x^2 - \varphi(a)} = \frac{x^2 - a}{x^2 - \varphi(a)} \qquad (3)$$

With this transformation we can start to explore the dynamics of (1) in the interior of L_f, analysing the bifurcation diagrams of the critical orbit $x = 0$. We choose in this paper to explore just the cases where φ is a straight line with positive slope.
We can see in figure 3 the line $b = \varphi(a) = -1.14723 + 2.09677a$, in cyan, crossing all the basins of attraction of the super stable lines, and analysing the correspondent f_a bifurcation diagram, figure 4, we can identify at least one value $a = 0.76$, where the orbit of the critical point $x = 0$ will produce a periodic $n = 3$ super stable orbit.

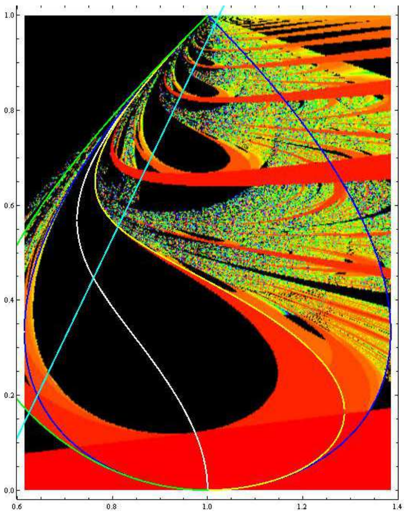

Fig. 3. Example line $b = -1.14723 + 2.09677a$

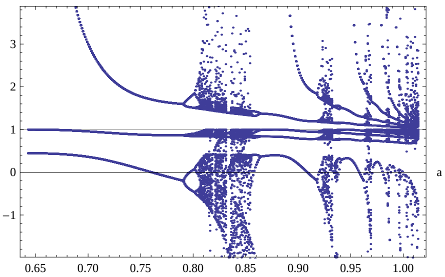

Fig. 4. f_a bifurcation diagram, $\varphi(a) = -1.147{+}2.096a$, $0.57 < a < 1.43$

Also we can observe intervals of stability for f_a and others where chaos prevail. For certain intervals of the value a we can identify phenomena like reverse bifurcations, double period bifurcations and, hidden among chaos windows, saddle-node bifurcations. Using Lyapunov Exponent diagram, figure 5 we can calculate the maximum value of topological entropy for $0.80 < a < 0.85$, that is, approximately $h = 0.409038$.

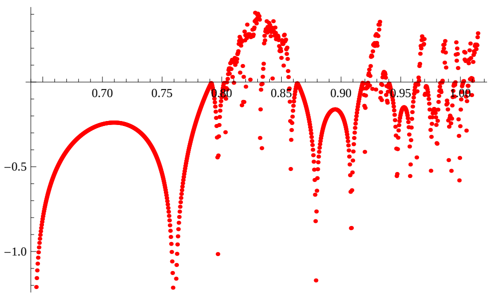

Fig. 5. f_a Lyapunov Exponents, $\varphi(a) = -1.147 + 2.096a$

The analysis of the bifurcation diagram is not sufficient to produce a deep study about the dynamics of function (3). Hidden, in intervals of supposed chaos, we can observe some regularity, like it happens in classic bifurcation diagrams for continuous maps. Also, to explore analytically the dynamics of f_a, it can be a very hard process due to the nature of rational maps iteration. Nowadays, most of the results, arising from the low dimension dynamics study, for real rational maps, are initial triggered by computational numeric calculus in association with a very deep knowledge of Implicit Theorem application. To avoid the analytic difficulties created by the conditions necessary to apply the Implicit Theorem, we show that the combined use of Lyapunov Exponent and Bifurcation diagrams, can be a great tool, providing a good initial approximation, on the search for intervals of chaos or regularity of f_a.
As an example, let $\varphi(a) = 0.02025 + 0.26625a$, the straight line in figure 6, and the bifurcation diagram in figure 7, that shows the behaviour of the orbit of $x = 0$, under iteration of f_a, with $0.57 < a < 1.43$.

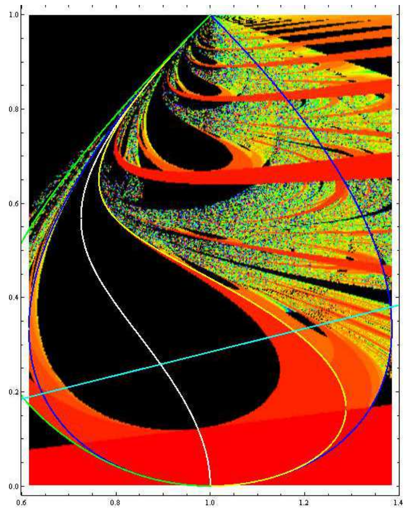

Fig. 6. $\varphi(a) = 0.02025 + 0.26625a$ crossing $P_{a,b}$

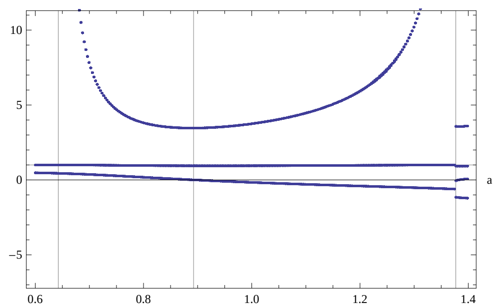

Fig. 7. Bifurcation diagram for f_a with $\varphi(a) = 0.02025 + 0.26625a$,and $0.57 < a < 1.43$

Close to the value $a = 0.8925$ we have a super stable orbit of the critical point and at $a = 1.377$ we have a border collision bifurcation. But what happens at $a = 0.6425$? Is it another border collision bifurcation? If yes, it is not so visible. Merging both diagrams, bifurcation an Lyapunov Exponent, we have the figure 8. As mentioned in section II, if $\lambda \to \infty$ then we have the presence of super stable orbit, and that is the case of $a = 0.6425$, and $a = 1.377$, where the orbit of the critical point $x = 0$ falls in an super stable orbit of the other critical point $x = \infty$. We can observe that these two values corresponds to the intersection of $\varphi(a)$ with the solution line of $f_a^3(1) = 1$. The only super stable orbit of $x = 0$ is at $a = 0.8925$, easily identified because it corresponds to the intersection of $\varphi(a)$, with the solution line of $f_a^3(0) = 0$, see figure 6. Also, in figure 8 we can see, for $1.2 < a < 1.3$, that we will have at least one value where $\lambda = 0$, revealing a region where we will find another bifurcation point, and it must be a period doubling or saddle-node bifurcation. So the points $a = 0.6425$ and $a = 1.377$ are border collision bifurcation points of $x = 0$, where the orbit undergoes in super stable orbit of $x = \infty$.

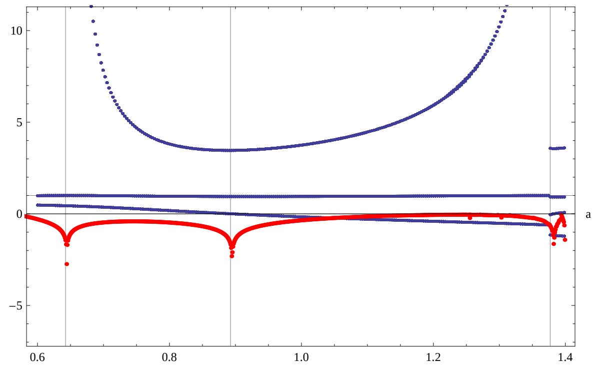

Fig. 8. Lyapunov Exponents (in red) and bifurcation diagram (in blue) for f_a with $\varphi(a) = 0.02025 + 0.26625a$, $0.57 < a < 1.43$, with vertical lines in the position where (2) assumes infinite values

Graphically, a border collision can be wrongly identified as a saddle-node bifurcation, but with the help of Lyapunov Exponents we can avoid this graphic confusion. Let's take another example, zooming $P_{a,b}$ to the region represented in figure 9.

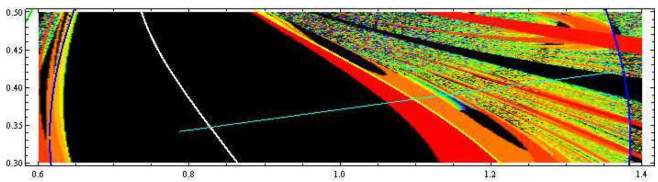

Fig. 9. Line $\varphi(a) = 0.23353 + 0.13721a$ crossing $P_{a,b}$

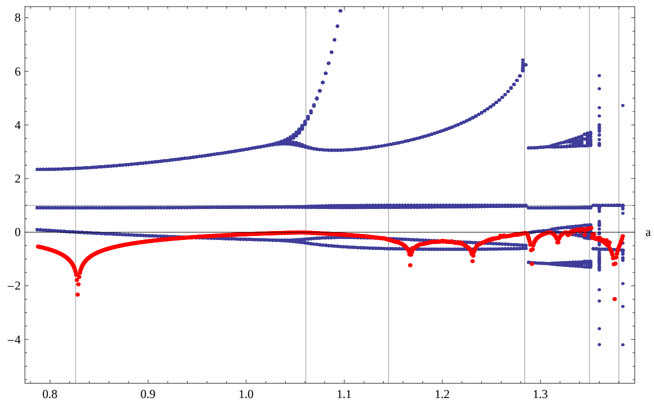

Fig. 10. Lyapunov Exponents (in red) and bifurcation diagram (in blue) for f_a with $b = 0.23353 + 0.13721a$, $0.786 < a < 1.3844$

Selecting $\varphi(a) = 0.23353 + 0.13721a$ we get a interesting f_a dynamic, as presented in figure 10. We have the presence of a super stable orbit, at $a = 0.826$, with $\lambda = \infty$, a double period bifurcation, at $a = 0.6425$, with $\lambda = 0$, and most important a bifurcation at $a = 1.284$, which at first glance, probably could be identified as a border collision bifurcation, but since $\lambda = 0$, at that position, then it must be a saddle node bifurcation, as also happens at $a = 1.35$, occurring the border collision bifurcation at $a = 1.38$.

V. Results

Using $P_{a,b}$ as a guide map, we can find the roads $b = \varphi(a)$, construct the bifurcation diagram, the Lyapunov Exponent diagram and write conclusions about the dynamic of map (1), related with the parameter a change. Clearly, the association between these two graphics is a powerful tool, allowing the researcher collect precious information, and since the hunt for some properties and new kind of bifurcations can be done, using numeric computational calculus, they can be the trigger for new ideas and a good start to initiate the analytic proof of the graphically observed phenomena.

As we show, in this work, only using the fundamentals of discrete dynamical systems, we can discover very easily, some special regions in $P_{a,b}$, where we can find, for f_a, well known behaviours, observed on the dynamics of continuous logistic maps and also in piecewise continuous *m*-modal maps, but also other behaviour not so common. We also remember that we focused our attention in L_f, and due to its fractal nature and self similarity it is easy to see that all the phenomena described graphically in last section for period 3 orbits also happens for all other periodic orbits.

Let's examine figure 11.

ISSN 2184-3945

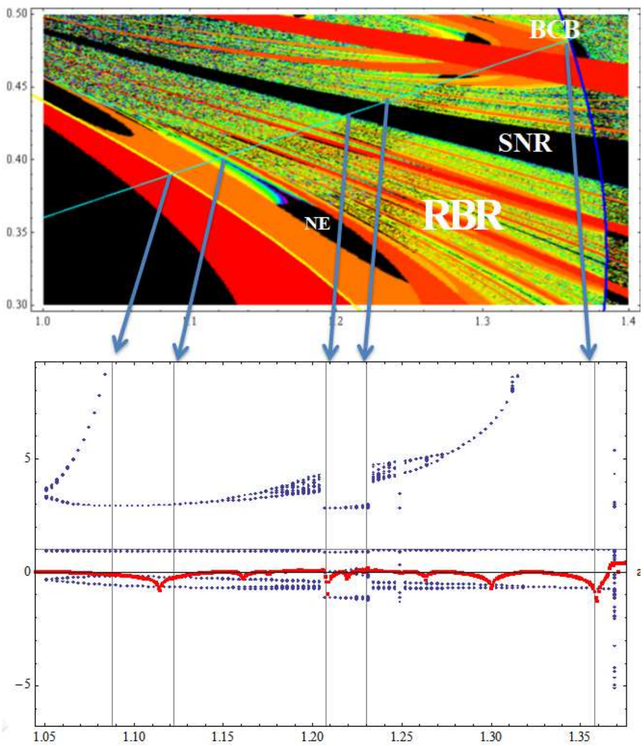

Fig. 11. Comparison between $P_{a,b}$ and the bifurcation and Lyapunov Exponents diagrams for the line $b = \varphi(a) = 0.0.01972 + 0.3404a$, with the presence of a reverse bifurcation with saddle node bifurcations at its centre.

We use $\varphi(a) = 0.01972 + 0.3404a$ and signalize the values $a \in \{1.088, 1.122, 1.2074, 1.2302, 1.3582\}$ with arrows. In 11 we enhance the region designated by **SNR**, in which borders the values a produce a saddle-node bifurcation. Indeed this kind of bifurcation will happen for $a = 1.2074$ and $a = 1.2302$. Also, we enhance the presence of a region designated by **RBR** where the values a on its south border will be the responsible for the appearance of a double period bifurcation, which one that goes in a reversion process inside of this region building a reverse bifurcation, until the north border when phenomena ends, entering region **SNR**. The BCB point, where the value a produces a Border Collision Bifurcation, is already signalized before and it is part of the solution line $f_a^3(1) = 1$. Another special region, designated by **NE**, is a region where the values at its south border starts a double period bifurcation, but at the north border, all the process reverts in a single point to a period order before doubling and then starts a reverse bifurcation process already inside **RBR**.
If we shift the line $\varphi(a)$, just enough to cross all 4 regions, we obtain an amazing representation of the dynamics of f_a, as represented in figure 12, and it is easy to identify the points where occur reverse bifurcation, saddle-node bifurcations and also border collision bifurcations.

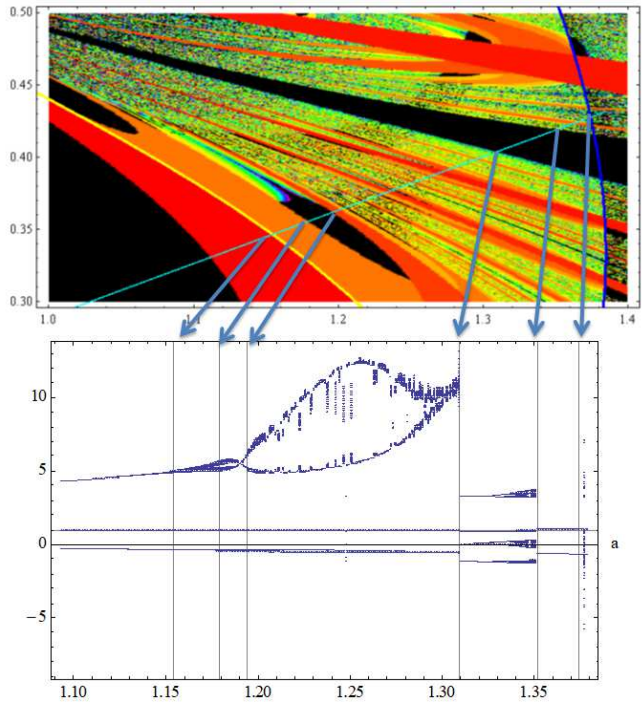

Fig. 12. Effects when the parameter a crosses the borders of regions NE, RBR and SNR, with a clear presence of a reverse bifurcation.

With the use of parameter space $P_{a,b}$ as a map to study the behaviour of family f_a, we encounter a fertile ground where can lead to discoveries related with the amazing properties of this family of maps, building proper roads. Further, with the adaptation and extension of some tools of piecewise continuous maps, the main goal is to prove that maps like $f_{a,b}$ exhibits a behaviour that resemble the one presented by the *m-modal* families.

References

[1] L. Alsedà and M. Misiurewicz, “Combinatorial Dynamics and Entropy in Dimension One,” Second Edition, Advanced Series in Nonlinear Dynamics, World Scientific, vol.5, 2000.
[2] J. Cabral and M. C. Martins, “Mapping Stability: Real Rational Maps of Degree Zero,”Applied Math. and Info. Sciences, 9(5), 2015, pp. 2265-2271.
[3] A. Katok, “Lyapunov exponents, entropy and periodic orbits for diffeomorphisms,” Publications Mathématiques de l’IHÉS 51, 1980, pp. 137-173.
[4] J. Milnor and W. Thurston, “On iterated maps of the interval,” Lec. Notes in Math, Springer-Verlag, 1988, pp. 465-563.
[5] H. E. Nusse and J. Yorke, “Border-collision bifurcations including ”period two to period three” for piecewise smooth systems,” Physica D: Nonlinear Phenomena , 57(1), 1992.
[6] R. Makrooni, F. Khellat and L. Gardini, “Border collision and fold bifurcations in a family of one-dimensional discontinuous piecewise smooth maps: unbounded chaotic sets,” Journal of Difference Equations and Applications, 21(8), 2015.
[7] L. Young, “Mathematical theory of Lyapunov exponents,” Journal of Physics A: Mathematical and Theoretical, 46(25), 2013.

Control of Invariants in Quasi-Polynomial Models

Alexander Fradkov
Lab.Control of Complex Systems
Institute for Problems of Mechanical Engineering
ITMO University
Saint Petersburg, Russia
a.fradkov@ieee.org

Irina Pchelkina
Dept. Robotics
Kaluga branch of Bauman Technical University
Kaluga, Russia
irinaashikhmina@gmail.com

Anatolii Tomchin
ITMO University
Saint Petersburg, Russia
ttomchin@yandex.ru

***Abstract*—An approach to control of invariant sets of quasi-polynomial systems in the presence and absence of bounded disturbances or bounded uncertainty in the model is proposed. The control strategy is based on introduction of an invariant functional for uncontrolled system and posing the control task as achieving the desired value of the invariant functional by means of control. The design is based on the reduction to the generalized Lotka-Volterra system and employing the speed-gradient control method.**

***Index Terms*—Invariants, nonlinear control, stability**

I. Introduction

Quasi-polynomial systems represent an important type of mathematical models because a wide class of smooth nonlinear systems can be represented in a quasi-polynomial form [1], [2]. In turn, quasi-polynomial systems can be reduced to generalized Lotka-Volterra form [3], [4] that is a well known model for description of multispecies populations [9]. Besides, other standard modeling forms of biological or biochemical interest, such as S-systems or mass-action systems, are naturally embedded into the generalized Lotka-Volterra form [3]. Generalized Lotka-Volterra model has been proved useful in the analysis and control of the systems described by a set of differential and algebraic equations. However most of existing results are related to stabilization of equilibrium points [2], [5], [6],

In a number of interesting applications the problem of control of invariants arises [10], [11], [12], [13]. A feature of control of invariants is in that the goal limit set is a manifold rather than a point. Therefore some set stability problems may arise. For a class of multispecies Lotka-Volterra systems a solution for an invariant control problem based on speed-gradient (SG)-method was proposed in [16].

In this paper an approach of [16] is extended to a class of quasi-polynomial systems. We present a control strategy that can improve stability and robustness of quasi-polynomial systems in the presence and absence of bounded disturbances or bounded uncertainty in the model. In this way, we introduce an invariant functional and pose the control task as achieving a desired value of the invariant functional.

Problem formulation is given in Section 2. Section 3 describes the control design. Section 4 and 5 provide formulations and proofs of the closed loop system properties in the absence and presence of bounded disturbances or bounded uncertainty in the model respectively.

II. Problem Formulation

A. Mathematical Model

Quasi-polynomial model is described by the following system of differential equations

$$\dot{y}_j = y_j \left(L_j + \sum_{i=1}^{m} A_{ji} \prod_{k=1}^{n} y_k^{B_{ik}} \right),\ j = 1, \dots, n, \qquad (1)$$

where $y \in int\left(R_+^n\right)$, $A \in R^{n\times m}$, $B \in R^{m\times n}$, $L_i \in R$, $j = 1, \dots, n$. Besides $L = (L_1, \dots, L_n)^T$. It is assumed that $rankB = n$ and $m \geq n$.

In [7] the authors show that the model (1) can be reduced to the generalized Lotka-Volterra also known as classical model of multispecies populations [8], [9]:

$$\dot{x}_i = x_i \left(N_i + \sum_{j=1}^{m} M_{ij} x_j \right),\ i = 1, \dots, m, \qquad (2)$$

where

$$M = B \cdot A,\ N = B \cdot L, \qquad (3)$$

and x_i is presented by

$$x_i = \prod_{k=1}^{n} y_k^{B_{ik}},\ i = 1, \dots, m. \qquad (4)$$

Let us choose initial values of variables x_i, $i = 1, \dots, m$ according to initial values of variables y_j, $i = 1, \dots, m$ and equations (4). Then dynamics of the multispecies populations (2) are equivalent to dynamics of the original quasi-polynomial model (1). Since the system (2) includes the variables y_i, $i = 1, \dots, n$, the stability of this system implies stability of the original system (1).

ISSN 2184-3945

Introduce control inputs $u_l,\ l = l_* + 1, \ldots, m,\ l_* \geq 1$ in (2). The controlled model of multispecies populations introduced in [16] is as follows:

$$\begin{cases} \dot{x}_i = x_i(t) \cdot \left(N_i + \sum_{j=1}^{m} M_{ij} x_j(t)\right),\ i = 1, 2, \ldots, l_* \\ \dot{x}_l = x_l(t) \cdot \left(N_l + \sum_{j=1}^{m} M_{lj} x_j(t) + u_l(t)\right),\ l = l_*, \ldots, m. \end{cases} \tag{5}$$

B. Invariant Functional

Assume that there exists at least one positive equilibrium in the uncontrolled system (2) for some values of the system parameters:

$$x_i = n_i > 0,\ i = 1, \ldots, m, \tag{6}$$

and the quantities $M_{ij}, i \neq j$ evaluating the type and intensity of the interaction between i-th and j-th variables form an antisymmetric matrix

$$M_{ii} = 0,\ M_{ij} = -M_{ji},\ i, j = 1, \ldots, m. \tag{7}$$

then the function

$$V_{qp}(x) = \sum_{i=1}^{m} n_i \left(\frac{x_i}{n_i} - \log\frac{x_i}{n_i}\right), \tag{8}$$

is an invariant of (5) for $u_l = 0,\ l = l_* + 1, \ldots, m,\ l_* \geq 1$ [8]. Besides, Hessian matrix of $V_{qp}(x)$ is positive definite and, therefore, $V_{qp}(x) > V_{qp}(n)$ for $x \neq n$. Hence $V_{qp}(x)$ can measure the amplitude of oscillations. Below it is used to achieve the desired amplitude of oscillations.

Introduce the control goal as an achievement of the desired level of the quantity $V_{qp}(x(t))$ as $t \to\propto$:

$$V_{qp} \to V_{qp}^*, t \to\propto . \tag{9}$$

If $V_{qp}^* = V_{qp}(n) = \min V_{qp}(x)$, then the goal (9) means achievement of the equilibrium $x = n$. In the case $V_{qp}(n) < V_{qp}^* < V_{qp}(x(0))$ achievement of the goal (9) means decrease of the oscillations level. If $V_{qp}^* > V_{qp}(x(0))$, then achievement of the goal (9) corresponds to the growth of the oscillations intensity. The problem is to find control function $u(t)$ in (5), ensuring achievement of the control goal (9).

III. Control Design

Apply the speed gradient (SG) method [14] to solve the problem. To this end introduce the so called goal function Q:

$$Q(x) = \frac{1}{2}\left(V_{qp}(x) - V_{qp}^*\right)^2. \tag{10}$$

In order to achieve the goal (9), it is necessary and sufficient that $Q(x(t)$ converges to zero as $t \to \infty$. According to the SG method one needs to evaluate A) derivative (speed of change) of Q with respect to the system (5) and B) the gradient of $\dot{Q}$ with respect to u.

Calculation of the time derivative of Q with respect to system (5) yields:

$$\dot{Q}(x, u) = \left(V_{qp}(x) - V_{qp}^*\right) \sum_{l=l_*}^{m} \left(x_l(t) - n_l\right) u_l. \tag{11}$$

Partial derivatives $\dot{Q}(\cdot)$ with respect to u_l are evaluated as follows:

$$\frac{\partial}{\partial u_l}\dot{Q}(x, u) = \left(V_{qp}(x) - V_{qp}^*\right)\left(x_l(t) - n_l\right),\ l = l_*, \ldots, m. \tag{12}$$

According to the SG method the control action is chosen as follows:

$$u_l(t) = -\gamma_l \left(V_{qp}(x) - V_{qp}^*\right)\left(x_l(t) - n_l\right), \tag{13}$$

where $\gamma_l > 0$, $l = l_*, \ldots, m$, $l_* \geq 1$.

IV. Control of quasi-polynomial systems in the absence of bounded disturbances or uncertainty

The first result of this section is the following statement.

Theorem 1. *Assume that there exists an equilibrium in the system (5) such that the conditions (6), (7) hold.*
Then either the algorithm (13) provides the goal (9), or the quantities of the controlled variables x_l tend to their equilibrium values n_l, $l = l_*, \ldots, m$, $l_* \geq 1$.
If the desired level $V_{qp}^* \geq V_{qp}^e$, where V_{qp}^e is a minimum of the invariant, and $V_{qp}(x(0)) > V_{qp}^e$, then the control goal (9) is achieved.

Proof.

Consider the time derivative of the goal function Q (11):

$$\dot{Q}(x, u) = -2\gamma Q \sum_{l=l_*}^{m} \left(x_l - n_l\right)^2 \leq 0. \tag{14}$$

Since Q does not increase, there exists a finite limit of $Q(t)$ as $t \to\propto$. Denote it as $\overline{Q}$. Suppose the goal (10) does not hold. Then $\overline{Q} > 0$. Hence $Q(t) \geq 0$ for all $t \geq 0$ and

$$\dot{Q}(x, u) = -2\gamma\overline{Q} \sum_{l=l_*}^{m} \left(x_l - n_l\right)^2 \leq 0. \tag{15}$$

Integration (15) yields

$$\begin{gathered} 0 \leq Q\left(x(t), u(t)\right) \leq Q\left(x(0), u(0)\right) - \\ -2\gamma\overline{Q} \sum_{l=l_*}^{m} \int_0^t \left(x_l(s) - n_l\right)^2 ds \leq 0. \end{gathered} \tag{16}$$

Therefore

$$\sum_{l=l_*}^{m} \int_0^t \left(x_l(s) - n_l\right)^2 ds <\propto . \tag{17}$$

Since the integrand is nonnegative and uniformly continuous, it converges to zero according to Barbalat Lemma [15], that is

$$x_l(t) \to n_l,\ t \to \infty,\ l = l_*, \ldots, m. \tag{18}$$

Thus either the algorithm (13) provides the control goal (5), or a number of the controlled variables $x_l(t)$ converges to its equilibrium n_l, $l = l_*, \dots, m$, $l_* \geq 1$.

The above assertion implies that the function $V_{qp}(x)$ either achieves the desired level V_{qp}^*, or converges to $V_{qp}(n) = V_{qp}^e$. Therefore at $x_i = n_i$, $i = 1, \dots, m$ the function $Q(x) = 0.5\left(V_{qp}(x) - V_{qp}^*\right)^2$ has its minimum. Thus for all $t \geq 0$ $V_{qp}(0) \geq V_{qp}^e$. Provided that $V_{qp}(0) = V_{qp}^e$, the system is always in its equilibrium, i.e. to achieve the control goal for $V_{qp}^* \geq V_{qp}^e$ it is necessary $V_{qp}(0) > V_{qp}^e$ ◄

Remark. In Theorem 1 it is supposed that the system (2) has at least one positive equilibrium for some values of its parameters. For a nonsingular matrix composed of M_{ij} we always can choose values of the birth rate N_i such that (6) holds [17]. For a nonsingular matrix composed of M_{ij} positivity conditions depending only on M_{ij} were found in [8].

V. Control of quasi-polynomial systems in the presence of bounded disturbances or uncertainty

A. Control of nonlinear systems in the presence of bounded disturbances or uncertainty

Consider the nonlinear system

$$\begin{cases} \dot{x} = f(x) + g(x)u + \eta, \\ y = h(x) \end{cases} \tag{19}$$

where $x \in X \subset R^n$ is a vector of state variables, $u \in U \subset R^m$ is a vector of control actions, $y \in R^p$ is an output vector. The vector $\eta \in R^n$ characterizes disturbances or uncertainty of the system (19). X, U are open sets in the space of dimension n and m accordingly; g is a $n \times m$ matrix function; f, h are smooth vector functions of dimension n and p accordingly. Moreover, $h(x)$ is an invariant function of (19) by $u = 0$.

Assume that in the system there exists an unique solution $x(t)$ for all $x(0) \in X$ and $u \in U$, and this solution is defined on $[0, +\infty)$ and entirely contained in the set X.

Introduce a control goal as achieving such quantity of the invariant $h(x)$ that will be the closest one to the desired value with the required accuracy:

$$\overline{\lim_{t \to \infty}}\, Q\left(x(t)\right) \leq C_Q, \tag{20}$$

where $Q = y^2$.

Apply the speed gradient (SG) method [14] to solve this problem. As a goal function take the function Q:

$$u = -\tilde{\gamma} \nabla_u \dot{Q} = -\gamma y^T \nabla h^T. \tag{21}$$

The second result of this paper is the following statement.

Theorem 2. *Suppose that the following conditions on the system (19) hold:*

- $f, g, h \in C^1$.
- $\|\eta(t)\| \leq C_\eta$.
- $L_f h\left(x\right) = 0$, *i.e.* $h\left(x\right)$ *is an invariant function in* (19) *by* $u = 0$.
- *There exists* $\xi > 0$ *such that a set* $Q_\xi = \{x \in R^n : Q(x) \leq \xi\}$ *is compact.*
- $x(0) \in Q_\xi$.
- $\forall x \in Q_\xi$ $\|h(x)^T \nabla h(x)^T\| \leq C$.
- *The minimum eigenvalue of the matrix* $A\left(x\right)^T A\left(x\right)$ *is uniformly positive, where* $A\left(x\right) = \nabla h\left(x\right)^T g\left(x\right)$*:*

$$\epsilon = \inf_{X \in R^n} \lambda_{min}\left(A(x)^T A(x)\right) > 0.$$

Then the designed control algorithm (21) *will provide the control goal* (20) *with* $C_Q = 2CC_\eta/\epsilon$.

Proof.

Consider the time derivative of the goal function Q along trajectories of (19):

$$\begin{array}{c} \dot{Q} = \frac{\partial Q}{\partial x}\dot{x} = 2y^T \nabla h^T\left(f + gu + \eta\right) = \\ 2y^T \nabla h^T f + 2y^T \nabla h^T gu + 2y^T \nabla h^T \eta. \end{array} \tag{22}$$

According to the first condition of Theorem 2 the first term of (22) is 0. Denote the second and third items of (22) as R_1, R_2 and estimate them:

$$R_1 = 2y^T \nabla h^T gu = y^T\left[\left(\nabla h^T g\right)\left(\nabla g^T h\right)\right] y = y^T A^T A y, \tag{23}$$

where $A = \nabla h^T g$. According to the fifth condition of Theorem 2 we obtain

$$A^T A \geq \epsilon I, \tag{24}$$

and, therefore

$$R_1 \leq -\epsilon \left\|y\right\|^2 = -\epsilon Q. \tag{25}$$

According to the first and forth conditions of Theorem 2 the functions f, g, h are bounded in the compact set Q_ξ, and ξ is bounded according to the second condition of Theorem 2. Therefore

$$R_2 = 2y^T \nabla h^T \eta \leq CC_\eta, \tag{26}$$

where C is a positive constant such that $\left\|2y^T \nabla h^T\right\| \leq C$. Then time derivative of Q

$$\dot{Q} \leq -\epsilon Q + CC_\eta. \tag{27}$$

that implies

$$\overline{\lim_{t \to \infty}}\, Q(x) \leq \frac{CC_\eta}{\epsilon}. \tag{28}$$

Thus, if the system (19) has bounded disturbances or uncertainty, the controls (21) limit the function Q, although the controls do not result in tending function Q to zero, and the upper estimate for the function Q is (28) ◄

ISSN 2184-3945

B. Quasi-Polynomial Model in the presence of bounded disturbances or uncertainty

Quasi-polynomial model with bounded disturbances or uncertainty is presented by the system

$$\dot{x}_i = x_i(t)\cdot\left(N_i + \sum_{j=1}^{m} M_{ij}x_j(t) + u_i(t)\right)+\eta_i,\ i = 1, \ldots, N, \tag{29}$$

where $\eta = (\eta_1, \ldots, \eta_N)^T$ is a vector containing disturbances or uncertainty.

Introduce a control goal as achieving such quantity of the invariant (8) that will be the closest one to its desired value V^*_{qp} with the required accuracy:

$$\overline{\lim_{t\to\infty}}\, h^2\left(x(t)\right) \le C_{V_{qp}}. \tag{30}$$

where $h(x) = V_{qp}\left(x\right) - V^*_{qp}$.

Apply the control algorithm (13) based on the speed gradient method to achieve the control goal (30).

The following result holds.

Theorem 3. *Suppose in the system* (29) *the conditions hold:*

- $\|\eta(t)\| \le C_\eta$.
- *There exists* $0 < \xi < \left(V^*_{qp}\right)^2$ *such that a set* $Q_\xi = \{x \in R^n : Q(x) \le \xi\}$ *is compact.*
- $x(0) \in Q_\xi$.
- $\forall x \in Q_\xi\ \|h(x)^T \nabla h(x)^T\| \le C$.
- *Take*
$$\epsilon = \inf_{i;\ x\in Q_\xi} x_i^2 \cdot \sum_{i=1}^{N}\left(1 - \frac{n_i}{x_i}\right)^2.$$

Then the algorithm (13) *will provide the goal* (30) *with* $C_{V_{qp}} = 2CC_\eta/\epsilon$.

Proof.

Theorem 3 is a consequence of Theorem 2. Indeed, in Theorem 3 all requirements from Theorem 2 except the sixth one hold. We have to verify this requirement, namely that the minimum eigenvalue of the matrix A^TA is uniformly positive, where the matrix $A = \triangledown hg^T$.

For the system (29) functions $h(x)$, $g(x)$ are as follows

$$h(x) = \sum_{i=1}^{N}\left(\frac{x_i}{n_i} - \log\frac{x_i}{n_i}\right) - W^*. \tag{31}$$

$$g(x) = \left(x_1, \ldots, x_N\right)^T. \tag{32}$$

Then

$$\triangledown h(x) = \left(\tilde{h_1}, \ldots, \tilde{h_N}\right)^T,\ \tilde{h_i} = 1 - \frac{x_i}{n_i},\ i = 1\ldots, N. \tag{33}$$

$$A(x)^TA(x) = g(x)\triangledown h(x)^T \triangledown h(x)g(x)^T = \sum_{i=1}^{N}\left(1 - \frac{x_i}{n_i}\right)^2 \cdot diag\{x_i^2\}_{i=1}^N. \tag{34}$$

Therefore the eigenvalues of the matrix $A(x)^TA(x)$ are

$$\lambda_i = x_i^2 \cdot \sum_{i=1}^{N}\left(1 - \frac{x_i}{n_i}\right)^2. \tag{35}$$

Thus, all eigenvalues of the matrix $A(x)^TA(x)$ are strictly positive. Therefore the system (29) satisfies all requirements of Theorem 2 ◄

VI. Conclusion

An approach to control of invariant sets of quasi-polynomial systems in the presence and absence of bounded disturbances is proposed. The control strategy is based on introduction of an invariant functional and posing the control task as achieving a desired value of the invariant functional. The design is based on the reduction to the generalized Lotka-Volterra system control. The proposed method may improve stability of the closed loop system and its robustness under action of bounded disturbances or under bounded uncertainty in the model. To implement the proposed algorithm an instant information exchange between different agents (species) is needed. In some cases it may be implemented based on Distributed Ledger Technology.

Further research may be devoted to application of the proposed algorithms to control of various biological or biochemical systems and numerical examination of the designed systems behavior. Examples of such system models can be fount, e.g. in [1].

Another avenue of research is study of speed-gradient algorithms for modeling of the biological evolution based on maximum entropy principle and its dynamical speed-gradient version [18].

The work was partly supported by RFBR grant 17-08-01728, by the Government of Russian Federation (Grant 08-08) and by the Distributed Ledger Technology Competence Center of SPbSU.

References

[1] G. Szederknyi, A. Magyar, K.M. Hangos, Analysis and Control of Polynomial Dynamic Models with Biological Applications (Academic Press, New York, 2018.

[2] Nader Motee, Bassam Bamieh, Mustafa Khammash. Stability analysis of quasi-polynomial dynamical systems with applications to biological network models. Automatica, 48 (2012) – pp. 2945–2950.

[3] Hernandez-Bermejo B., Fairen V. Lotka-Volterra representation of general nonlinear system. Mathematical Biosciences, Vol. 140, Issue 1, Feb. 1997, pp. 1–32.

[4] Hernandez-Bermejo B., Fairen V. Local Stability and Lyapunov Functionals for n–Dimensional Quasipolynomial Conservative Systems. Journal of Mathematical Analysis and Applications, 2001. – pp.242–256.

[5] G. Szederkenyi, K.M. Hangos. Global stability and quadratic Hamiltonian structure in Lotka-Volterra and quasi-polynomial systems. Physics Letters A, 324, 2004, pp.437–445.

[6] A. Magyar, G. Szederkenyi, K.M. Hangos. Quasi-polynomial system representation for the analysis and control of nonlinear systems. Proc. of the 16th IFAC World Congress, Prague, Czech Republic, 2005, pp.1–6.

[7] A. Magyar, G. Szederkenyi, K.M. Hangos. Globally stabilizing feedback control of process systems in generalized Lotka-Volterra form // Journal of Process Control, 2008. – Is. 18. – pp. 80–91.

[8] Yu. M. Svirezhev, D. O. Logofet. Stability of Biological Communities. MIR Publishers, 1983.

[9] Lotka A. J. Elements of Mathematical Biology. – Dover, New York, 1956.

[10] Fradkov A.L. Swinging control of nonlinear oscillations. International J. Control, V.64, Is. 6, 1996, pp.1189–1202.

[11] Astrom K.J., Furuta K. Swing up a pendulum by energy control. Automatica, 36 (2) (2000), pp. 287–295.

[12] Shiriaev A.S., Fradkov A.L. Stabilization of invariant sets for nonlinear systems with applications to control of oscillations. Intern. J. Robust Nonlinear Control, 2001, vol.11, pp.215–240.

[13] Shiriaev, A. S.; Freidovich, L. B.; Spong, M. W. Controlled Invariants and Trajectory Planning for Underactuated Mechanical Systems IEEE Transactions On Automatic Control Volume: 59 Issue: 9, pp. 2555–2561, 2014.

[14] Andrievskii B.R, Stotskii A. A., Fradkov A. L. Velocity-gradient algorithms in control and adaptation problems. Automation And Remote Control 49 (12), pp. 1533–1564, Part 1, 1988.

[15] Fradkov A.L., Miroshnik I.V., Nikiforov V.O. Nonlinear and Adaptive Control of Complex Systems. Dordrecht: Kluwer Academic Publ., 1999.

[16] Pchelkina I.V., Fradkov A.L., Control of oscillatory behavior of multispecies populations. Ecological Modelling. Elsevier, Vol. 227, Jan. 2012. pp. 1–6.

[17] Chakrabarti C.G., Koyel G. Non-equilibrium thermodynamics of ecosystems: Entropic analysis of stability and diversity. – Ecological Modeling. Is. 220, pp. 1950–1956, 2009..

[18] Shalymov D., Fradkov A., Liubchich S., Sokolov B. Dynamics of the relative entropy minimization processes. Cybernetics And Physics, Vol. 6, No. 2, 2017, 80-87.

ISSN 2184-3945

On the stability of 1D discrete dynamical systems: applications to population dynamics

Rafael Luís
Department of Mathematics, University of Madeira, Funchal, Portugal
Center for Mathematical Analysis, Geometry and Dynamical Systems, University of Lisbon, Lisbon, Portugal
rafael.luis.madeira@gmail.com

***Abstract*—In this paper we present a survey in the theory of stability of one-dimensional discrete-time dynamical systems. The main goal is to write a document that may be used as a pedagogical instrument in stability analysis for researchers that are not familiar with these techniques. Hence, we present the principal definitions and results in this field and a collection of classical population models widely used in population ecology. The dynamics of these models is, in general, a time-parameter dependent and the idea is to describe what factors in the parameter affect population size and how and why a population changes over time. Moreover, the presented techniques may be extended for different fields of science since the addressed results and examples are standard and may be adapted for a particular situation.**

***Index Terms*—Local Stability, Global Stability, Population Dynamics, Applications**

I. Introduction

One-dimensional discrete models are an appropriate mathematical tool to model the behavior of populations with non-overlapping generations. This subject has been intensely investigated by different researchers and is part of the solid foundations of the modern theory of discrete dynamical systems.

A discrete dynamical system (or difference equation) is a relation governed by the rule

$$x_{n+1} = f_n(x_n), \quad n = 0,\ 1,\ 2,\ \ldots, \tag{1}$$

where $x \in X$ and X is a topological space. Here, the orbit of a point x_0 is generated by the composition of the sequence of maps

$$f_0, f_1, f_2, \ldots.$$

Explicitly,

$$\begin{aligned} x_1 &= f_0(x_0), \\ x_2 &= f_1(x_1) = f_1 \circ f_0(x_0), \\ &\vdots \\ x_{n+1} &= f_n \circ f_{n-1} \circ \ldots \circ f_1 \circ f_0(x_0), \\ &\vdots \end{aligned}$$

If $f_0 = f_1 = f_2 = \ldots$, then the equation is said to be autonomous, otherwise it is non-autonomous. If the sequence of maps is periodic, i.e., $f_{n+p} = f_n$, for all $n = 0,\ 1,\ 2,\ \ldots$ and some positive integer $p > 1$, then we deal with non-autonomous periodic difference equations. Systems where the sequence of maps is periodic, model population with fluctuation habitat, and they are commonly called periodically forced systems.

Notice that the non-autonomous periodic difference equation (1) does not generate a discrete (semi)dynamical system [6] as it may not satisfy the (semi)group property. One of the most effective ways of converting the non-autonomous difference equation (1) into a genuine discrete (semi)dynamical system is the construction of the associated skew-product system as described in a series of papers by Elaydi and Sacker [6]–[8], [10]. It is noteworthy to mention that this idea was originally used to study non-autonomous differential equations by Sacker and Sell [22].

An ordered set of points $C_r = \{\overline{x}_0, \overline{x}_1, \ldots, \overline{x}_{r-1}\}$ is an $r-$periodic cycle in X if

$$f_{(i+nr) \bmod p}(\overline{x}_i) = \overline{x}_{(i+1) \bmod r},\ n = 0,\ 1,\ 2,\ \ldots.$$

In particular,

$$f_i(\overline{x}_i) = \overline{x}_{i+1},\ 0 \le i \le r-2,$$

and

$$f_t(\overline{x}_{t \bmod r}) = \overline{x}_{(t+1) \bmod r},\ r-1 \le t \le p-1.$$

It should be noted that the $r-$periodic cycle C_r in X generates an $s-$periodic cycle on the skew-product $X \times Y$ ($Y = \{f_0, f_1, \ldots, f_{p-1}\}$) of the form

$$\widehat{C}_s = \{(\overline{x}_0, f_0), (\overline{x}_1, f_1), ..., (\overline{x}_{(s-1) \bmod r}, f_{(s-1) \bmod p})\},$$

where $s = lcm[r, p]$ is the least common multiple of r and p.

To distinguish these two cycles, the $r-$periodic cycle C_r on X is called an $r-$geometric cycle (or simply $r-$periodic cycle when there is no confusion), and the $s-$periodic cycle $\widehat{C}_s$ on $X \times Y$ is called an $s-$complete cycle. Notice that either $r < p$, or $r = p$ or $r > p$.

Define the composition operator Φ as follows

$$\Phi_n^i = f_{n+i-1} \circ \ldots \circ f_{i+1} \circ f_i.$$

When $i = 0$ we write Φ_n^0 as Φ_n.

This work was partially supported by FCT/Portugal through project PEst-OE/EEI/LA0009/2013.

As a consequence of the above remarks it follows that the $s-$complete cycle $\widehat{C}_s$ is a fixed point of the composition operator Φ_s^i. In other words we have that

$$\Phi_s^i(\overline{x}_{i \bmod r}) = \overline{x}_{i \bmod r}.$$

If the sequence of maps $f_i,\ i = 0,\ 1,\ 2,\ \ldots$ is a parameter family of maps one-to-one in the parameter, then by [11] we have that $\overline{x}_{i \bmod p}$ is a fixed point of Φ_p.

Before ending this short introduction, we mention that in section II we present the principal results concerning the stability of fixed points in autonomous discrete dynamical systems. The results presented in this section may be extended to periodic systems substituting the map f for the composition operator Φ. The next two sections are devoted to applications. In section III we present the principal models for one-dimensional population dynamics. In the next section we refer some studies in non-autonomous periodic equations.

Finally, this survey may be used as a pedagogical instrument in stability analysis for students or researchers that are not familiar with these techniques and aims to study discrete dynamical systems. Moreover, it may be used for researchers in other fields that are familiar with some basic tools in Analysis. The presented examples in population dynamics are known and may be extended for other areas following the exposed techniques.

II. General results

Consider an interval $I \subseteq \mathbb{R}$ and an autonomous map $f : I \to I$. A point $x^* \in \mathbb{R}$ is said to be a fixed point (or equilibrium point) of f if $f(x^*) = x^*$, and given $x_0 \in \mathbb{R}$, we define its orbit $O(x_0)$ as the set of points

$$O(x_0) = \{x_0,\ f(x_0),\ f^2(x_0),\ f^3(x_0),\ \ldots\},$$

where $f^n = f \circ f^{n-1}$, for $n \in \mathbb{N}$, where $\mathbb{N}$ is the set of positive integers and $\circ$ represents the composition of functions.

One of the main objectives of the stability theory of discrete dynamical systems is to study the behavior of orbits when the starting points are near fixed points.

Let $f : I \to I$ be a map and x^* be a fixed point of f, where I is an interval of real numbers. Then:

1) The fixed point x^* is said to be locally stable if, for any $\epsilon > 0$, there exits $\delta > 0$ such that, for all $x_0 \in I$ with $|x_0 - x^*| < \delta$, we have $|f^n(x_0) - x^*| < \epsilon$, for all $n \in \mathbb{N}$. Otherwise, the fixed point x^* will be called unstable.
2) The fixed point x^* is said to be attracting if there exists $\eta > 0$ such that $|x_0 - x^*| < \eta$ implies $\lim\limits_{n\to\infty} f^n(x_0) = x^*$.
3) The fixed point x^* is said locally asymptotically stable if it is both stable and attracting. If in the previous item $\eta = \infty$, then x^* is said to be globally asymptotically stable.

Fig. 1 illustrates the idea behind the definition of stability.

Working with concrete examples, the definition of stability may not be the most practical tool to show the stability of a fixed point. There exists a simple but powerful criterion for knowing the local stability of fixed points. We may divide the fixed point into two categories: hyperbolic and nonhyperbolic. A fixed point x^* of a map f is said to be hyperbolic if $|f'(x^*)| \neq 1$, where f' denotes the derivative of the function f. Otherwise, the fixed point is nonhyperbolic.

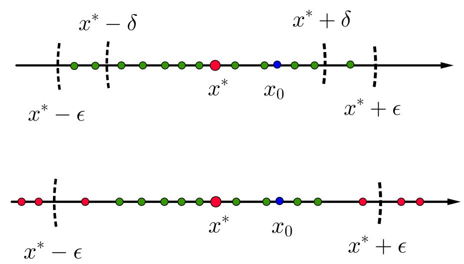

Fig. 1. Stable vs unstable fixed point. In the first case, the orbit of a starting point x_0 in a neighborhood δ of x^* stay in a neighborhood ϵ of x^* while in the second case, after certain order, the orbit start to be out of a neighborhood ϵ of x^*.

Theorem(Elaydi [4], page 25):

Let x^* be a hyperbolic fixed point of a map f, where f is continuous and differentiable at x^*. The following statements hold true:

1) If $|f'(x^*)| < 1$, then x^* is locally asymptotically stable.
2) If $|f'(x^*)| > 1$, then x^* is unstable.

The stability criteria for nonhyperbolic fixed points are more complex and are summarized in the following theorem. Before presenting it we need to introduce the notion of Schwarzian derivative.

The Schwarzian derivative, Sf, of a function f, is defined by

$$Sf(x) = \frac{f'''(x)}{f'(x)} - \frac{3}{2}\left(\frac{f''(x)}{f'(x)}\right)^2.$$

In particular, when $f'(x^*) = -1$, we have $Sf(x^*) = -f'''(x^*) - \frac{3}{2}\left[f''(x^*)\right]^2$.

Theorem(Elaydi [4], pages 28-30): Let x^* be a fixed point of a map f and f', f'' and f''' be continuous at x^*.

1) Let $f'(x^*) = 1$.
   a) If $f''(x^*) > 0$, then x^* is unstable but semi-stable from the left.
   b) If $f''(x^*) < 0$, then x^* is unstable but semi-stable from the right.
   c) If $f''(x^*) = 0$ and $f'''(x^*) > 0$, then x^* is unstable.
   d) If $f''(x^*) = 0$ and $f'''(x^*) < 0$, then x^* is locally asymptotically stable.
2) Let $f'(x^*) = -1$.
   a) If $Sf(x^*) < 0$, then x^* is locally asymptotically stable.
   b) If $Sf(x^*) > 0$, then x^* is unstable.

In applications it is important to know whenever the conditions of local stability imply global stability. The precedent results gives conditions on local stability. In 1955 W. Coppel stated the following result:

Theorem(Coppel [1]): Let $I = [a, b] \subseteq \mathbb{R}$ and $f : I \to I$ be a continuous map. If the equation $f(f(x)) = x$ has no roots, with the possible exception of the roots of the equation $f(x) = x$, then every orbit under the map f converges to a fixed point.

Coppel's theorem is not enough to ensure global stability. It is necessary to have uniqueness of the fixed point. In certain cases, depending the model we can establish global stability since only a unique fixed point will play a rule, as we will illustrate in the next sections.

III. Autonomous models

In this section we apply the results stated in the previous section to some important autonomous models in applications. We will start by the Ricker model which is a fishing model.

Example I - Ricker model: The Ricker model is given by

$$x_{n+1} = x_n e^{p - x_n},$$

where $x_n \geq 0$ is the density of the population at the period of time n and $p > 0$ is the carrying capacity of the population.

The map of the model is given by $f(x) = xe^{p-x}$. There are two fixed points, namely $x^* = 0$ and $x^* = p$. The origin is an unstable fixed point provide that $f'(0) = e^p > 1$. The positive fixed point is locally asymptotically stable whenever $0 < p \leq 2$ and unstable when $p > 2$. Notice that $|f'(p)| < 1$ implies that $0 < p < 2$ and since $f'(2) = -1$ we have $Sf(2) = -1 < 0$.

Now, solving the equation $f(f(x)) = x$, one can show that there are only two solutions whenever $0 < p \leq 2$, the origin and $x = p$, precisely the fixed pints of the map f. Since the origin is unstable, and $x^* = p$ is the unique fixed point in the positive real line, we have that the conditions of local stability of $x^* = p$ will implies global stability with respect to the positive real line. This means that every orbit starting at $x_0 > 0$ will converge to $x^* = p$ whenever $0 < p \leq 2$.

In Figure 2 is presented a cobweb diagram for this model. Notice that, a cobwebbing diagram is a geometrical toll where one can see the location of the values in the orbit of a starting point x_0. These values are located in the diagonal line $y = x$. In this case, it is clear that the orbit of $x_0 = 0.1$ converge to $x^* = 1.73$.

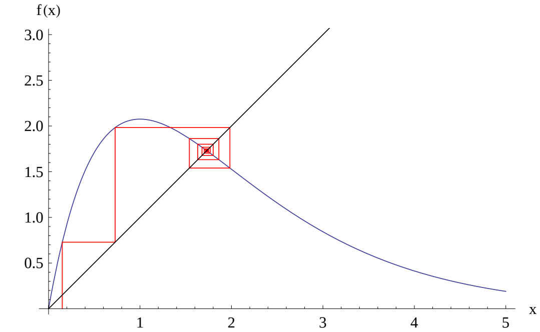

Fig. 2. Cobweb diagram for the Ricker model $x_{n+1} = x_n e^{p-x_n}$ when $p = 1.73$ and the starting point $x_0 = 0.1$. This example illustrates that the origin is an unstable fixed point and the positive fixed point is globally asymptotically stable.

It follows a difference equation which is the discrete version of the Verhulst model [24], [25] also called logistic map, a population model well known and studied in this field. We recall that the dynamics of this equation has played a paramount importance and it is present in the foundations and in the development of the modern theory of discrete dynamical systems.

Example II - Logistic model: The 1D logistic equation is given by

$$x_{n+1} = \mu x_n (1 - x_n),$$

where $x_n \in [0,\ 1]$ is the density and $\mu \in (0, 4)$ is a control parameter that represents a combined rate for reproduction and starvation.

We remark that this equation is found to be the most suitable model for the study of the surplus production of the population biomass of species in the presence of limiting factors such as food supply or disease. The above logistic model can possess stable, unstable, periodic and chaotic behaviors and thus receives wide attention due to the great implications of it in chaos theory (see May [20] for details at this point).

Since the map is given by $f(x) = \mu x(1 - x)$, the model has two fixed points, the origin and $x^* = \frac{\mu - 1}{\mu}$.

From the relation $f'(0) = \mu$ we have that the origin is locally asymptotically stable when $0 < \mu < 1$ and unstable when $\mu > 1$. When $\mu = 1$ we have $f'(0) = 1$. It follows that $f''(0) = -2 < 0$ and thus the origin is semi-stable from the right.

It is a straightforward computation to see that $x^* = \frac{\mu - 1}{\mu}$ is locally asymptotically stable whenever $1 < \mu \leq 3$ and unstable when $\mu \in (0, 1] \cup (3, 4)$.

Following a similar idea as the precedent example, one can show that the solutions of the equation $f(f(x)) = x$ are $x = 0$ and $x^* = \frac{\mu - 1}{\mu}$ whenever $0 < \mu \leq 3$. There are two cases: (i) $x^* = 0$ is globally asymptotically stable when $0 < \mu \leq 1$ provide that it is the unique fixed point of f in $[0, 1]$ and (ii) when $1 < \mu \leq 3$ the fixed point $x^* = \frac{\mu - 1}{\mu}$ is globally asymptotically stable with respect to the interior of the unit interval since it is the unique fixed point in this region.

Example III - Beverton-Holt model: The 1D Beverton-Holt map is given by

$$f(x) = \frac{rKx}{K + (r - 1)x},$$

where $x \geq 0$ is the density, $K > 0$ is the carrying capacity and $r > 0$ is the growth rate of the population. There are two fixed points, the origin which is locally asymptotically stable when $0 < r \leq 1$ and a positive fixed point $x^* = K$ which is locally asymptotically stable whenever $r > 1$.

In this example we do not need to apply Coppel's theorem to establish global stability since the model is monotone. Hence, the origin is globally asymptotically stable with respect to the interval $[0, K)$ whenever $0 < r \leq 1$, and $x^* = K$ is globally asymptotically stable with respect to the positive real line whenever $r > 1$.

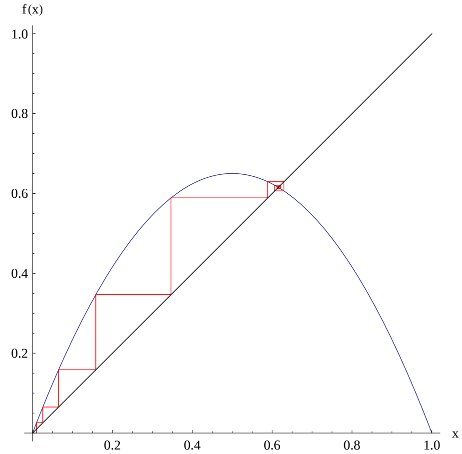

Fig. 3. Cobweb diagram for the logistic map when $x_0 = 0.15$ and $\mu = 2.6$. An orbit of starting point in the interior of the unit interval converges to the positive fixed point since it is globally stable in this set.

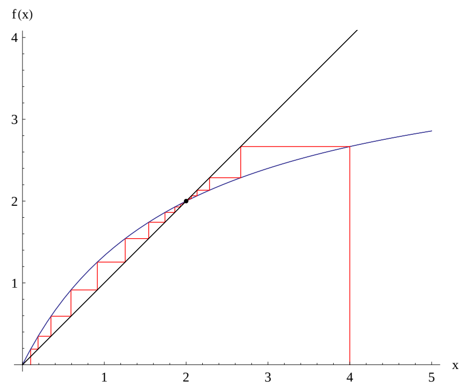

Fig. 4. Cobweb diagram for the Beverton-Holt model when $r = 2$ and $K = 2$. In this case we present the orbit of two initial points. It illustrates the unstability of the origin and the globally stability of the positive fixed point.

Example IV - Ricker with Allee effect: The modified Ricker model with Allee effect is given by

$$x_{n+1} = x_n^2 e^{p-x_n},$$

where $x_n \geq 0$ is the density of the population and $p > 0$ is the carrying capacity.

The fixed points of the model are the solutions of the equation $x^2 e^{p-x} = x$. From this relation it follows $x^* = 0$ and $xe^{p-x} = 1$. This last equation has no solution if $p < 1$, exactly one solution $x^* = 1$ if $p = 1$ and two solution, $x^* = \mathbf{A} < 1$ and $x^* = \mathbf{K} > 1$ if $p > 1$. In population dynamics these last fixed points are known as threshold point ($\mathbf{A}$) and carrying capacity ($\mathbf{K}$).

Hence, there are 3 cases to consider:

(i) $p < 1$. In this case the origin is a globally asymptotically stable fixed point provide that it is the unique fixed point in the non-negative real line. Notice that $f'(0) = 0$.

(ii) $p = 1$. There are two fixed points in the model, the origin and $x^* = 1$. The origin is locally asymptotically stable since $f'(0) = 0$ and its basin of attraction[1] is the set $[0,\ 1[\cup]\mathbf{A_r},\ +\infty[$, where $\mathbf{A_r}$ is the right pre-image of 1, i.e., the greatest solution of the equation $x^2 e^{1-x} = 1$ which is in this case ≈ 3.51286. The fixed point $x^* = 1$ is semistable from the right since $f'(1) = 1$ and $f''(1) = -1 < 0$. Its basin of attraction is the set $[1,\ \mathbf{A_r}]$.

(iii) $p > 1$. There are three fixed points, the origin, $x^* = \mathbf{A} < 1$ and $x^* = \mathbf{K} > 1$. The origin is locally asymptotically stable fixed point and its basin of attraction is the set $[0, \mathbf{A_r}[\cup]\mathbf{A_r},\ +\infty[$, where $\mathbf{A_r}$ is the right pre-image of $\mathbf{A}$.
In order to determine the stability of $\mathbf{A}$ and $\mathbf{K}$ notice that

$$f'(x) = x(2-x)e^{p-x},$$

and for the non-trivial values we have

$$f'(x) = \frac{(2-x)}{x} f(x).$$

Hence $|f'(\mathbf{A})| = |2 - \mathbf{A}|$ and $|f'(\mathbf{K})| = |2 - \mathbf{K}|$. Since $0 < \mathbf{A} < 1$ and $\mathbf{K} > 1$ we have that $\mathbf{A}$ is an unstable fixed point whereas $\mathbf{K}$ is locally asymptotically stable whenever $1 < \mathbf{K} < 3$. If this is the case, then its basin of attraction is $]\mathbf{A}, \mathbf{A_r}[$.

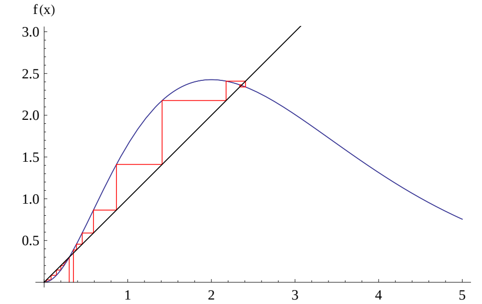

Fig. 5. Cobweb diagram of the Ricker model with Allee effect when the parameter $p = 2$. It illustrates the local stability of the origin and the carrying capacity and the instability of the threshold point.

Example V - Polynomial with Allee effect: Let us consider the difference equation given by

$$x_{n+1} = \mu_n x_n^{k_n} (1 - x_n), \tag{2}$$

where $x_n \in [0,1]$, $\mu_n > 0$ and $k_n = 2, 3, 4, \ldots$ for all non negative integer n. For more details about this equation please see [18].

Equation (2) may be represented by the map

$$f_n(x) = \mu_n x^{k_n} (1 - x).$$

Notice that when $\mu_n = \mu$ and $k_n = 1$ for all n, Equation (2) is the logistic equation studied in Example III.

In order to insure that $x_n \in I = [0,1]$ for all n, we make the following assumption concerning the parameters

[1]The basin of attraction (or the stable set) of a fixed point consists of all points that are forward asymptotic to it.

H: $\mu_n \leq \left(\frac{k_n+1}{k_n}\right)^{k_n}(k_n+1),\ n=0,1,2\ldots.$

Assumption **H** guarantees that all the orbits in (2) are bounded. Furthermore, it guarantees that f_n maps the interval I into the interval I for all $n=0,1,2\ldots$.

Let us now study the dynamics of the particular map $f(x)=\mu x^k(1-x)$, with $x\in I$, $\mu>0$ and $k=2,3,\ldots$. To find the fixed points of f we determine the solutions of the equation $\mu x^k(1-x)=x$. After eliminating the trivial solution, $x=0$, the positive fixed points are the solutions of

$$\mu x^{k-1}(1-x)=1, \tag{3}$$

or equivalently

$$\ln(\mu)=-(k-1)\ln x-\ln(1-x). \tag{4}$$

Letting $g(x)=-(k-1)\ln x-\ln(1-x)$, we see that $g(x)>0$ for all $x\in(0,1)$. Moreover, g is convex in the unit interval since $g'(x)>0$, for all $x\in I$, and attains its minimum at $g(c_g)$ where $c_g=\frac{k-1}{k}$ is the unique critical point of g in the unit interval. Let $\mathbf{O}_\mu$ be the immediate basin of attraction of the origin.

1) If $g(c_g)>\ln(\mu)$, then Eq. (4) has no solution. Hence, $x^*=0$ is the unique fixed point of the map f whenever $\mu<k\left(\frac{k}{k-1}\right)^{k-1}$. Under this scenario $x^*=0$ is globally asymptotically stable, given that it is the unique fixed point in I. Notice that at the origin we have $f'(0)=0$ and that $\mathbf{O}_\mu=[0,1]$.
2) If $g(c_g)=\ln(\mu)$, then Eq. (4) has a unique solution, $x^*=\frac{k-1}{k}=c_g$. Hence, the map f has a unique positive fixed point when $\mu=k\left(\frac{k}{k-1}\right)^{k-1}$. In this case and using (3), we obtain $|f'(x^*)|=1$ and $|f''(x^*)|=-k^2<0$, that allows us to conclude that x^* is an unstable fixed point, but semi-stable from the right. Moreover, its immediate basin of attraction is the set $\left[x^*,\max f^{-1}(\{x^*\})\right]$ where $f^{-1}(\{x^*\})$ is the pre-image of $\{x^*\}$. Notice that $\mathbf{O}_\mu=I\setminus\left[x^*,\max f^{-1}(\{x^*\})\right]$.
3) If $g(c_g)<\ln(\mu)$, then Eq. (4) has two positive solutions. Hence, the map f possesses two positive fixed points whenever $\mu>k\left(\frac{k}{k-1}\right)^{k-1}$. The smaller, denoted as $\mathbf{A}_\mu$, is known as a threshold point and the greater, denoted by $\mathbf{K}_\mu$, is known as a carrying capacity. Under this scenario, the fixed point $\mathbf{A}_\mu$ is always unstable and the fixed point $\mathbf{K}_\mu$ is locally asymptotically stable in the interval $\left(\mathbf{A}_\mu,\max f^{-1}(\{\mathbf{A}_\mu\}\right)$ if $\left|k-\mu\mathbf{K}_\mu^k\right|<1$. Moreover, $\mathbf{O}_\mu=[0,\mathbf{A}_\mu)\cup\left(\max f^{-1}(\{\mathbf{A}_\mu\}),1\right]$.

Notice that the sequence $a_k=\left(\frac{k+1}{k}\right)^k(k+1)$ that is used to define Assumption **H** is increasing for $k=2,3,\ldots$. We now resume the precedent ideas in the following result, for a general integer $k=2,3,\ldots$:

Theorem: Let $f(x)=\mu x^k(1-x)$, $k=2,3,\ldots$. Then the following yields:

1) If $\mu<k\left(\frac{k}{k-1}\right)^{k-1}$, then $x^*=0$ is a globally asymptotically stable fixed point of f and its basin of attraction is the unit interval.
2) If $\mu=k\left(\frac{k}{k-1}\right)^{k-1}$, then the map has two fixed points, the origin and a positive fixed point $x^*=\frac{k-1}{k}$. This last one is locally asymptotically stable from the right and its immediate basin of attraction is the set $\left[x^*,\max f^{-1}(\{x^*\})\right]$. Moreover, $\mathbf{O}_\mu=I\setminus\left[x^*,\max f^{-1}(\{x^*\})\right]$.
3) If $\mu>k\left(\frac{k}{k-1}\right)^{k-1}$, then the map has three fixed points, the origin, a threshold fixed point $\mathbf{A}_\mu$ and a carrying capacity $\mathbf{K}_\mu$ such that $\mathbf{A}_\mu<\mathbf{K}_\mu$. The threshold fixed point is always unstable and if $|k-\mu\mathbf{K}_\mu^k|<1$ the carrying capacity is locally asymptotically stable with a basin of attraction given by the set $\left(\mathbf{A}_\mu,\max f^{-1}(\{\mathbf{A}_\mu\})\right)$. Moreover, $\mathbf{O}_\mu=I\setminus\left[\mathbf{A}_\mu,\max f^{-1}(\{\mathbf{A}_\mu\})\right]$.

Remark: Before ending this example let us have a particular look in the dynamics of the autonomous equation when $k=2$, i.e., the dynamics of the modified logistic equation with Allee effect when the map is given by $f(x)=\mu x^2(1-x)$.

1) If $\mu<4$, then the origin is a globally asymptotically stable fixed point provided that it is the unique fixed point in the unit interval.
2) If $\mu=4$, then the map possesses two fixed points, the origin and $x^*=\frac{1}{2}$. The basin of attraction of the origin is
$$\mathbf{O}_4=\left[0,\frac{1}{2}\right)\cup\left(\frac{1+\sqrt{5}}{4},1\right], \tag{5}$$
while the basin of attraction of the positive fixed point is $\left[\frac{1}{2},\frac{1+\sqrt{5}}{4}\right]$. Notice that $x^*=\frac{1}{2}$ is a fixed point semi-stable from the right.
3) If $4<\mu$, then the map has three fixed points, the origin, the threshold point $\mathbf{A}_\mu=\frac{1}{2}\left(1-\sqrt{\frac{\mu-4}{\mu}}\right)$ and the carrying capacity $\mathbf{K}_\mu=\frac{1}{2}\left(1+\sqrt{\frac{\mu-4}{\mu}}\right)$.
It is a straightforward computation to see that, when $\mu>4$,
$$|f'(\mathbf{A}_\mu)|=3+\frac{\mu}{2}\left(-1+\sqrt{\frac{\mu-4}{\mu}}\right)>1.$$
Hence, the fixed point $\mathbf{A}_\mu$ is unstable.
Similarly, we see that
$$|f'(\mathbf{K}_\mu)|=\left|3-\frac{\mu}{2}\left(1+\sqrt{\frac{\mu-4}{\mu}}\right)\right|<1 \text{ iff } 4<\mu<\frac{16}{3}.$$
When $\mu=\frac{16}{3}$ we have $f'(\mathbf{K}_\mu)=-1$. Forward computations show that the Schwarzian derivative evaluated at the fixed point is negative, i.e., $Sf(\mathbf{K}_\mu)<0$. It follows that the fixed point $\mathbf{K}_\mu$ is asymptotically stable. Thus, the fixed point $x^*=\mathbf{K}_\mu$ is locally asymptotically stable whenever $4<\mu\leq\frac{16}{3}$ and its basin of attraction is the set $\left(\mathbf{A}_\mu,\ \max f^{-1}(\{\mathbf{A}_\mu\})\right)$. Moreover,
$$\mathbf{O}_\mu=[0,\mathbf{A}_\mu)\cup\left(\max f^{-1}(\{\mathbf{A}_\mu\}),1\right]. \tag{6}$$

IV. NON-AUTONOMOUS MODELS

In this section we present some studies for particular periodic difference models. We notice that the study of this kind of equations is quite complicate and in certain cases it is not possible to find explicitly the fixed points due the complexity of computations, specially nontrivial fixed points.

Example VI - Periodic Ricker map:

Let us consider the periodic difference equation given by the following equation

$$x_{n+1} = R_n(x_n),$$

where the sequence of maps $R_n(x)$ is given by

$$R_n(x) = xe^{r_n - x}, \ n = 0, \ 1, \ 2 \dots, \tag{7}$$

$x \geq 0$ is the density of the population and $r_n > 0$, $n = 0, \ 1, \ 2 \dots$ is the sequence of individual carrying capacities.

Notice that the local stability condition for each individual map $R_i(x)$ is given by

$$0 < r_i \leq 2, \quad i = 0, \ 1, \ 2 \dots,$$

as is shown in Example III.

In order to have periodicity we require that $R_{n+p} = R_n$, for all $n = 0, 1, 2, \dots$, i.e., the sequence of parameters satisfies $r_n = r_{n \bmod p}$, for all n. It is clear that the composition map

$$\Phi_p(x) = R_{p-1} \circ \dots \circ R_1 \circ R_0(x)$$

is continuous in $\mathbb{R}_0^+$.

In [21] R. Sacker showed that the map Φ_p has a globally asymptotically stable fixed point whenever the periodic sequence of parameters satisfies $0 < r_n \leq 2$, $n = 0, 1, 2, \dots$. Since the sequence of maps is one-to-one relative to the parameters, it follows from [11] that the globally asymptotically stable fixed point of Φ_p generates a globally asymptotically stable $p-$periodic cycle of the form

$$\{\overline{x}_0, \ \overline{x}_1, \ \dots, \ \overline{x}_{p-1}\}.$$

Using the chain rule of derivative it follows that

$$\Phi_p'(\overline{x}_0) = R_{p-1}'(\overline{x}_{p-1}) R_{p-2}'(\overline{x}_{p-2}) \dots R_1'(\overline{x}_1) R_0'(\overline{x}_0).$$

Since $R_i'(x) = (1-x)e^{p_i - x}$ and the dynamics of the periodic orbit is $\overline{x}_{i+1} = \overline{x}_i e^{r_i - \overline{x}_i}$, $i = 0, \ 1, \ 2 \ \dots, \ p-1$, the stability condition of the periodic orbit is

$$\prod_{i=0}^{p-1} |1 - \overline{x}_i| < 1. \tag{8}$$

Later on, Elaydi et al. [12] noticed that the region of stability in the parameter space determined by Sacker may be larger as it is shown in Fig. 6 for a $2-$periodic equation. They have been determined the boundary of the region and in a recent paper, Liz [19] showed global stability in this region using the following result:

Theorem(Corollary 2.9 in [13] by El-Morshedy & López): Let $a \geq 0$, $b > a$ and $g : (a, \ b) \to [a, \ b]$ be a continuous map with a unique fixed point x^* such that $(g(x) - x)(x - x^*) < 0$ for all $x \neq x^*$. Assume that there are points $a \leq c < x^* < d \leq b$ such that the restriction of g to $(c, \ d)$ has at most one turning point and whenever it makes sense, $g(x) \leq g(c)$ for every $x \leq c$, and $g(x) \geq g(d)$ for every $x \geq d$. If g is decreasing at x^*, assume additionally that $Sg(x) < 0$ for all $x \in (c, \ d)$ except at most one critical point og g and $-1 < g'(x^*) < 0$. Then the fixed point x^* is globally stable.

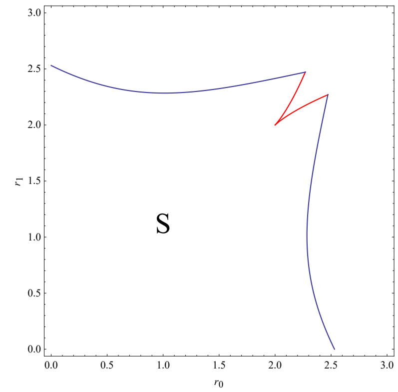

Fig. 6. Region S where the $2-$periodic Ricker equation has a globally asymptotically stable $2-$periodic cycle. The curves are part of the region of global stability. Once the parameters crosses these curves the $2-$periodic cycle becomes unstable.

It remains as an open problem to show global stability for $p \geq 3$.

Example VII - Periodic Beverton-Holt model:

Let $x_{n+1} = B_n(x_n)$, $n = 0, \ 1, \ 2, \dots$ where the map B_n is given by

$$B_n(x) = \frac{rK_n x}{K_n + (r-1)x}. \tag{9}$$

Here $x \geq 0$ is the density, the parameter $r > 1$ is the grow rate and the sequence of parameters $K_n > 0$ are the carrying capacities of each individual population. In Example III is established the conditions for stability of each individual map B_n.

Let us now assume that $K_{n+p} = K_n$ for all n and $p > 1$, i.e., the sequence of maps B_n is $p-$periodic. Since each individual map is monotone and the composition of monotone maps is monotone, we have that Φ_p is a monotone map. Moreover, the orbits are bounded since $B_n(x) < \frac{r}{r-1} K_n$ for all n.

It follows from the Brouwer's fixed point theorem that Φ_p has a fixed point. Due the monotonicity we have that the fixed point is globally asymptotically stable. This fixed point of Φ_p generates a globally asymptotically stable $p-$periodic cycle in the original equation (9) of the form

$$\{\overline{x}_0, \ \overline{x}_1, \ \dots, \ \overline{x}_{p-1}\}.$$

In a famous conjecture, Chushing and Hensen [2], [3] stated that the average of the individual carrying capacities is less than the average of the numbers in the $p-$periodic cycle, i.e.,

$$\frac{K_0 + K_1 + \dots + K_{p-1}}{p} < \frac{\overline{x}_0 + \overline{x}_1 + \dots + \overline{x}_{p-1}}{p}.$$

ISSN 2184-3945

Using Jensen's inequality some researchers solved positively this conjecture. To cite few [5]–[10], [15], [16], [23].

In conclusion, forcing the system may be beneficial for the population since the carrying capacity of the periodic population will be greater than the individual carrying capacities.

Example VIII - Generalized periodic logistic:

We start this example presenting a result related to the non-autonomous equation (2) when $k = 2$ (although it may be extended for other values of the parameter k as well). It is not hard to prove the following:

Lemma: Consider the non-autonomous difference equation given by

$$x_{n+1} = \mu_n x_n^2 \left(1 - x_n\right), \tag{10}$$

where $x_n \in [0, 1]$, $\mu_n \in \left(0, \frac{27}{4}\right]$, for $n = 0, 1, 2\ldots$, and $\mathbf{O}_\mu$ the immediate basin of attraction of the origin. Then

$$4 \leq \mu_1 \leq \mu_2 \leq \frac{27}{4} \Rightarrow \mathbf{O}_4 \supseteq \mathbf{O}_{\mu_1} \supseteq \mathbf{O}_{\mu_2} \supseteq \mathbf{O}_{\frac{27}{4}}, \tag{11}$$

where $\mathbf{O}_4$ is given by (5) and

$$\mathbf{O}_{\frac{27}{4}} = \left[0, \frac{9 - \sqrt{33}}{18}\right) \cup \left(\max f^{-1}\left(\left\{\mathbf{A}_{\frac{27}{4}}\right\}\right), 1\right], \tag{12}$$

where $\max f^{-1}\left(\left\{\mathbf{A}_{\frac{27}{4}}\right\}\right) \approx 0.971\,62$.

Let us now turn our attention to the non-autonomous periodic equation (2). We will study the case where the sequence of maps is $p-$periodic, *i.e.*, when $f_{n+p} = f_n$, for all $n = 0, 1, 2, \ldots$. Under this scenario, equation (2) is $p-$periodic.

The dynamics of the non-autonomous $p-$periodic equation (2) is completely determined by the following composition operator

$$\Phi_p = f_{p-1} \circ \ldots \circ f_1 \circ f_0.$$

From assumption $\mathbf{H}$ it follows that $\Phi_p(I) \subseteq I$ with $\Phi_p(0) = 0$ and $\Phi_p(1) = 0$. Hence, by the Brouwer's fixed point theorem [14], the composition operator Φ_p has a fixed point in the unit interval.

It is clear that $x^* = 0$ is a locally asymptotically stable fixed point of Φ_p provided that $|\Phi_p'(0)| = 0$. Now, if $\Phi_p(x) < x$, for all $x \in (0, 1)$, then $x^* = 0$ is the unique fixed point of the composition operator Φ_p in the unit interval. In this case, $x^* = 0$ is a globally asymptotically stable fixed point and its basin of attraction is the entire unit interval. This is the case where local stability implies global stability in the sense that every orbit of $x_0 \in I$ converge to the origin.

Notice that, if C_{Φ_p} is the set of critical points of Φ_p, i.e., if C_{Φ_p} contains all the solutions in the unit interval of the p equations $\Phi_i(x) = c_i$, $i = 0, 1, \ldots, p-1$, where c_i is the critical point of the map f_i, then $\Phi_p(x) < x$, for all $x \in (0, 1)$ if $\Phi_p(c_{\Phi_p}) < c_{\Phi_p}$, where $c_{\Phi_p} \in C_{\Phi_p}$.

Now, if $|\Phi_p(x)| > x$ for some $x \in (0, 1)$, the composition operator Φ_p has more than one fixed point. We know from Coppel's Theorem [1] that every orbit converges to a fixed point if and only if the equation $\Phi_p \circ \Phi_p(x) = x$ has no solutions with the exception of the fixed points of Φ_p.

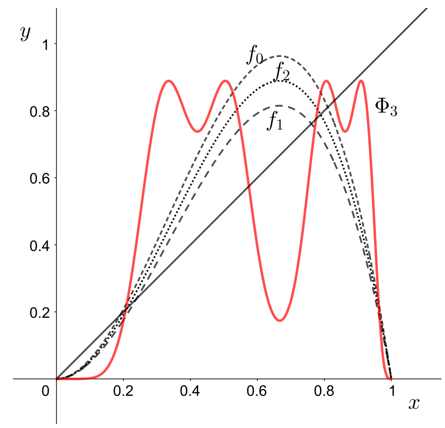

Fig. 7. Composition of three generalized logistic maps. The composition map Φ_3 is represented by the solid curve and the individual maps are represented by the dashed curves. The values of parameters are $k = 2$, $\mu_0 = 6.5$ (f_0), $\mu_1 = 5.5$ (f_1) and $\mu_2 = 6$ (f_2).

It is not possible, in general, to say much concerning the number of fixed points of Φ_p since we have many scenarios. However, if all maps f_i have a threshold fixed point $\mathbf{A}_i$ and we let $\mathbf{A}_m = \min\{\mathbf{A}_0, \mathbf{A}_1, \ldots, \mathbf{A}_{p-1}\}$ and $\mathbf{A}_M = \max\{\mathbf{A}_0, \mathbf{A}_1, \ldots, \mathbf{A}_{p-1}\}$, then one can show that the minimal positive fixed point of Φ_p, $\mathbf{A}_{\Phi_p}$, lies between $\mathbf{A}_m$ and $\mathbf{A}_M$ and is, in fact, an unstable fixed point. Under this scenario, the immediate basin of attraction of the origin is $\cup_{i \geq 1} J_i$ where $J_i \subset I$ and

$$\Phi_p(J_i) \subset [0, \mathbf{A}_{\Phi_p}).$$

See Fig. 7 for an example of this scenario.

We remark that each fixed point of the composition map Φ_p, with the exception of $x^* = 0$, generates a periodic orbit in equation (2). More precisely, if x^* is a non-trivial fixed point of Φ_p, then

$$\overline{C} = \{\overline{x}_0 = x^*, \overline{x}_1 = f_0(\overline{x}_0), \overline{x}_2 = f_1(\overline{x}_1), \ldots, \overline{x}_{p-1} = f_{p-2}(\overline{x}_{p-2})\}$$

is a periodic cycle of equation (2), which is locally asymptotically stable if

$$|\Phi_p'(x^*)| = \left|\prod_{i=0}^{p-1} f_i'(\overline{x}_i)\right| < 1.$$

Notice that, due the periodicity of the maps f_i, we have $\overline{x}_p = f_{p-1}(\overline{x}_{p-1}) = \overline{x}_0$, $\overline{x}_{p+1} = \overline{x}_1$, and so on.

From the dynamical point of view, it is interesting to know the region where the stability of the fixed points occurs. Since we are not able to find explicitly the fixed points of the composition map Φ_p for general values of the parameters k_i and μ_i, $i = 0, 1, \ldots, p-1$, we will particularize and study the cases where this is possible as are the cases when $p = 2, 3, 4$ and $k = 2$, i.e., we will study the dynamics of the system when the sequence of maps is $2-$periodic and given by

$$f_{n\ mod(2)}(x) = \mu_{n\ mod(2)}\ x^k(1 - x), \quad k = 2, 3, 4.$$

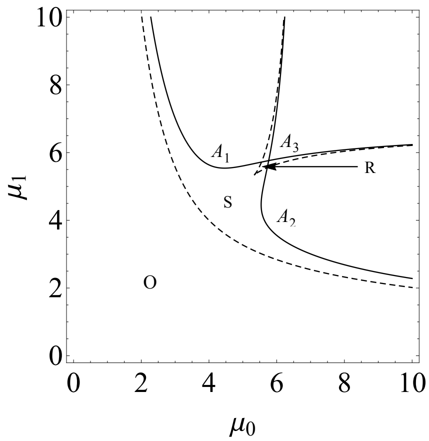

Fig. 8. Region of local stability, in the parameter space $\mu_0 O \mu_1$ where the fixed points of $f_1 \circ f_0$ are locally asymptotically stable and the maps are given by $f_i(x) = \mu_i x^2(1-x)$, $i = 0, 2$.

Let us start with the case $k = 2$. Following the techniques employed in [17], one can find the region of local stability of the fixed points of the composition map $\Phi_2 = f_1 \circ f_0$ by calculating the boundary where the absolute value of $\Phi_2'(x^*)$ is equal to one. This happens when

$$\begin{cases} f_1(f_0(x^*)) = x^* \\ f_1'(f_0(x^*))f_0'(x^*) = 1 \end{cases} \tag{13}$$

and

$$\begin{cases} f_1(f_0(x^*)) = x^* \\ f_1'(f_0(x^*))f_0'(x^*) = -1 \end{cases} . \tag{14}$$

Since the computations are long we will omit it here. Now, drawing implicitly, in the parameter space, the curves where the two previous equations are satisfied, we find the region where the stability of the fixed points of Φ_2 occurs. The stability regions are depicted, in the parameter space $\mu_0 O \mu_1$, in Fig. 8.

If the parameters μ_0 and μ_1 belong to the region O, then the origin is a fixed point globally asymptotically stable. Once the parameters cross the dashed curve, from Region O to Region S, a bifurcation occurs, known as saddle-node bifurcation. The fixed point $x^* = 0$ becomes unstable and a new locally stable fixed point of Φ_2 is born. This fixed point is, in fact, a $2-$periodic cycle of the $2-$periodic equation (2). Now if the parameters μ_0 and μ_1 cross the dashed curve from Region S to Region R, a saddle-node bifurcation occurs. The $2-$periodic cycle becomes unstable and a new locally asymptotically stable $2-$periodic cycle is born.

For a general framework of bifurcation in one-dimensional periodic difference equations, we refer the work of Elaydi, Luís, and Oliveira in [12].

Now, following the same techniques as before, we are able to find the regions of local stability of fixed points when $k = 3$ and $k = 4$. These regions are represented in Fig. 9. As we can observe, they are similar to the case $k = 2$ and the conclusions follow in the same fashion.

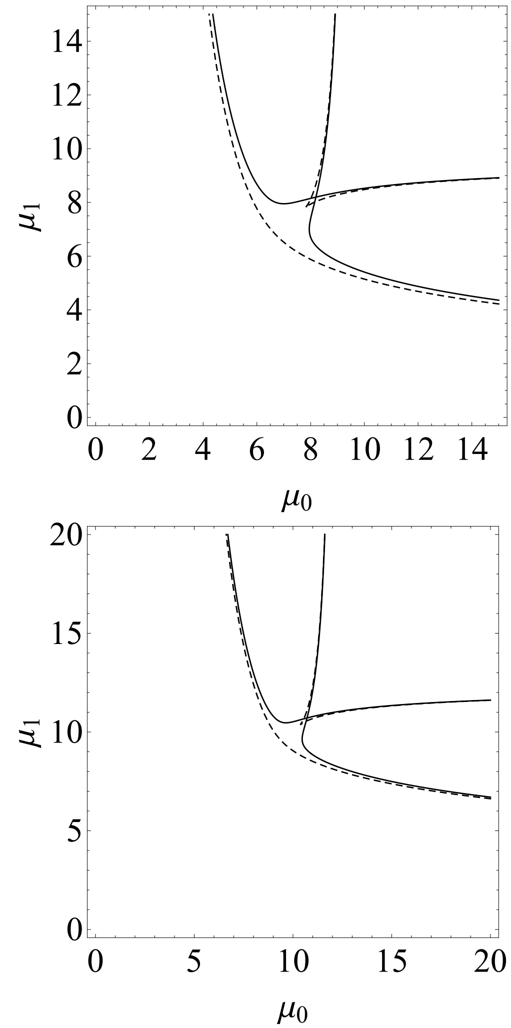

Fig. 9. Regions of local stability, in the parameter space, of the $2-$periodic equation when $k = 3$ (left) and $k = 4$ (right).

V. Conclusion

In this paper, we have presented a survey in local stability of discrete-time dynamical systems. The most important results concerning stability of hyperbolic and non-hyperbolic fixed points are addressed. Examples in both, autonomous and non-autonomous periodic models, are deeply studied. Some of these examples are widely used in the literature such as the Beverton-Holt model, the logistic model and the Ricker model. However, the examples with Allee effect are not so well known and studied. We should mention that, in the past two decades, the Allee effect was deeply studied in discrete dynamical systems.

Finally, this survey aims to be as a pedagogical instrument in stability analysis of discrete dynamical systems.

References

[1] W. A. Coppel. *The solution of equations by iteration*, Mathematical Proceedings of the Cambridge Philosophical Society, **51**(01) (1955), 41–43.

[2] J. Cushing, S. Henson, *Global dynamics of some periodically forced, monotone difference equations*, Journal of Difference Equations and Applications **7** (2001), 859–872.

[3] J. Cushing, S. Henson, *A periodically forced Beverton-Holt equation*, Journal of Difference Equation and Applications **8** (2002) 1119–1120.

[4] S. Elaydi. *Discrete Chaos: With Applications in Science and Engineering*. Chapman and Hall/CRC, Boca Raton, Second Edition, 2008.

[5] S. Elaydi, R. Sacker, *Basin of attraction of periodic orbits of maps in the real line*, Journal of Difference Equations and Applications **10** (2004) 881888.

[6] S. Elaydi, R. Sacker, *Skew-product dynamical systems: Applications to difference equations*, Proceedings of the Second Annual Celebration of Mathematics, United Arab Emirates.

[7] S. Elaydi, R. Sacker, Global stability of periodic orbits of nonautonomous difference equations and populations biology, J. Differential Equations **208** (2005) 258–273.

[8] S. Elaydi, R. Sacker, *Nonautonomous Beverton-Holt equations and the Cushing-Henson conjectures*, Journal of Difference Equations and Applications **11** (4-5) (2005), 337–346.

[9] S. Elaydi, R. Sacker, *Global stability of periodic orbits of nonautonomous difference equations in population biology and the Cushing-Henson conjectures*, in: S. Elaydi, G. Ladas, B. Aulbach, O. Dosly (Eds.), Proceedings of the Eighth International Conference on Difference Equations and Applications, Chapman and Hall/CRC, 2005, pp. 113–126.

[10] S. Elaydi, R. Sacker, *Periodic difference equations, population biology and the cushing-henson conjectures*, Mathematical Biosciences **201** (2006) 195–207.

[11] S. Elaydi, R. Luis, and H. Oliveira, *Towards a theory of periodic difference equations and its application to population dynamics*, in: M. M. Peixoto, A. A. Pinto, D. A. Rand (Eds.), Dynamics, Games and Science I, DYNA 2008, in Honor of Maurcio Peixoto and David Rand, University of Minho, Braga, Springer, 2011, pp. 287–321, series: Springer Proceedings in Mathematics, Vol. 1.

[12] S. Elaydi, R. Luís and H. Oliveira, *Local bifurcation in one-dimensional nonautonoous periodic difference equations*, International Journal of Bifurcation and Chaos, **23**(03) (2013), 1350049 18pp.

[13] H. A. El-Morshedy and V. J. López, *Global attractors for difference equations dominated by one-dimensional maps*, Journal of Difference Equations and Applications, **14**(4) (2008), 391–410.

[14] R. B. Kellogg, T. Y. Li, and J. Yorke. *A constructive proof of the Brower's fixed point theorem and computational results*, SIAM Journal on Numerical Analysis, **13**(4) (1976), 473–483.

[15] V. Kocic, *A note on the nonautonomous Beverton-Holt model*, Journal of Difference Equation and Applications **11** (4-5) (2005) 415–422.

[16] R. Kon, *A note on attenuant cycles of population models with periodic carrying capacity*, Journal of Difference Equation and Applications **10** (8) (2004) 791–793.

[17] R. Luís, S. Elaydi, and H. Oliveira, *Non-autonomous periodic systems with Allee effects*, Journal of Difference Equations and Applications, **16**(10) (2010), 1179–1196.

[18] R. Luís, and S. Mendona, *A STOCHASTIC STUDY FOR A GENERALIZED LOGISTIC MODEL*, REVSTAT - STATISTICAL JOURNAL (2019), to appear.

[19] E. Liz, *On the global stability of periodic Ricker maps*, Electronic Journal of Qualitative Theory of Differential Equations, **76** (2016), 1–8.

[20] R. May, *Simple mathematical models with very complicated dynamics*, Nature,, **261**(1976), 459–475.

[21] R. Sacker, *A note on periodic Ricker map*, Journal of Difference Equations and Applications **13** (1) (2007) 89–92.

[22] R. Sacker, J. Sell, *Lifting properties in skew-product flows with applications to differential equations*, AMS Memoirs 11 (190).

[23] S. Stevic, *A short proof of the Cushing-Henson conjecture*, Discrete Dynamics in Nature and Society, Hindawi Publishing Corporation, 2006.

[24] P. Verhulst; *Recherches mathematiques sur la loi daccroissement de la population*; Mem. Acad. Royale Belg., **18**(1845);1–38.

[25] P. Verhulst; *Deuxieme memoire sur la loi daccroissement de la population*, Mem. Acad. Royale Belg., **20**(1847);1–32.

ISSN 2184-3945

A Remark on An Annuity Payment Structure

Alexander Patkowski
Centerville, Massachusetts,
U.S.A.
alexpatk@hotmail.com

Krzysztof Ostaszewski
Department of Mathemaics
Illinois State University
Normal, Illinois, U.S.A.
krzysio@ilstu.edu

Abstract **— We discuss a possible occurrence of annuity payments which follow a basic-hypergeometric progression, relative to the associated spot rate. We give explicit formulas for calculating the outstanding balance in a particular model where a single interest rate is replaced with a particular interest rates structure.**

Keywords — Annuity, Basic hypergeometric series, Outstanding loan balance.

I. Introduction and Main Result

An annuity is a series of payments, typically following a pattern, e.g., level (i.e., same every period). Annuities are used for calculation of loan amortization schedules, bond prices, and in insurance applications. If a loan in the initial amount L is being paid off by a series of level payments P over n years with annual effective interest rate of i, with payments made at the end of each year, then the outstanding balance of a loan at time k (expressed in years), where k is an integer, just after the k-th payment was made at the end of the $(k-1)$-st year, is

$$OB_k = Pa_{\overline{n-k}|i} = P \cdot \frac{1-(1+i)^{-(n-k)}}{i}, \tag{1}$$

alternatively written as

$$OB_k = L(1+i)^k - Ps_{\overline{k}|i} = L(1+i)^k - P \cdot \frac{(1+i)^k - 1}{i}. \tag{2}$$

(1) is called the *prospective method* of calculation of a loan balance, and (2) is termed the *retrospective method* of calculation (see [1]). In the above k and n are natural numbers.

Loan repayments are not always level in practical scenarios. One possible alternative is to pay l times the interest due the loan whose initial balance was L, where l is a parameter greater than 1. With an annual effective interest rate of i, the loan balance would be: L at time 0,

$$L - L(l-1)i = L(1-(li-i))$$

at time 1, then

$$L(1-(li-i))\,(1-(li-i)) = L(1-(li-i))^2$$

at time 2, etc., so that in each payment the balance of the loan is multiplied by the expression $(1-(li-i))$ and with balance at time k equal to

$$\begin{aligned} L\big(1-(li-i)\big)^k &= L\big(1-(l-1)i\big)^k = \\ &= L \cdot \sum_{j=0}^{k} \binom{k}{j} \big(-(l-1)i\big)^j. \end{aligned} \tag{3}$$

The last step follows from the Binomial Theorem. Note that the terms $\big(-(l-1)i\big)^j$ for $j = 0, 1, \ldots$, etc., form a geometric progression as the ratio of two consecutive terms is always $-(l-1)i$.

Recall that a positive integer x, the *falling factorial* is defined as

$$(x)_n = x(x-1)(x-2)\ldots(x-(n-1)) = \sum_{k=0}^{n-1}(x-k),$$

for a positive integer n, and $(x)_0 = 1$. Note that $\frac{(x)_n}{n!} = \binom{x}{n}$.

Also, the *q-shifted factorial* is defined as

$$(a;q)_n = \prod_{k=0}^{n-1}\left(1-aq^k\right) = (1-a)(1-aq)\left(1-aq^2\right)\ldots\left(1-aq^{n-1}\right).$$

We say that a series of the form $\sum_{n=0}^{+\infty} a_n x^n$ is a *basic hypergeometric series* if $\frac{a_{n+1}}{a_n} = \frac{p(q)}{r(q)}$, for every n, where, s $p(q)$ and $r(q)$ are polynomials of arbitrary degree in q, q is a parameter such that $|q| < 1$, and $|x| < 1$, assuring convergence of the series.

We use the concepts and notation of basic hypergeometric series (see [2]) throughout this note. We have

$$(1-x)(1-xq)\ldots\left(1-xq^{n-1}\right) = (x:q)_n.$$

Note that

$$\lim_{n\to\infty}(x:q)_n = \prod_{n=0}^{\infty}\left(1-xq^n\right).$$

We see that for large values of *k,* the expression from (3)

$$L \cdot \sum_{j=0}^{k} \binom{k}{j} \left(-(l-1)i\right)^{j}$$

representing the outstanding loan balance at time *k,* can reach the value of 0, resulting in full repayment of the loan, provided that $1 < l < 2$ and $0 < i < 1$ (a very natural assumption for interest rates).

II. Varying Interest Rates

A more complicated scenario occurs if we instead use a varying interest rate. Let us assume that the interest rate (*forward rate,* or *short rate*) from time $j - 1$ to time j is $f_j = i^j$. This assumption is a special model for persistently falling interest rates, a scenario akin to the recent experience of developed economies such as Japan, or Germany, and, to a degree, the United States. We then have the following

Proposition 1. *Suppose a loan L' is to be repaid at l times the forward rate (or short rate) from time j – 1 to time j* given as $f_j = i^j$. *Then the loan will need either a single final payment (a balloon payment) or an additional annuity of scheduled payments, written as A, to complete the loan repayment, since*

$$OB_k = L'\left(1-(l-1)i\right)\left(1-(l-1)i^2\right)\ldots\left(1-(l-1)i^k\right) = \\ = \left((l-1)i;i\right)_k. \tag{4}$$

Note that the proposition is stated to imply that we require

$$L' = L'\left((l-1)i;i\right)_k + A,$$

if the original term of the payment structure was k periods.

We note that (4) is a special case of q-binomial formula [2, p. 5, eq. (6.23)]:

$$(x;q)_n = \sum_{j \geq 0} \frac{(q)_n (-x)^j q^{\binom{j}{2}}}{(q)_j (q)_{n-j}}. \tag{5}$$

Additionally, the left-hand side reduces to $(1-x)^n$ when $q = 1$, which may be interpreted to be the case illustrated for (3).

Proof of the Proposition 1. In order to prove our claim, we need to show that for arbitrarily large *k,* or equivalently for $k \to \infty$, $OB_k > 0$. To see this, we use the limiting case of the q-binomial formula (1.5):

$$(xq;q)_\infty = \sum_{n=0}^{\infty} \frac{(-x)^n q^{\frac{n(n+1)}{2}}}{(q)_n},$$

and select $x = l - 1$, $1 < l < 2$, and $q = i$. The terms in the series are clearly declining, tending to zero, and alternating from the first term of 1, which shows that the series converges to a value in the open interval (0, 1). Hence

$$L'\left((l-1)i;i\right)_\infty < L'$$

and

$$A = L'\left(1-\left((l-1)i;i\right)_\infty\right).$$

We also note that in the case when $0 < l < 1$, the value of A is larger than in the case when $1 < l < 2$, as in this unusual arrangement at the end of k periods there is an outstanding balance greater than the original loan *L',* by (4). Clearly, this means a final balloon payment is required.

III. Final Comments

If A is selected as a final payment and satisfies $A > L'li$ for $1 < l < 2$, then this is the balloon payment in the traditional sense, as the first payment is the otherwise largest one in such a scenario. While it seems unlikely that the short rate f_j may decline as rapidly as i^j, we believe that our model is still feasible. It may be of interest to apply our model in scenarios where it is believed than short rates will decline consistently in the future. Our main objective is to highlight the appearance of basic hypergeometric progression within the scope of financial mathematics.

References

[1] Wai-Sum Chan and Yin-Kuen Tse, *Financial Mathematics for Actuaries,* World Scientific Pub. Co. Inc., Second Edition, 2017.

[2] N. J. Fine, *Basic Hypergeometric Series and Applications,* Math. Surveys 27, American Mathematical Society, Providence, Rhode Island, U.S.A., 1985 (revision from orignal 1980 edition).

Application of Paraconsistent Annotated Logic in Prototype of Autonomous Vehicle in 1:24 Scale

Henry Costa Ungaro
Graduate Program in Production Engineering
Paulista University
São Paulo, Brazil
henry@paradecision.com

Jair Minoro Abe
Graduate Program in Production Engineering
Paulista University
São Paulo, Brazil
jairabe@uol.com.br

Fábio Vieira do Amaral
Paulista University
São Paulo, Brazil
fabio@paradecision.com

Kazumi Nakamatsu
University of Hyogo
Hyogo, Japan
nakamatu@shse.u-hyogo.ac.jp

***Abstract* — Google, Tesla, and GM are companies that worry about creating a IA-based stand-alone vehicle. These vehicles comprehend the world depends on the data extraction from sensors, radars, cameras, among other devices. One detail that must be considered is the inconsistencies, which appear to be caused by the conditions of the environment in which the evidence is placed. This paper applies the concepts of Paraconsistent Annotated Evidential Et in an embedded software environment from Arduino Uno microcontroller board, ultrasonic sensors, DC motors, vehicle chassis available in Arduino basic kit, in 1:24 scale. The project is to provide an initial knowledge base that can evolve into a more complex situation. The scope of this work is limited to the identification of obstacles and the application of actions that avoid the collision. As proposition: "there are no obstacles ahead". During the tests, the prototype easily recognized obstacles that occur by adopting the measurements determined by the twelve logical states.**

Keywords—paraconsistent logic; paraconsistent annotated logic; autonomous vehicle; Arduino

I. Introduction

Autonomous vehicles tend to benefit society, referring to locomotion, ensuring more safety in critical conditions, reducing the stress generated by large cities' traffic, and others. [1]

II. Theoretical Foundation

Decision making is the cognitive process by which a plan of action is chosen from several others (based on various scenarios, environments, analyzes, and factors) for a problem situation. Every decision-making process produces a final choice. The output may be an action or an opinion. Decision-making refers to the process of choosing the most appropriate path in a given circumstance. [2]

In the real world, we deal with uncertainties, situations of inconsistencies, and often we have only a partial recognition of facts and objects – However, this does not prevent the development of human reasoning that is beyond the binary relation of truth and falsity [3]. The need to demonstrate and treat contradictory and non-trivial situations led to the emergence of an underlying logic for formal systems called paraconsistent logics [4].

A. Paraconsistent logic

The necessity to make decisions occurs at a moment of deadlock, which there are more than one option to follow. We make decisions based on subjective aspects; subjectivity has no perfect measure; it is organized, systematically and objectively. [2]

Paraconsistent Logic is among the non-classical logical since it contains provisions contrary to some of the basic principles of Aristotelian Logic, such as the principle of contradiction. Under Aristotelian view, any statement is necessarily true or false. According to the Paraconsistent Logic, a sentence and its negation may both be true [4]. It works with propositions of type p (μ, λ), where p is a proposition and (μ, λ) indicate the degrees of favorable evidence and contrary evidence, respectively. The pair (μ, λ) is called the annotation constant, with the values of μ and λ being limited between 0 and 1 [5]. The input data processing takes place through the application of minimization and maximization connectives between the atomic formulas A and B that define the output state, considering the propositional ones with their respective degrees of certainty and uncertainty pA (μ_1, λ_1) and pB (μ_2, λ_2), the highest value is obtained between the degrees of certainty (μ_1 OR μ_2), obtaining the resulting degree of certainty (μ_R), then minimizing the degrees of uncertainty (λ_1 OR λ_2) obtaining the degree of resulting uncertainty (λ_R) [5].

Considering the scenario of two expert groups A (E1, E2) and B (E3, E4), we can demonstrate the application of the OR connective represented by the disjunction A v B:

E1 (μ_1, λ_1) OR E2 (μ_2, λ_2) = (Max $\{\mu_1, \mu_2\}$, Min $\{\lambda_1, \lambda_2\}$) = AR (μ_1, λ_1)

E3(μ_1, λ_1) OR E4(μ_2, λ_2) = (Max $\{\mu_1, \mu_2\}$, Min $\{\lambda_1, \lambda_2\}$) = AR (μ_2, λ_2)

Then the application of the AND connective between the annotated AR and BR signals, representing the AR Conjunction $\wedge$ BR:

R = AR (μ_1, λ_1) AND BR (μ_2, λ_2) = (Min $\{\mu_1, \mu_2\}$, Max $\{\lambda_1, \lambda_2\}$) = R (μ_1, λ_1)

After maximization and minimization, the degrees of certainty and uncertainty are obtained by:

• Degree of certainty: $Gce(\mu, \lambda) = \mu - \lambda$
• Degree of Uncertainty: $Gun(\mu, \lambda) = \mu + \lambda - 1$
Two external and arbitrary boundary values (Vcve = Truth control value and Vcfa = False control value) determine when the resulting degree of certainty is high enough that the proposition analyzed is considered totally true or totally false.
Likewise, two external and arbitrary boundary values (Vcic = Control value of inconsistency and Vcpa = Control value of paracompleteness) determine when the value of the degree of uncertainty resulting from the analysis is so high that the proposition can be considered totally inconsistent or totally paracomplete (Table 1).

TABLE I. EXTREME VALUES [6]

External Limit Values	
Vcve	Truth control value
Vcfa	False control value
Vcic	Inconsistency control value
Vcpa	Paracomplete control value

After determining the four limit values and the results of the degree of certainty and uncertainty, it is possible to identify the resulting logical state. Through the use of such concepts, we arrive in Figure 1.

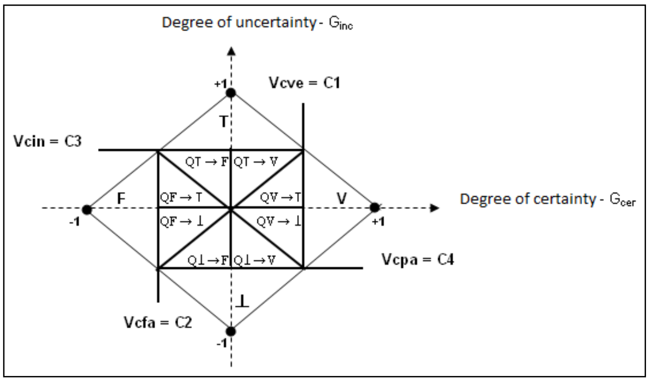

Fig. 1. Diagram with the degrees of certainty and uncertainty, with adjustable values of limit control, indicated in the axes [6]

The logical states which are represented by regions that occupy the vertices of the lattice are: True, False, Inconsistent and Paracomplete. These are called extreme logic states. The output logic states represented by internal regions in the lattice that is not the extreme logic states are called non-extreme logic states. Each non-extreme logical state is named according to its proximity to the extreme logic states.
The following are four logical states extreme Table 2 and eight non-extreme Table 3 that make up the lattice of Figure 2.

TABLE II. EXTREME STATES [6]

Extreme State	Symbol
True	V
False	F
Inconsistent	T
Paracomplete	⊥

TABLE III. NON-EXTREME STATES [6]

Non-Extreme State	Symbol
Quasi-true tending to Inconsistent	QV→T
Quasi-true tending to Paracomplete	QV→⊥
Quasi-false tending to Inconsistent	QF→T
Quasi-false tending to Paracomplete	QF→⊥
Quasi-Inconsistent tending to True	QT→t
Quasi-Inconsistente tending to False	QT→F
Quasi-Paracomplete tending to True	Q⊥→V
Quasi-Paracomplete tending to False	Q⊥→F

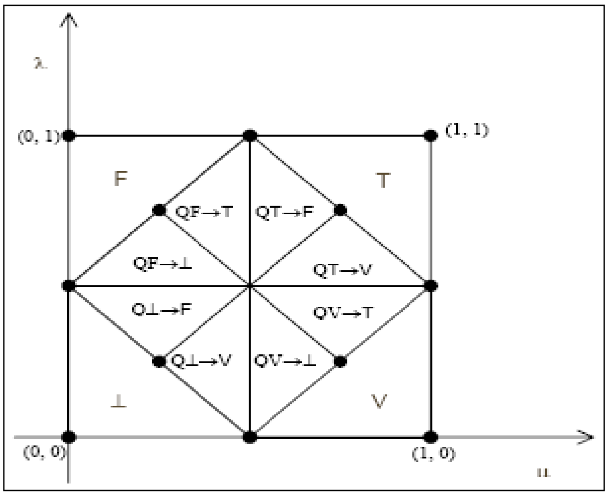

Fig. 2. Division of the lattice in 12 regions [6]

The characterization the resulting logical states, the following rules are considered (Table 4):

TABLE IV. MATHEMATICAL CHARACTERIZATION OF THE STATES [5]

Condition	Resulting State
If $Gcer(\mu, \lambda) \geq Vcve$	True
If $Gcer(\mu, \lambda) \leq Vcfa$	False
If $Ginc(\mu, \lambda) \geq Vcic$	Inconsistent
If $Ginc(\mu, \lambda) \leq Vcpa$	Paracomplete
If $0 \leq Gcer(\mu, \lambda) < Vcve$ and $0 \leq Ginc(\mu, \lambda) < Vcic$ and $Gcer(\mu, \lambda) \geq Ginc(\mu, \lambda)$	Quasi-true tending to Inconsistent
If $0 \leq Gcer(\mu, \lambda) < Vcve$ and $0 \leq Ginc(\mu, \lambda) < Vcic$ and $Gcer(\mu, \lambda) < Ginc(\mu, \lambda)$	Quasi-Inconsistent tending to true
If $0 \leq Gcer(\mu, \lambda) < Vcve$ and $Vcpa < Ginc(\mu, \lambda) \leq 0$ and $Gcer(\mu, \lambda) \geq \lvert Ginc(\mu, \lambda)\rvert$	Quasi-true tending to Paracomplete
If $0 \leq Gcer(\mu, \lambda) < Vcve$ and $Vcpa < Ginc(\mu, \lambda) \leq 0$ and $Gcer(\mu, \lambda) < \lvert Ginc(\mu, \lambda)\rvert$	Quasi-Paracomplete tending to true
If $Vcfa < Gcer(\mu, \lambda) \leq 0$ and $Vcpa < Ginc(\mu, \lambda) \leq 0$ and $\lvert Gcer(\mu, \lambda)\rvert \geq \lvert Ginc(\mu, \lambda)\rvert$	Quasi-false tending to Paracomplete
If $Vcfa < Gcer(\mu, \lambda) \leq 0$ and $Vcpa < Ginc(\mu, \lambda) \leq 0$ and $\lvert Gcer(\mu, \lambda)\rvert < \lvert Ginc(\mu, \lambda)\rvert$	Quasi-Paracomplete tendending to False
If $Vcfa < Gcer(\mu, \lambda) \leq 0$ and $0 \leq Ginc(\mu, \lambda) < Vcic$ and $\lvert Gcer(\mu, \lambda)\rvert \geq Ginc(\mu, \lambda)$	Quasi-false tending to Inconsistent'

If Vcfa < Gcer(μ, λ) ≤ 0 and 0 ≤ Ginc(μ, λ) < Vcic and |Gcer(μ, λ)| < Ginc(μ, λ)	Quasi-inconsistent tending to False

B. *Hardware*

Arduino is an open source hardware platform, designed on the Atmel AVR microcontroller, which can be programmed through a programming language similar to C / C ++, allowing the preparation of projects with a basic or no programming and electronic knowledge. [7]

Motors and H-Bridge. The basic principle of DC motors is to let the electric current flow through a coil, creating a magnetic field. This magnetic field applied to a magnet results in the rotation of the shaft, which may be connected to wheels, propellers or any other type of gear. [7]

The H-Bridge is an integrated circuit that facilitates the assembly of circuits for the use of motors, allowing the movement of these motors clockwise and counter clockwise. These plates protect the motor circuit of the others, avoiding damages. [9]

Ultrasonic Sensor. The ultrasonic sensor HC-SR04 allows detecting objects that are in the distance between 1 and 200 cm.

This sensor emits an ultrasonic signal that reflects in an object and returns to the sensor, allowing to calculate the distance of the object concerning the sensor, adopting as a base the time of trajectory of the signal. [7]

Chassis. The chosen chassis was the standard model of the kits supplied with the Arduino microcontroller. Acrylic structure, with three wheels being two associated with motors and the third wheel, formed by bearing without motor control. [10]

C. *Methodology*

Experimental implementation of paraconsistent logic concepts through the construction of a prototype based on the Arduino platform

III. PROTOTYPE

Figure 4 shows the circuit with all the components used. PowerBank Lotus LT55, lithium battery with a capacity of 10000mAh @ 3.7V, DC input 5V 2A output DC 5V 1A / 2.1A output:> 6800MAH> 31.5WH, with two USB inputs where the USB1 feeds Arduino and USB2 power the motors.

Two ultrasonic sensors were used, in which one corresponded to a "favorable degree of evidence" and the other to "opposite degree of evidence." Arduino pins 4, 5, 6 and seven are used to control the two motors connected to H-Bridge.

The pins 9 (Trigger) and 12 (Echo) is responsible for controlling the left-hand ultrasonic (μ) and the pins 10 (Trigger) and 13 (Echo) the right (λ) pins.

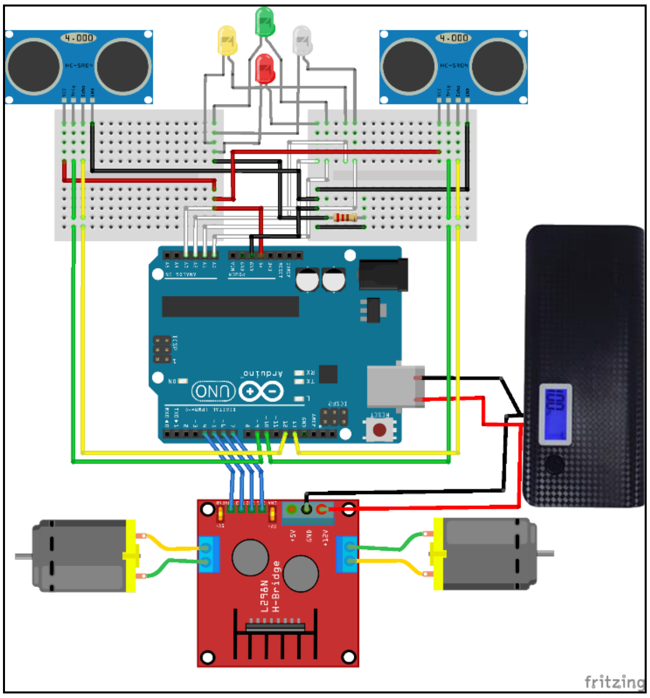

Fig. 3. Prototype Wiring Scheme

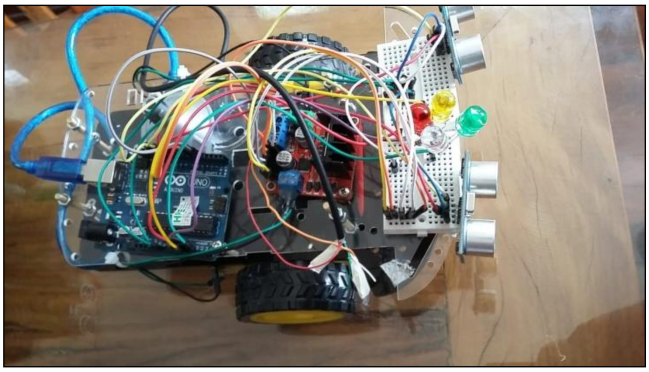

Fig. 4. Prototype

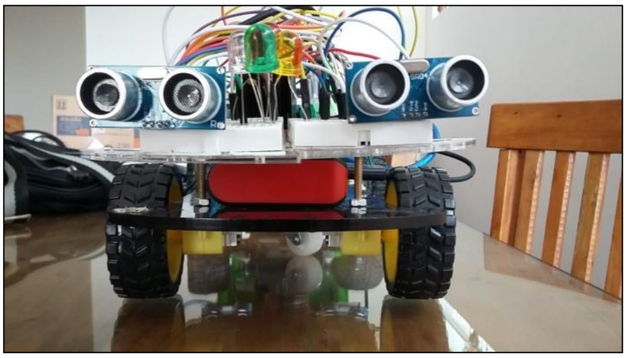

Fig. 5. Prototype

IV. EVENT DEFINITIONS

As proposition, it was considered that there are no obstacles in front of the vehicle.

Maximum distance was taken by sensors: 120 cm.

For maximum distance, was assigned μ value 1 and for λ value 0, in correspondence for the minimum distance, was assigned μ value 0 and for λ value 1. For control values, Vcve was assigned +0 value, 5, for the Vcfa was assigned value -0.5, for the Vcic was assigned +0.5 value and for Vcpa was assigned value -0.5. Figures 11 and 12 correlate extreme and non-extreme logic states with regions that were considered as possible obstacle holders. The center line comprises the perfectly defined line, where the degree of certainty becomes more decisive about the presence of obstacles. As it moves away from the center line towards the vertical extremes, the level of inconsistency and indetermination increases, as a consequence, the actions referring to the states near the center line and μ tending to 0 indicate the presence of an obstacle closer and closer to the vehicle. Therefore, more actions should be taken.

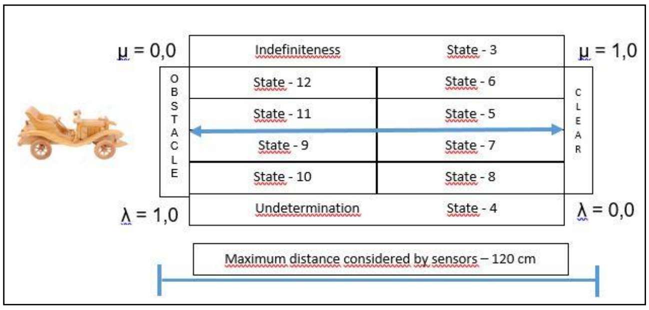

Fig. 6. Prototype decisions in logic state

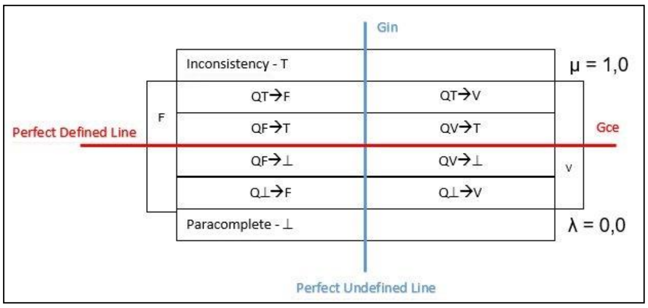

Fig. 7. Prototype extreme state

V. SOURCE CODE

```
#include <Ultrasonic.h>
//Ultrasonic pins
#define pino_trigger_mi     9      // The sensor sends a ultrasonic wave
#define pino_trigger_lambda 10     // The object reflect this wave and
#define pino_echo_mi        12     // Echo recive the wave
#define pino_echo_lambda    13
//Ultrasonic Start Up
Ultrasonic sensor_mi(pino_trigger_mi, pino_echo_mi);
Ultrasonic sensor_lambda(pino_trigger_lambda, pino_echo_lambda);
// Control Variables
float distancia_mi;          // distance value for sensor_mi
float distancia_lambda;      // distance value for sensor_lambda
float vcve = 0.5;            // control variable for true
float vcfa = -0.5;           // control variable for false
float vcic = 0.5;            // control variable for inconsistency
float vcpa = -0.5;           // control variable for de paracomplete
// ParaAnaliser
int paraAnalisador(float mi, float lambda) {
  // Normalization of evidence degree between 0 and 1
  mi   = mi / 100;                 // Favorable degree -  0 , 1
  lambda = lambda / 100;           // Unfavorable degree - 0 , 1
  float Gce  = mi - lambda;        // Gce - certainty degree  - Gce = mi - lambda
  float Gin  = ((mi + lambda) - 1);  // Gin - uncertainty degree - Gin = mi + lambda - 1
  int estado = 0;                  // Logic States, Extreme and Non-Extreme
  float modulo_Gce;                // Module Value for certainty
  float modulo_Gin;                // Module Value for uncertainty
  if (Gce < 0)
   modulo_Gce = Gce * (-1);
  else
   modulo_Gce = Gce;
  if (Gin < 0)
   modulo_Gin = Gin * (-1);
  else
   modulo_Gin = Gin;
  // Extreme states definition
  // Proposition: path ahead is clear
  if(Gce >= vcve)
   estado = 1; //true - path is clear
  else if(Gce <= vcfa)
     estado = 2; //False - it will hit - Stop, backwards, turn right and left
    else if(Gin >= vcic)
        estado = 3; //Inconsistent - turn slightly right
       else if(Gin <= vcpa)
           estado = 4; //Paracompleto - turn slightly left
          else if( (Gce >= 0) && (Gce < vcve) && (Gin >= 0) && (Gin < vcic) && (Gce >= Gin))
              estado = 5; //Quasi-true tending to inconsistent - Turn right, more than state 3
             else if((Gce >= 0) && (Gce < vcve) && (Gin >= 0) && (Gin < vcic) && (Gce < Gin))
                 estado = 6; //inconsistent tending to true - turn slightly left , less than state 5
                else if((Gce >= 0) && (Gce < vcve) && (Gin > vcpa) && (Gin <= 0) && (Gce >= modulo_Gin))
                    estado = 7; //Quasi-true tending paracomplete- turn left, more than state 8
                   else if((Gce >= 0) && (Gce < vcve) && (Gin > vcpa) && (Gin <= 0) && (Gce < modulo_Gin))
                       estado = 8; // paracomplete tending to true - turn slightly left , more than state 4
                      else if((Gce > vcfa) && (Gce <= 0) && (Gin > vcpa) && (Gin <= 0) && (modulo_Gce >= modulo_Gin))
                          estado = 9; // quasi-false tending to paraconsistent - Stop, turn left
                         else if((Gce > vcfa ) && (Gce <= 0) && (Gin > vcpa) && (Gce < Gin) && (Gin <= 0))
                             estado = 10; // paracomplete tending to false - Stop, turn left
```

```
                    else if((Gce > vcfa) && (Gce
    <= 0) && (Gin >= 0) && ( Gin < vcic) && (Gce >=
    Gin))
                        estado = 11; // quasi-false
    tending to inconsistent- Stop, turn right
                       else if((Gce <= 0) && (Gce
    < vcfa) && (Gin >= 0) && (Gin < vcic) && (Gce <
    Gin))
                          estado = 12;
    //inconsistent tending to false - Stop, turn slightly right
  return estado;
}
// H-Bridge variables (L293D)
int in1 = 7;            // input 1
int in2 = 6;            // input 2
int in3 = 5;            // input 3
int in4 = 4;            // input 4
// Distance ajustment
float ajusteDistancia(Ultrasonic sensor) {
  float cmMsec;
  long microsec = sensor.timing();
  cmMsec = sensor.convert(microsec, Ultrasonic::CM);
  if (cmMsec > 120)          //Define maximum distance
    cmMsec = 120;
  else if (cmMsec < 5)        //Define minimum distance
    cmMsec = 5;
  return cmMsec;
}
void setup() {
  Serial.begin(9600);
  pinMode(in1, OUTPUT);
  pinMode(in2, OUTPUT);
  pinMode(in3, OUTPUT);
  pinMode(in4, OUTPUT);
  pinMode(verde_verdadeiro     , OUTPUT);
  pinMode(vermelho_falsidade   , OUTPUT);
  pinMode(amarelo_inconsistente, OUTPUT);
  pinMode(branco_paracompleto  , OUTPUT);
}
// Motor Control
void para(){
    digitalWrite(in2,LOW);
    digitalWrite(in1,LOW);
    digitalWrite(in3,LOW);
    digitalWrite(in4,LOW);
}
void anda(){
    digitalWrite(in1,LOW);
    digitalWrite(in3,HIGH);
    digitalWrite(in2,HIGH);
    digitalWrite(in4,LOW);
}
void re(){
    digitalWrite(in1,HIGH);
    digitalWrite(in3,LOW);
    digitalWrite(in2,LOW);
    digitalWrite(in4,HIGH);
}
void direita(){
    digitalWrite(in1,LOW);
    digitalWrite(in3,LOW);
    digitalWrite(in2,HIGH);
    digitalWrite(in4,LOW);
}
void esquerda(){
    digitalWrite(in1,LOW);
    digitalWrite(in3,HIGH);
    digitalWrite(in2,LOW);
    digitalWrite(in4,LOW);
}
void esquerda_f(){
    digitalWrite(in1,HIGH);
    digitalWrite(in3,HIGH);
    digitalWrite(in2,LOW);
    digitalWrite(in4,LOW);
}
void direita_f(){
    digitalWrite(in1,LOW);
    digitalWrite(in3,LOW);
    digitalWrite(in2,HIGH);
    digitalWrite(in4,HIGH);
}
// --- LOOP ---
void loop() {
  distancia_mi = map(ajusteDistancia(sensor_mi), 10, 120,
    0, 100);
  distancia_lambda = map(ajusteDistancia(sensor_lambda),
    10, 120, 100, 0);
  int estado =
    paraAnalisador(distancia_mi,distancia_lambda);
  Serial.println(String("Distance-mi : ") + distancia_mi +
    String("| Distance-lambda : ") + distancia_lambda +
    String("| State : ") + estado );
  if(estado == 1){
   anda();
  }
  else if(estado == 2){
   re();
  }
  else if(estado == 3){
   direita_f();
   anda();
   esquerda_f();
  }
  else if(estado == 4){
   esquerda_f();
   anda();
   direita_f();
  }
  else if(estado == 5){
   direita_f();
  }
  else if(estado == 6){
   direita();
  }
  else if(estado == 7){
   esquerda_f();
  }
  else if(estado == 8){
   esquerda();
  }
  else if(estado == 9){
   para();
   esquerda_f();
```

```
    delay(500);
  }
  else if(estado == 10){
    para();
    esquerda();
  }
  else if(estado == 11){
    para();
    direita_f();
    delay(500);
  }
  else if(estado == 12){
    para();
    direita();
  }
}
```

VI. CONCLUSIONS

During the tests, all the logical states were identified, when facing obstacles, in diagonal, the position of the sensors did not prove useful and are in need of adjustments. Although the hardware limitations, the decision making process proved to be efficient in relation of response time, deviating obstacles with relative ease, the number of collisions presented an index with less than 5% in relation of sample universe formed by 123 obstacles.

REFERENCES

[1] Jung, C.R. et al. Computação embarcada: Projeto e implementação de veículos autônomos inteligentes. Anais do CSBC (in Portuguese), v. 5, p. 1358-1406, 2005.

[2] Shimizu, T. (2006). Decisão nas Organizações (Vol. 2 ed.) (in Portuguese), São Paulo, SP, Brasil: Atlas, 2006.

[3] Martins, H. G. (2003). A Lógica Paraconsistente Anotada de Quatro Valores LPA4v aplicada em Sistemas de Raciocínio Baseado em Casos para o Restabelecimento de Subestações Elétricas. Tese de Doutorado apresentada à Universidade Federal de Itajubá, 2003.

[4] Akama, S., "Towards Paraconsistent Engineering," Intelligent Systems Reference Library, Volume 110, 234 pages, 2016.

[5] Abe, J.M., S. Akama, K. Nakamatsu, "Introduction to Annotated Logics - Foundations for Paracomplete and Paraconsistent Reasoning," Series Title Intelligent Systems Reference Library, Volume 88, Springer International Publishing, Copyright Holder Springer International Publishing Switzerland, ISBN 978-3-319-17911-7, Edition Number 1, 190 pages, 2015.

[6] Abe, J.M., "Paraconsistent Intelligent Based-Systems: New Trends in the Applications of Paraconsistency," editor, Book Series: "Intelligent Systems Reference Library," Springer-Verlag, Vol. 94, ISBN:978-3-319-19721-0, 306 pages, 2015.

[7] Oliveira, C.L.V., H.A.P. Zanetti, Descomplicado: como elaborar projetos de eletrônica (in Portuguese), Saraiva Educação SA, 2015.

[8] Fritzing. Available at: http://fritzing.org/home/ Retrieved 2018-11-10

[9] Thomsen, Adilson. Motor DC com Driver Ponte H L298N. 2013. Available in: https://www.filipeflop.com/blog/motor-dc-arduino-ponte-h-l298n/. Retrieved 2018-11-10

[10] MSS Eletrônica Available at: https://www.msseletronica.com/detalhes/kit-chassis-2-rodas-2-motores-eletricos-dc-cc-para-robos-robotica-carrinho-2wd/990.html. Retrieved 10/11/2018

Authors' Index